Summer 7-15-2022

THERMODYNAMIC AND KINETIC INVESTIGATION OF U(VI) AND AS(V) REACTIONS: INSIGHTS FOR RISK ASSESSMENT AND REMEDIATION

MARIA ISABEL MEZA
UNIVERSITY OF NEW MEXICO

Maria Isabel Meza
Candidate

Civil, Construction & Environmental Engineering
Department

This dissertation is approved, and it is acceptable in quality and form for publication:

Approved by the Dissertation Committee:

Jose M. Cerrato , Chairperson

Kerry J. Howe

Abdul-Mehdi S. Ali

Peter C. Burns

Jorge Gonzalez-Estrella

Peter Lichtner

THERMODYNAMIC AND KINETIC INVESTIGATION OF

U(VI) AND AS(V) REACTIONS:

INSIGHTS FOR RISK ASSESSMENT AND REMEDIATION

BY

ISABEL MEZA

B.S., Environmental Engineering, Universidad San Francisco de Quito, 2007
MSc. Environmental Management and Natural Resources, Ball State University, 2009

DISSERTATION

Submitted in Partial Fulfillment of the

Requirements for the Degree of

Doctor of Philosophy

Engineering

The University of New Mexico

Albuquerque, New Mexico

July, 2022

ACKNOWLEDGEMENTS

I want to express my sincere thanks to Dr. José Cerrato who believed in me and gave me the opportunity to pursue this PhD. José, thanks for being a great advisor, mentor, and friend who guided me wisely during my Ph.D. journey. I learned patience, passion, and decision to always pursue top-notch research which helped me to become an excellent independent researcher.

I also thank my committee members; Dr. Mehdi Ali (for all your patience and great research insights, even if I was about to break your ICP-MS), Dr. Peter Burns (for hosting me at your incredible laboratory at Notre Dame and never stopping mentoring me), Dr. Jorge Gonzalez-Estrella (for teaching me all the basics about laboratory work, writing, and the best tips of how to become an excellent researcher), Dr. Peter Lichtner (for all your patience teaching me by Zoom about PFLOTRAN, and catching every single typo in the documents), and Dr. Kerry Howe (for your valuable recommendations, encouragement, and scientific questions that made me grow as a researcher a lot). All of you are a main component of my dissertation.

I want to sincerely acknowledge Dr. Mike Spilde, Dr. Eric Peterson, Dr. Tori Forbes, Dr. Juan Lezama-Pacheco, Virginia Rodriguez, and Kaelin Gagnon, for their input and guidance on my research, manuscript writing, and data interpretation. I deeply appreciate working and analyzing all my results with them. I appreciate the feedback and help provided by my fellow students in the E-H_2O research group and the graduate student office, with experimental designs, presentations, manuscripts or just to share lunch or a cup of coffee.

I want to say a thank you very much to my extraordinary support network who kept me as sane as possible, especially during COVID. Thank you, Carmen Adelita, for being

there for me during many hard moments. Thank you to my Bible Study Group: Justin, Daniel, Bethany, Sarah, Kristin, Michael, Clarissa, Joe, Shiloh, Jacqueline, Bart, Elizabeth, Jillian, and Ashleigh.

Finally, I must recognize the support and inspiration of my family, especially my daughter, Amelie, thank you for your patience, you have been an excellent daughter even though the hard circumstances. I dedicate this dissertation and years to you Mami Nancy, Papi Fico, David, and Dany. Thank you for your never-ending support, patience, and understanding during my doctoral journey. Even though we have been far away physically, I was always blessed with your wisdom every step of the way. I could not have done this without you Peluchines.

THERMODYNAMIC AND KINETIC INVESTIGATION OF U(VI) AND AS(V) REACTIONS:

INSIGHTS FOR RISK ASSESSESMENT AND REMEDIATION

by

Isabel Meza

B.S. in Environmental Engineering, 2007
MSc. Environmental Management and Natural Resources, 2009
Ph.D. Engineering, 2022

ABSTRACT

The goal of this dissertation was to investigate the mechanisms of immobilization of uranium (U) and arsenic (As) in waters nearby to Native American Communities for remediation applications. This work sought to identify the physical or chemical processes affecting the complexation, sorption, and precipitation of U and As with calcium (Ca), carbonates $(CO_3)^{2-}$, and phosphate $(PO_4)^{3-}$. The current knowledge about the mechanisms affecting the reaction of metal mixtures such as U, As, and other co-occurring elements in natural waters with minerals such as limestone[1-5] and hydroxyapatite for remediation applications is limited. A better understanding of thermodynamics and kinetics affecting the reaction of metal mixtures is essential for the development of water remediation strategies for the application of natural abundant minerals in the southwestern US and other areas of the world. The research objectives were: **1)** Determine the solubility product and thermodynamic variables ($\Delta G°, \Delta H°, \Delta S°$) for uranyl arsenate solids with the monovalent cations sodium (Na) and potassium (K). **2)** Determine the kinetic rate law for dissolution of uranyl arsenate solids at acidic pH. **3)** Determine conditions that favor precipitation of U and As with phosphate and limestone at pH 3 and 7 for water remediation. The information gained from this research will be relevant for risk assessment and remediation.

TABLE OF CONTENTS

LIST OF FIGURES

Chapter 3

Chapter 4

Chapter 5

LIST OF TABLES

Chapter 3

Chapter 4

CHAPTER 1

1.1 INTRODUCTION

The concentrations of U^6 and As can exceed the maximum contaminant level (MCL) established by EPA,[6, 7] and these elements can co-occur with other elements in abandoned waste sites in Native American Communities in the SW US.[8, 9] The co-occurrence of these elements at elevated concentrations has also been reported in natural geologic formations and sites affected by mining legacy and other anthropogenic activities in other parts of the US, Canada, Australia, and other parts of the world. [8-10] Understanding the physical-chemical processes affecting the mobilization of U and As in these environments is necessary for the development of feasible risk assessment and remediation strategies.

The goal of this dissertation was to investigate the mechanisms of immobilization of uranium (U) and arsenic (As) in waters nearby Native American Communities for remediation applications. This dissertation is organized in five chapters. Chapter 1 is the introduction and Chapter 2 is the literature review. Chapters 3, 4 and 5 are the main body of work of the dissertation and each is formatted as a research paper.

Chapter 3 has been submitted for publication in *Environmental Science and Technology* and relates to the solubility products of NaUAs and KUAs with its thermodynamic variables. Chapter 3 includes a discussion about the impact that substitution of cations can have in the solubility of uranyl arsenate solids ($UAs_{(s)}$).

Chapter 4 focuses on obtaining the dissolution rates of NaUAs and KUAs and interpreting the solubility of these $UAs_{(s)}$ in relation to the concentrations of U and As in water. The manuscript resulting from this chapter will be submitted to the journal *ACS Earth and Space Chemistry*.

Chapter 5 focuses on understanding the effects of naturally occurring minerals and rocks like limestone and hydroxyapatite, in the concentration of U and As in the environment. The manuscript resulting from this chapter will be submitted to the journal *Environmental Science Water Research and Technology.* Appendices A, B and C contain supplementary information for the Chapters 3, 4 and 5 respectively.

This study represents a relevant contribution given the limited existing literature related to the solubility of uranyl arsenate minerals. Furthermore, the information obtained in this dissertation can be useful for reactive transport models for risk assessment and remediation initiatives.

CHAPTER 2: LITERATURE REVIEW

2. Background

2.1 Uranium, arsenic, and their occurrence in mining legacy sites and other anthropogenic processes.

Uranium (U) and Arsenic (As) are naturally occurring elements, commonly associated in uranium deposits.[11] The most relevant oxidation states for U in natural environments are U(VI) and U(IV)[12], though it can exist in nature in oxidation states ranging from +4 to +6[13] and it occurs as oxides, peroxides, oxide-hydroxy-hydrates, precipitates, and complexes.[13] Uranium speciation and mobility depend on the presence of dissolved inorganic carbon and organic matter, the solution pH, redox potential, hydrolysis, dissolution, complexation, and sorption.[14] Uranium (IV) exists in reduced subsurface environments and is a less mobile than U(VI). Uranium (VI) is the most prevalent oxidation form in the environment, and occurs in oxic conditions across the pH range, and forms more soluble and toxic compounds compared to U(IV).[12] The U(VI) cation in the environment is invariably present as a $(UO_2)^{2+}$ uranyl ion.

The predominant oxidation states of As in natural waters are As(III) and As(V),[15] but it can also occur in nature in oxidation states ranging from -3 to +5. Arsenic speciation depends on pH and redox potential of the environment.[16] For instance, As(V) predominates in oxidizing conditions and pH values lower than 6.9 as H_2AsO_4, in higher pH values as $HAsO_4^{2-}$, in extremely acidic conditions as H_3AsO_4, and extreme alkaline conditions as AsO_4^{3-}. Arsenic (III), on the other hand, will predominate under reducing conditions and pH values lower than 9.2 mainly as H_3AsO_3.[15] Both As(V) and As(III) are toxic; however, As (III) is 20 to 50 times more toxic than As(V).[16]

The co-occurrence of U and As caused by natural and anthropogenic processes is a concern to communities living in the proximity of contaminated sites.[11, 17-22] Minerals containing U and As occur in various locations worldwide. [21, 23, 24] For example, some of the largest U mines are located in Key Lake, Saskatchewan, Canada, St. Austell District of Cornwall, England, and in several Southwestern US sites.[21, 23, 24] Communities that surround the mine sites have been impacted by the release of U and As, which is of major concern for public health as both are toxic and carcinogenic, and U is radioactive.[11, 25, 26]

Exposure to U can lead to chemical and radiological toxicity.[12] Its main chemical effect is associated with kidney disease while its primary radiological effect is associated with cancer.[27] Research evaluating the effect of uranium on Navajo communities have related U exposure to an increased probability of developing one or more chronic diseases such as hypertension, kidney disease, and diabetes.[28] On the other hand, exposure to As can lead to its accumulation in skin, hair, and nails resulting in clinical conditions such as hyperpigmentation or keratosis. It also increases the risk of skin, lung, and internal organ cancer. In addition, other conditions such as cardiovascular diseases, neuropathy, low verbal IQ, loss of long term memory, fetal loss and premature delivery, and decreased birth weights of infants have been associated with exposure to As.[29] Consequently, reclamation and environmental restoration of abandoned U mine sites are now being addressed under the Superfund law by the USEPA, state agencies, and tribes.[30]

Considering areas not influenced directly by mining operations, U and As can co occur as contaminants and impact human health as well. For example, literature relates to the spatial relationship between U and As in Northern Plains Native lands that were

evaluated and U and As were found elevated in samples taken from three regions in North and South Dakota.[20] Also, it was stated that there was a spatial correlation of ground water wells containing U and As which are associated with flow along a geologic contact; however, the underlying mechanisms enabling the U and As correlation warranted further study.[20] Therefore, it is crucial to develop a greater understanding of U and As and their behavior in natural waters.

2.2 Importance of understanding the thermodynamics and kinetics of uranyl arsenate solids.

Uranyl arsenate solids ($UAs_{(s)}$) are one of the most diverse chemical groups of U minerals but have been less characterized than the analogues phosphate phases.[23, 31] Arsenate and phosphate-bearing anionic units are generally isostructural, have similar size and charge, precipitate as uranyl minerals at elevated concentrations, and form ternary complexes on surfaces at low concentrations.[11, 32-35] Uranyl phosphates have generally low solubilities ranging from log K_{sp} of -13.17 for uranyl hydrogen phosphate to -49.36 and -50.39 for uranyl orthophosphate.[35, 36] The solubility curves and solubility products (log K_{sp}) of $UAs_{(s)}$ like $(UO_2)_3(AsO_4)_2 12H_2O$, $NaAsUO_6 3H_2O$, and $KAsUO_6 3H_2O$ were measured.[35, 37] However, the previous measurements were done only within heterogenous water-salt systems or saturated conditions,[35,37] and the literature suggests that solubility measurements should be confirmed under both supersaturation and undersaturation.[35, 38, 39] The changes in U and As soluble concentration as a function of pH could also be affected by the formation of secondary phases. Secondary phases that have been reported in the literature, include trögerite $(UO_2)_3(AsO_4)_2 12H_2O_{(s),}$[35, 40] and $(UO_2)(H_2AsO_4)_2(H_2O)_{(s)}$[41, 42].

These previous studies indicate that the thermodynamics and solubility constants of $UAs_{(s)}$ need more documentation.[41, 43]

Understanding the kinetics of the dissolution of UAs(s) is also essential to gain fundamental knowledge of U and As mobilization in environmentally relevant conditions. This knowledge is necessary for the use of reactive transport models as a tool to interpret and predict the fate of these toxic elements in the environment and to develop risk assessment and remediation strategies.

2.3. Limestone (calcium carbonate) and phosphate occurrence in the SW and its remediation applications.

Active and passive treatments are remediation strategies for treating acid mine drainage (AMD) and waste of abandoned mine sites. Active treatments involve the application of alkaline materials to remediate acidic mine waters and precipitate metals, while passive treatments use the application of natural and constructed wetlands.[44] Limestone is a sedimentary rock mainly composed of calcium carbonate ($CaCO_3$) commonly applied in both passive and active treatments for the neutralization of acid mine drainage.[1] Passive treatments that depend exclusively on the application of limestone are commonly used in post-closure/low acidic mine sites and are relatively inexpensive and easy to maintain.[1]

Several studies have evaluated the use of limestone to remove heavy metals from contaminated water.[2-5] Limestone (95.6% $CaCO_3$) showed removal efficiencies higher than 82% for cadmium (Cd), copper (Cu), chromium (Cr), lead (Pb), nickel (Ni), and zinc (Zn).[2] Limestone columns (95% $CaCO_3$) removed 99% of As.[4] Limestone (77 and 99 % $CaCO_3$) exhibited removal efficiencies higher than 88% for Cd, Cu, and Zn.[5] Finally, limestone has

also shown removal efficiencies for Pb as high as 90%.[3] However, very few studies have assessed the application of limestone to treat main waste containing U in co-occurrence with As.

Research has indicated that there are various processes involved in the sorption mechanisms of heavy metals in limestone.[3, 5, 45] Earlier findings suggest that at a low pH, the rapid dissolution of calcium carbonate is the first mechanism for heavy metal sorption forming carbonate complexes with limestone;[5] for example, Godelitsas et al.[3] showed formation of $PbCO_3$. Labastida et al.[45] indicated that metal removal also occurs due to precipitation and co-precipitation of metals. However, other results have indicated that the presence of some heavy metals such as Cd inhibited the dissolution of carbonate [$(CO_3)^{2-}$] to some extent, suggesting that there are other mechanisms involved in the removal of metals by limestone.[5] Iron hydroxides have also decreased the $(CO_3)^{2-}$ dissolution from limestone grains.[46] Overall, these studies indicate that the mechanism involved in the sorption of metals in limestone are complex and metal-specific. The presence of co-occurring U and As may likely have a unique sorption mechanism in a limestone matrix.

Precipitation of U and As in water will also depend on the working pH. Environmentally relevant conditions limit remediation approaches based on adsorption and precipitation with natural minerals. The formation of ternary uranyl aqueous complexes such as $Ca_2UO_2(CO_3)_3{}^0_{(aq)}$ increase U mobility. [24, 47] In a previous study it was observed that $UAs_{(s)}$ are stable in aqueous solution at pH 3.0 but at pH 7.0 dissolution is enhanced by formation of ternary calcium (Ca) uranyl carbonate complexes.[48] The availability of environmentally relevant ions in solution, like bicarbonate and $(PO_4)^{3-}$, can release $(AsO_4)^{3-}$ through competitive ion displacement.[49] Research has also found that $(UO_2)^{2+}$ and $(AsO_4)^{3-}$

can decrease in concentration when amendments with $(PO_4)^{3-}$, and both limestone and apatite have been used in batch experiments at pH 3.0 and 7.0.

The surface charge of any abundant mineral like calcite or apatite has to be considered when U and As are removed from aqueous solutions. Zeta potential analyses indicated the limestone used in this study is negatively charged from pH 2.0 to 9.0 at 25°C. Considering previous research, if the limestone is made up of quartz, albite, and calcite, we might have a negative charge that as well will influence U and As immobilization from water through adsorption and surface precipitation.[50-52]

2.4. Gaps in the Literature and Research Objectives.

This dissertation work addresses a current gap in the literature related to understanding the mechanisms for the immobilization of U and As in waters nearby to Native American Communities for remediation applications. While there is thermodynamic information from uranyl phosphates (uranyl arsenates analogues), there is limited information about the solubility and thermodynamic values for $UAs_{(s)}$ containing alkali or alkali-earth cations.[1,35, 36]

Thermodynamics and log K_{sp} were measured for $UAs_{(s)}$, but only within heterogenous water-salt systems,[35] and the literature suggests that solubility measurements should be confirmed under both supersaturation and undersaturation.[38] A previous study by Dzik et al.[11] provided calorimetry measurements for $UAs_{(s)}$ of the meta-autunite group containing potassium (K^+), lithium (Li^+), cesium (Cs^+), strontium (Sr^{2+}), and copper (Cu^{2+})[11] but did not provide solubility values or kinetic rates. These previous studies indicate that the thermodynamics, solubility constants, and kinetic rates of $UAs_{(s)}$

need more documentation.[41, 43]Additionally, the role of interlayer H_3O^+ substitution with monovalent cations in meta-autunite $UAs_{(s)}$ needs further investigation.[35, 42, 43, 53, 54]

Interaction of aqueous solutions containing $(UO_2)^{2+}$ and $(AsO_4)^{3-}$ with naturally abundant minerals such as calcite and apatite can cause immobilization of these metals, and amendments with both have been considered as potential remediation pathways.[4, 55, 56] Uranyl and $(AsO_4)^{3-}$ can adsorb and precipitate onto and with calcium phosphate minerals including autunite, hydroxyapatite, and fluorapatite.[55-59] Uranyl and $(AsO_4)^{3-}$ immobilization may be the result of adsorption to apatite; formation of $(UO_2)^{2+}$ and $(AsO_4)^{3-}$-phosphate ternary surface complexes with strong sediment surface binding.[56, 58] However, the mechanisms involved in the sorption and coprecipitation of $(UO_2)^{2+}$ and $(AsO_4)^{3-}$ onto and with limestone and $(PO_4)^{3-}$ remain limited.

The integration of experiments using well characterized $UAs_{(s)}$, laboratory-controlled experiments with advanced analytical techniques provided new information about the thermodynamics, solubility products, and kinetic rates for $UAs_{(s)}$. Furthermore, we also revealed the role of Ca in removal of $(UO_2)^{2+}$ and $(AsO_4)^{3-}$ in an aqueous system amended with $(PO_4)^{3-}$ and natural limestone.

2.5. Research Objectives

This project seeks to identify the physical or chemical processes affecting the complexation, sorption, and precipitation of U and As with calcium (Ca), carbonates $(CO_3)^{2-}$, and phosphate $(PO_4)^{3-}$. This project has three specific objectives:

Objective 1: Determine the solubility product (log K_{sp}) and thermodynamic variables ($\Delta G°$, $\Delta H°$, $\Delta S°$) for uranyl arsenate solids with monovalent cations sodium (Na) and potassium (K). (Paper in revision in **ES&T**)

Hypothesis 1: Potassium uranyl arsenate solid [$K(UO_2)(AsO_4)](H_2O)_3$] will have similar solubility product as sodium uranyl arsenate [$Na(UO_2)(AsO_4)](H_2O)_3$].

Objective 2: Determine the kinetic rate law for dissolution of uranyl arsenate solids at acidic pH.

Hypothesis 2: $NaUAs_{(s)}$ and $KUAs_{(s)}$ will have similar dissolution rates.

Objective 3: Determine conditions that favor chemical precipitation of U and As with limestone, PO_4, and Ca at pH 3 and pH 7 for water remediation**.**

Hypothesis 3: Precipitation of hydroxyapatite and uranyl phosphates will decrease the solubility of U and As.

REFERENCES

1. Santomartino, S.; Webb, J. A., Estimating the longevity of limestone drains in treating acid mine drainage containing high concentrations of iron. *J. Appl. Geochem.* **2007,** *22*, (11), 2344-2361.

2. Aziz, H. A.; Adlan, M. N.; Ariffin, K. S., Heavy metals (Cd, Pb, Zn, Ni, Cu and Cr(III)) removal from water in Malaysia: Post treatment by high quality limestone. *Bioresour. Technol.* **2008,** *99*, (6), 1578-1583.

3. Godelitsas, A.; Astilleros, J. M.; Hallam, K.; Harissopoulos, S.; Putnis, A., Interaction of Calcium Carbonates with Lead in Aqueous Solutions. *Environ. Sci. Technol.* **2003,** *37*, (15), 3351-3360.

4. Lizama-Allende, K.; Henry-Pinilla, D.; Diaz-Droguett, D. E. J. W., Air,; Pollution, S., Removal of Arsenic and Iron from Acidic Water Using Zeolite and Limestone: Batch and Column Studies. *Water Air Soil Pollut.* **2017,** *228*, (8), 275.

5. Sdiri, A.; Higashi, T.; Jamoussi, F.; Bouaziz, S., Effects of impurities on the removal of heavy metals by natural limestones in aqueous systems. *J. Environ. Manage.* **2012,** *93*, (1), 245-253.

6. Agency, E. P., National Primary Drinking Water Regulations. In Regulations, N. P. D. W., Ed. Environmental Protection Agency, 2019.

7. Roccaro, P.; Vagliasindi, F. G. A., Coprecipitation of vanadium with iron(III) in drinking water: a pilot-scale study. *Desalination Water Treat.* **2015,** *55*, (3), 799-809.

8. Avasarala, S.; Lichtner, P. C.; Ali, A.-M. S.; González-Pinzón, R.; Blake, J. M.; Cerrato, J. M., Reactive Transport of U and V from Abandoned Uranium Mine Wastes. *Environ. Sci. & Technol.* **2017,** *51*, (21), 12385-12393.

9. Blake, J. M.; Avasarala, S.; Artyushkova, K.; Ali, A.-M. S.; Brearley, A. J.; Shuey, C.; Robinson, W. P.; Nez, C.; Bill, S.; Lewis, J., Elevated concentrations of U and co-occurring metals in abandoned mine wastes in a northeastern Arizona Native American community. *Environ. Sci. Technol.* **2015,** *49*, (14), 8506-8514.

10. Jose Cerrato, P., and Scott Fendorf, PhD, Environmental Project 1 Mineral phases influence toxic transport from mine wastes Immobilization of Uranium, Arsenic, and Co-occurring Metals in Mine Wastes. In National Institute of Environmental Health Sciences: Tribal lands in the Southwest (UNM Metals) Superfund Research Program Center, 2016.

11. Dzik, E. A.; Lobeck, H. L.; Zhang, L.; Burns, P. C., High-temperature calorimetric measurements of thermodynamic properties of uranyl arsenates of the meta-autunite group. *Chem. Geol.* **2018,** *493*, 353-358.

12. Wufuer, R.; Wei, Y.; Lin, Q.; Wang, H.; Song, W.; Liu, W.; Zhang, D.; Pan, X.; Gadd, G. M., Chapter Four - Uranium Bioreduction and Biomineralization. In *Adv. Appl. Microbiol*, Sariaslani, S.; Gadd, G. M., Eds. Academic Press: 2017; Vol. 101, pp 137-168.

13. Burns, P. C.; Sigmon, G. E., *Uranium: cradle to grave*. Mineralogical Association of Canada Winnipeg: 2013; Vol. 43.

14. Blake, J. M.; De Vore, C. L.; Avasarala, S.; Ali, A.-M.; Roldan, C.; Bowers, F.; Spilde, M. N.; Artyushkova, K.; Kirk, M. F.; Peterson, E.; Rodriguez-Freire, L.; Cerrato, J. M., Uranium mobility and accumulation along the Rio Paguate, Jackpile Mine in Laguna Pueblo, NM. *Environ. Sci.: Process. Impacts* **2017,** *19*, (4), 605-621.

15. Smedley, P. L.; Kinniburgh, D. G., A review of the source, behaviour and distribution of arsenic in natural waters. *Appl Geochem* **2002,** *17*, (5), 517-568.

16. Crognale, S.; Amalfitano, S.; Casentini, B.; Fazi, S.; Petruccioli, M.; Rossetti, S., Arsenic-related microorganisms in groundwater: a review on distribution, metabolic activities and potential use in arsenic removal processes. *Rev. Environ. Sci. Bio-Technol.* **2017,** *16*, (4), 647-665.

17. Coyte, R. M.; Vengosh, A., Factors controlling the risks of co-occurrence of the redox-sensitive elements of arsenic, chromium, vanadium, and uranium in groundwater from the eastern United States. *Environ. Sci. Technol.* **2020,** *54*, (7), 4367-4375.

18. Das, N.; Das, A.; Sarma, K. P.; Kumar, M., Provenance, prevalence and health perspective of co-occurrences of arsenic, fluoride and uranium in the aquifers of the Brahmaputra River floodplain. *Chemosphere* **2018,** *194*, 755-772.

19. Yadav, S. K.; Ramanathan, A. L.; Kumar, M.; Chidambaram, S.; Gautam, Y. P.; Tiwari, C., Assessment of arsenic and uranium co-occurrences in groundwater of central Gangetic Plain, Uttar Pradesh, India. *Environ. Earth Sci.* **2020,** *79*, (6), 154.

20. Sobel, M.; Sanchez, T. R.; Zacher, T.; Mailloux, B.; Powers, M.; Yracheta, J.; Harvey, D.; Best, L. G.; Bear, A. B.; Hasan, K.; Thomas, E.; Morgan, C.; Aurand, D.; Ristau, S.; Olmedo, P.; Chen, R.; Rule, A.; O'Leary, M.; Navas-Acien, A.; George, C. M.; Bostick, B., Spatial relationship between well water arsenic and uranium in Northern Plains native lands. *Environ. Pollut.* **2021,** *287*, 117655.

21. Corkhill, C. L.; Crean, D. E.; Bailey, D. J.; Makepeace, C.; Stennett, M. C.; Tappero, R.; Grolimund, D.; Hyatt, N. C., Multi-scale investigation of uranium attenuation by arsenic at an abandoned uranium mine, South Terras. *NPJ Mater. Degrad.* **2017,** *1*, (1), 19.

22. Hoover, J.; Gonzales, M.; Shuey, C.; Barney, Y.; Lewis, J., Elevated arsenic and uranium concentrations in unregulated water sources on the Navajo Nation, USA. *Expos. Health.* **2017,** *9*, (2), 113-124.

23. Dzik, E. A. L., Haylie L.; Zhang, Lei; Burns, Peter C., Thermodynamic properties of phosphate members of the meta-autunite group: A high-temperature calorimetric study. *J. Chem. Thermodyn.* **2017,** *114*, 165-171.

24. Blake, J. M.; Avasarala, S.; Ali, A.-M. S.; Spilde, M.; Lezama-Pacheco, J. S.; Latta, D.; Artyushkova, K.; Ilgen, A. G.; Shuey, C.; Nez, C.; Cerrato, J. M., Reactivity of As and U co-occurring in mine wastes in northeastern Arizona. *Chem. Geol.* **2019,** *522*, 26-37.

25. Hoover, J. H.; Coker, E.; Barney, Y.; Shuey, C.; Lewis, J., Spatial clustering of metal and metalloid mixtures in unregulated water sources on the Navajo Nation – Arizona, New Mexico, and Utah, USA. *Sci. Total Environ.* **2018,** *633*, 1667-1678.

26. Brockgreitens, J. W.; Heidari, F.; Abbas, A., Versatile process for the preparation of nanocomposite sorbents: phosphorus and arsenic removal. *Environ. Sci. Technol.* **2020,** *54*, (14), 9034-9043.

27. National Research Councial, *Uranium mining in Virginia: scientific, technical, environmental, human health and safety, and regulatory aspects of uranium mining and processing in Virginia*. National Academies Press: 2012.

28. Hund, L.; Bedrick, E. J.; Miller, C.; Huerta, G.; Nez, T.; Ramone, S.; Shuey, C.; Cajero, M.; Lewis, J., A Bayesian framework for estimating disease risk due to exposure to uranium mine and mill waste on the Navajo Nation. *J. R. Stat. Soc. Ser. A-Stat. Soc.* **2015,** *178*, (4), 1069-1091.

29. Kapaj, S.; Peterson, H.; Liber, K.; Bhattacharya, P., Human Health Effects From Chronic Arsenic Poisoning–A Review. *J. Environ. Sci, Part A* **2006,** *41*, (10), 2399-2428.

30. USEPA, Federal Actions to Address Impacts of Uranium Contamination in the Navajo Nation Five-Year Plan Summary Report. In US Environmental Protection Agency: Pacific Southwest, Region 9: San Francisco CA, 2013.

31. Finch, R.; Murakami, T., Systematics and paragenesis of uranium minerals. **1999**.

32. Troyer, L. D.; Tang, Y.; Borch, T., Simultaneous reduction of arsenic(v) and uranium(vi) by mackinawite: role of uranyl arsenate precipitate formation. *Environ. Sci. Technol.* **2014,** *48*, (24), 14326-14334.

33. Liu, H.-K.; Ramachandran, E.; Chen, Y.-H.; Chang, W.-J.; Lii, K.-H., High-temperature, high-pressure hydrothermal synthesis, characterization, and structural relationships of layered uranyl arsenates. *Inorg. Chem.* **2014,** *53*, (17), 9065-9072.

34. Chernorukov, N. G.; Karyakin, N. V., The physical chemistry of the compounds $MIP(As)UO_6$ (MI=H, Li, Na, K, Rb, Cs) and their crystalline hydrates. *Russ. Chem. Rev.* **1995,** *64*, (10), 913-927.

35. Nipruk, O.; Chernorukov, N.; Pykhova, Y. P.; Godovanova, N.; Eremina, A., State of uranyl phosphates and arsenates in aqueous solutions. *Radiochemistry* **2011,** *53*, (5), 483-490.

36. Gorman-Lewis, D.; Shvareva, T.; Kubatko, K.-A.; Burns, P. C.; Wellman, D. M.; McNamara, B.; Szymanowski, J. E. S.; Navrotsky, A.; Fein, J. B., Thermodynamic properties of autunite, uranyl hydrogen phosphate, and uranyl orthophosphate from solubility and calorimetric measurements. *Environ. Sci. Technol.* **2009,** *43*, (19), 7416-7422.

37. Nipruk, O. V.; Chernorukov, N. G.; Elipasheva, E. V.; Klinshova, K. A.; Bakhmetev, M. O., State of uranyl arsenates $M^{I}AsUO_6 \cdot nH_2O$ (M^{I}–H^+, Li^+, Na^+, K^+, Rb^+, Cs^+, $NH4^+$) in aqueous solution. *J. Radioanal. Nucl. Chem.* **2020,** *324*, (1), 233-244.

38. Gorman-Lewis, D.; Burns, P. C.; Fein, J. B., Review of uranyl mineral solubility measurements. *J. Chem. Thermodyn.* **2008,** *40*, (3), 335-352.

39. Gorman-Lewis, D.; Fein, J. B.; Burns, P. C.; Szymanowski, J. E.; Converse, J., Solubility measurements of the uranyl oxide hydrate phases metaschoepite, compreignacite, Na–compreignacite, becquerelite, and clarkeite. *J. Chem. Thermodyn.* **2008,** *40*, (6), 980-990.

40. Chernorukov, N.; Nipruk, O.; Knyazev, A.; Pykhova, Y. P., Synthesis and study of uranyl arsenate $(UO_2)_3(AsO_4)_2 \cdot 12H_2O$. *Russ. J. Inorg. Chem.* **2011,** *56*, (2), 163-167.

41. Gezahegne, W. A.; Hennig, C.; Tsushima, S.; Planer-Friedrich, B.; Scheinost, A. C.; Merkel, B. J., EXAFS and DFT investigations of uranyl arsenate complexes in aqueous solution. *Environ. Sci. Technol.* **2012,** *46*, (4), 2228-2233.

42. He, M.; Liu, X.; Cheng, J.; Lu, X.; Zhang, C.; Wang, R., Uranyl arsenate complexes in aqueous solution: Insights from first-principles molecular dynamics simulations. *Inorg. Chem.* **2018,** *57*, (10), 5801-5809.

43. Rutsch, M.; Geipel, G.; Brendler, V.; Bernhard, G.; Nitsche, H., Interaction of uranium(VI) with arsenate(V) in aqueous solution studied by time-resolved laser-induced fluorescence spectroscopy (TRLFS). In *Radiochim. Acta*, 1999; Vol. 86, p 135.

44. Johnson, D. B.; Hallberg, K. B., Acid mine drainage remediation options: a review. *Sci. Total Environ.* **2005,** *338*, (1), 3-14.

45. Labastida, I.; Armienta, M. A.; Lara-Castro, R. H.; Aguayo, A.; Cruz, O.; Ceniceros, N., Treatment of mining acidic leachates with indigenous limestone, Zimapan Mexico. *J. Hazard. Mater.* **2013,** *262*, 1187-1195.

46. Robbins, E. I.; Cravotta, C. A.; Savela, C. E.; Nord, G. L., Hydrobiogeochemical interactions in 'anoxic' limestone drains for neutralization of acidic mine drainage. *Fuel* **1999,** *78*, (2), 259-270.

47. Dong, W.; Ball, W. P.; Liu, C.; Wang, Z.; Stone, A. T.; Bai, J.; Zachara, J. M., Influence of calcite and dissolved calcium on uranium(VI) sorption to a Hanford subsurface sediment. *Environ. Sci. Technol.* **2005,** *39*, (20), 7949-7955.

48. Gonzalez-Estrella, J.; Meza, I.; Burns, A. J.; Ali, A.-M. S.; Lezama-Pacheco, J. S.; Lichtner, P.; Shaikh, N.; Fendorf, S.; Cerrato, J. M., Effect of bicarbonate, calcium, and pH on the reactivity of As(V) and U(VI) mixtures. *Environ. Sci. Technol.* **2020**.

49. DeVore, C.; Freire, L. R.; Gonzalez-Estrella, J.; Villa, N.; Ali, A. M.; Ducheneaux, C.; Artyushkova, K.; Cerrato, J., Investigation of the effect of microbial processes on arsenic stability in sediments from Cheyenne River, South Dakota, USA. *Abstr. Pap. Am. Chem. Soc.* **2019,** *257*, 1.

50. Kaya, A.; Yukselen, Y., Zeta potential of clay minerals and quartz contaminated by heavy metals. *Can. Geotech. J.* **2005,** *42*, (5), 1280-1289.

51. Alroudhan, A.; Vinogradov, J.; Jackson, M. D., Zeta potential of intact natural limestone: Impact of potential-determining ions Ca, Mg and SO4. *Colloids Surf. A: Physicochem. Eng. Asp.* **2016,** *493*, 83-98.

52. Jie, Z.; Weiqing, W.; Jing, L.; Yang, H.; Qiming, F.; Hong, Z., Fe(III) as an activator for the flotation of spodumene, albite, and quartz minerals. *Miner. Eng.* **2014,** *61*, 16-22.

53. Moldovan, B. J.; Hendry, M. J., Characterizing and Quantifying Controls on Arsenic Solubility over a pH Range of 1−11 in a Uranium Mill-Scale Experiment. *Environ. Sci. Technol.* **2005,** *39*, (13), 4913-4920.

54. Qafoku, N. P.; Zachara, J. M.; Liu, C.; Gassman, P. L.; Qafoku, O. S.; Smith, S. C., Kinetic Desorption and Sorption of U(VI) during Reactive Transport in a Contaminated Hanford Sediment. *Environ. Sci. Technol.* **2005,** *39*, (9), 3157-3165.

55. Rakovan, J.; Reeder, R. J.; Elzinga, E. J.; Cherniak, D. J.; Tait, C. D.; Morris, D. E., Structural Characterization of U(VI) in Apatite by X-ray Absorption Spectroscopy. *Environ. Sci. Technol.* **2002,** *36*, (14), 3114-3117.

56. Moore, R. C.; Szecsody, J.; Rigali, M. J.; Vermuel, V.; Leullen, J. *Assessment of a Hydroxyapatite Permeable Reactive Barrier to Remediate Uranium at the Old Rifle Site Colorado*; United States, 2016; p 9.

57. DeVore, C. L.; El Hayek, E.; Busch, T.; Long, B.; Mann, M.; Rudgers, J. A.; Ali, A.-M. S.; Howard, T.; Spilde, M. N.; Brearley, A.; Ducheneaux, C.; Cerrato, J. M., Arsenic Accumulation in Hydroponically Grown Schizachyrium scoparium (Little Bluestem) Amended with Root-Colonizing Endophytes. *ACS Earth Space Chem.* **2021,** *5*, (6), 1278-1287.

58. Wen Hang, H.; Pan, Z.; Giammar, D.; Li, L., Enhanced uranium immobilization by phosphate amendment under variable geochemical and flow conditions: insights from reactive transport modeling. *Environ. Sci. Technol.* **2018,** *52*, (10), 5841-5850.

59. Pan, Z.; Giammar, D. E.; Mehta, V.; Troyer, L. D.; Catalano, J. G.; Wang, Z., Phosphate-Induced Immobilization of Uranium in Hanford Sediments. *Environ. Sci. Technol.* **2016,** *50*, (24), 13486-13494.

CHAPTER 3. SOLUBILITY AND THERMODYNAMIC INVESTIGATION OF META-AUTUNITE GROUP URANYL ARSENATE SOLIDS WITH MONOVALENT CATIONS SODIUM (NA) AND POTASSIUM (K)

Isabel Meza,[1,2] Jorge Gonzalez-Estrella,[3] Peter C. Burns,[4] Virginia Rodriguez[4], Carmen A. Velasco,[1,2] Ginger Sigmon,[4] Jennifer Szymanowski,[4] Tori Z. Forbes,[5] Lindsey M. Applegate,[5] Abdul-Mehdi S. Ali,[6] Peter Lichtner,[2] and José M. Cerrato[1,2]*

*Corresponding email address: jcerrato@unm.edu

Telephone: (001) (505) 277-0870

Fax: (001) (505) 277-1918

[1] Department of Civil, Construction & Environmental Engineering, MSC01 1070, University of New Mexico, Albuquerque, NM, 87131, USA

[2] Center for Water and the Environment, UNM, Albuquerque, NM, 87131, USA

[3] School of Civil and Environmental Engineering, College of Engineering, Architecture, and Technology, Oklahoma State University, Stillwater, OK, 74078, USA

[4] Department of Civil and Environmental Engineering and Earth Sciences, University of Notre Dame, Notre Dame, Indiana 46556, USA and Department of Chemistry and Biochemistry, University of Notre Dame, Notre Dame, IN, 46556, USA

[5] Department of Chemistry, University of Iowa, Iowa City, IA, 52242, USA

[6] Department of Earth and Planetary Sciences, MSC03 2040, University of New Mexico, Albuquerque, NM, 87131, USA

Abstract.

We investigated the aqueous solubility and thermodynamic properties of meta-autunite group Na and K-bearing uranyl arsenate solids. The measured solubility products (log K_{sp}) for NaUAs and KUAs ranged from -23.50 to -22.96 and -23.87 to -23.38, respectively. These values were confirmed in dissolution and precipitation experiments at equilibrium pH ranging from 1.5 to 3**.** The secondary phase $(UO_2)(H_2AsO_4)_2(H_2O)_{(s)}$ was identified by powder X-ray diffraction in the reacted solids recovered from the KUAs precipitation experiments at pH ranging from 1.5 to 2. Trögerite, $(UO_2)_3(AsO_4)_2 12H_2O_{(s)}$, was identified as a secondary phase in the reacted solids recovered from dissolution and precipitation experiments at pH ranging from 2.6 to 3 for NaUAs. The standard-state enthalpy of formation from the elements ($\Delta H°_{f-el}$) of NaUAs is -3025 ± 22 kJ mol^{-1} and for KUAs is -3000 ± 28 kJ mol^{-1} derived from measurements by drop solution calorimetry. Changes in interlayer bonding associated with the occurrence of hydronium together with Na or K are expected to impact the solubility of NaUAs and KUAs as the linkages between the interstitial complex and the uranyl arsenate sheets are important in determining solubility. This work provides novel thermodynamic information for reactive transport models to interpret and predict the influence of uranyl arsenate solids on soluble concentrations of U and As contaminated waters affected by mining legacy and other anthropogenic activities.

INTRODUCTION

The chemical behavior of uranyl arsenate solids (UAs) is important because they are found within uranium mining operations and have been noted as co-occurring contaminants within drinking water sources.[1-7] Communities near these sites can be impacted by the release of U and As, which is of major concern for public health as both are toxic and carcinogenic.[6, 8, 9] Minerals containing uranium (U) and arsenic (As) occur in the major uranium mines in Key Lake, Saskatchewan, Canada, St. Austell District of Cornwall, England, and in several Southwestern US sites.[5, 10, 11] Even in areas that are not impacted by mining operations, U and As can co-occur naturally in waters and soils in community lands. For instance, the spatial relationship between U and As in Northern Plains was evaluated and both were found elevated in drinking water samples taken from groundwater wells in three regions in North and South Dakota in the proximity of communities.[4] Also, it was noted that there was a spatial correlation of wells containing U and As associated with a flow along a geologic contact; however, the underlying mechanisms enabling the U and As correlation warrant further study.[4] Native American communities near these sites are concerned about the release of toxic U and As levels in their water sources.[7, 12, 13] Therefore, it is crucial to develop a greater understanding of UAs and their behavior in natural waters.

Uranyl arsenates are one of the most diverse chemical groups of U minerals but less characterized than the related phosphate phases.[10, 14] Currently, the International Mineralogical Association lists 36 mineral species that contain both essential U and As.[15] Arsenates and phosphates populate the meta-autunite group ($A^{n+}[(UO_2)(TO_4)]\,(H_2O)$), where A^{n+} is a mono-, di- or trivalent cation; T = P, As) with the same structural topology.[16] This group of minerals contain uranyl ions $[(UO_2)^{2+}]$[17] in square bipyramidal polyhedra linked through equatorial corner-sharing with phosphate or arsenate tetrahedra. This unit then links to neighboring UO_2^{2+} cations to form a 2-D sheet and charge balancing cations [i.e. sodium (Na^+), potassium (K^+), calcium (Ca^{2+})] and

water molecules are located between the U(VI) layers to form the final 3-D crystalline lattice.[6, 10] Arsenate and phosphate-bearing anionic units are generally isostructural, have similar size and charge, precipitate as uranyl minerals at elevated concentrations, and form ternary complexes on surfaces at low concentrations.[6, 18-21] Uranyl phosphates have generally low solubilities ranging from log K_{sp} of -13.17 for uranyl hydrogen phosphate to -49.36 and -50.39 for uranyl orthophosphate.[20, 22] The solubility of $(UO_2)_3(AsO_4)_2 12H_2O$ was measured, but only within heterogenous water-salt systems,[20] and the literature suggests that solubility measurements should be confirmed under both supersaturation and undersaturation.[23, 24] These previous studies indicate that the thermodynamics of UAs need more documentation.[25, 26]

There is incomplete information about the thermodynamic values for UAs containing alkali or alkali-earth cations.[6, 20] The formation of U-As-Ca precipitates has been identified at acidic pH, and that bicarbonate facilitates the dissolution of U, As, Ca-bearing solids at circumneutral pH.[27] A previous study by Dzik et al.[6] provided calorimetry measurements for UAs of the meta-autunite group containing K^+, lithium (Li^+), cesium (Cs^+), strontium (Sr^{2+}), and copper (Cu^{2+})[6] but did not provide solubility values. Additionally, the role of H^+ in the form of hydronium (H_3O^+ substituted with monovalent cations in meta-autunite UAs remains poorly understood.

The objective of this study is to determine the solubility and thermodynamic properties of two uranyl arsenate phases: sodium uranyl arsenate $(Na_{0.5}(H_3O)_{0.5}[(UO_2)(AsO_4)](H_2O)_{2.5(s)}$ (NaUAs) and potassium uranyl arsenate $K_{0.9}[(H_3O)_{0.1}(UO_2)(AsO_4)](H_2O)_{2.5(s)}$ (KUAs). While the inclusion of cations (e.g. Na^+, K^+, Ca^{2+}) in the interlayer region of meta-autunite UAs is widely documented, [6, 28, 29] our understanding about how this substitution affects the solubility of these solids remains limited.

The novelty of this investigation is the identification of the impact of monovalent cations such as Na^+, K^+, and H_3O^+ on the solubility of UAs at acidic pH using various aqueous chemistry, solid-state chemistry, thermodynamic techniques, and speciation calculations. This knowledge informs understanding of U and As mobility in the environment, expanding on the limited existing data related to the solubility of uranyl arsenate solids and minerals. The results from this study will develop reliable and internally consistent thermodynamic data to be incorporated into reactive transport models.

3.1. Materials and methods

3.1.1. Synthesis.

Uranyl arsenate solids (NaUAs and KUAs) were synthesized at room temperature over the course of one to two weeks by the slow mixing of reactants emerging from two vials inside of a barrier solution in a beaker as described by Dzik et al.[10] This method is known for providing high quality, purity, and yield of the material required for calorimetric measurements. Additional details describing this synthesis process are included in the Supplementary Information (see additional materials and methods and Table S1 in SI).

3.1.2. Analytical Methods.

Powder X-ray diffraction (p-XRD), electron microprobe analysis, scanning electron microscopy (SEM), energy dispersive X-ray spectroscopy (EDS), and thermogravimetric analyses (TGA) were used with the unreacted and reacted solids. The soluble concentrations of U, As, Na and K in solution were measured using inductively coupled plasma optical emission spectrometry (ICP-OES) and inductively coupled plasma mass spectrometry (ICP-MS). Acid digestions were conducted to assess the acid extractable elements from the synthesized solids. The acid digestions involved ~1 mL of nitric acid and 2 mL of hydrochloric acid. Additional details describing the

solution analyses are included in the Supplementary Information. Additional details describing the solid analyses are included in the Supplementary Information (Figures S1-S4 in SI).

3.1.3. Solubility experiments.

All solubility measurements were conducted in batch reactors at 25°C using Teflon Nalgene® bottles for days (d) reaction time. A Thermo Orion Ross pH micro electrode was used for pH measurements and was calibrated daily with 3 NIST standard solutions (pH 4, 7, and 10). All experiments were conducted in triplicate (n=3) at initial acidic pH ranging from 1.5 to 3, and using a ratio of 1.4 in terms of mass of each uranyl arsenate solid and mass of 18 MΩ H_2O (e.g., ~40 mg of NaUAs in 28 mL of water which can dissolve into ~690 mg L^{-1} of U and 217 mg L^{-1} of As). The conversion of volume of water to mass was conducted by assuming that the density of water was 997 g L^{-1}.[30] Two types of experiments were performed to accurately evaluate the solubility of the NaUAs and KUAs solids. The first type was a dissolution experiment whereby UAs (NaUAs or KUAs) were added first to the vial and then the 18 MΩ H_2O. The second type was a precipitation experiment where besides the UAs and 18 MΩ H_2O, Na or K, As, and U were added as $NaNO_3$ or KNO_3, $(NO_3)_2(H_2O)_6$, As_2O_5, and UO_2, respectively in that order. For the precipitation experiments carried out at pH ranging from 1.5 to 2, the initial concentration was ~2.7 mM of U, As, Na for the assays amended with NaUAs and ~2.5 mM of U, As, and K for the assays amended with KUAs. Chemical equilibrium modeling determined higher saturation indices at pH values ranging from 2.6-3 compared to those obtained at pH 1.5 to 2. Thus, for the precipitation experiments carried out at pH ranging from 2.6 to 3, the initial concentration was ~1.5 mM of U, As, Na, and K for the assays amended either with NaUAs and KUAs. We determined that precipitation occurred if at least one of the final concentrations of U, As, or Na decreased from the starting values.

The pH ranging from 1.5 to 3 was chosen because the chemical speciation of U and As is well-constrained at low pH. For example, chemical equilibrium modeling indicates that UO_2^{2+} is the predominant species of U, while H_3AsO_4 and $H_2AsO_4^{1-}$ are the predominant species of As with limited influence of the carbonate system (i.e., carbonic acid is predominant at this acidic pH). We attempted to make a solution at pH 4, but the pH stabilized in the proximity of 3 so decided to stay in the acidic range from 1.5 to 3. To adjust the pH ranging from 1.5 to 2 and from 2.6 to 3 of each experiment solution, a small quantity of concentrated HNO_3 was used. The pH was set initially at the target value and monitored daily, after the UAs and the additions were already in the reactors, and no adjustment of the pH was necessary over the 30 d.

Throughout the two different types of experiments, batch reactors were sealed and agitated at 60 rpm in an analog rotisserie tube rotator (Scologex MX-RL-E, Rocky Hill, CT, US) at room temperature. Aliquots of the solution were extracted at various times (0 min, 15 min, 30 min, 60 min, 120 min, 4 h, 6 h, 8 h, 12 h, 24 h, 8 d, 15 d, 22 d, 31 d), filtered through 0.1 μm MilliporeSigma Millex filters, and diluted for ICP-OES or MS analyses to determine dissolved concentrations of U, As, and Na or K. One control reactor was used with the dissolution experiments, where no aliquots were withdrawn during the 30 d, to validate that the withdrawal of aliquots did not change the dissolved concentrations of the elements. To verify the composition of the remaining solid at the end of each experiment, ~20 mg of reacted material was collected for p-XRD analysis of reacted solid samples.

3.1.4. Thermodynamic modeling.

Calculations were carried out using the open-source computer code PFLOTRAN that runs on MacOSX, Linux, and Windows.[31] PFLOTRAN applies the law of mass action to obtain the aqueous species complexes as a function of he free ion concentrations. Table 1 shows the reaction stoichiometry used for each uranyl arsenate solid in the log K_{sp} calculations. Solubility product calculations were only performed using data points that corresponded to samples taken from each batch reactor after they had achieved equilibrium (using the average concentration values calculated over a ± 10% interval during 30 d). Once the dissolution and precipitation experiments were completed, we were able to verify if equilibrium was reached in these experiments. The measured U, As, Na, and K concentrations and pH values at equilibrium used for the log K_{sp} speciation calculations are listed in the Supporting Information Table S2 in SI. Table S3 in SI shows the speciation equations and thermodynamic relations that are described below in detail. For each solubility value, we calculated the ionic strength of the solution (I) using Table S3, Eq. 5 in SI. We used the Debye-Hückel algorithm to correct the concentrations (valid for ionic strength lower than 0.1 M) described in Table S3, Eq. 6 in SI.

To obtain the log K_{sp} we used Table S3, Eq. 4 in SI, the mineral law of mass action equation, a function of the free ion concentrations of the primary species including the pH. From the experimental total concentrations (from solubility experiments) at equilibrium $\left(C_j^{tot}\right)$ using Table S3, Eq. 3, we obtained the primary (C_j) and secondary (C_i) species concentrations. Then, using the mass action equation (Table S3, Eq. 4 in SI) corresponding to the concentrations obtained from a speciation calculation, the saturation index (*SI*) was calculated (Table S3, Eq. 8 in SI). From the value obtained for the *SI*, we subsequently adjusted the solubility product constant (log K_{sp}) by the log *SI* so that the log *SI* = 0 was achieved (log K_{sp} = log K_{sp} - log *SI*).

Standard states used in this research for solid phases and for H_2O are the pure mineral or fluid at the temperature and pressure of the experiments. Molal activity coefficients of neutral aqueous species are assumed to be unity. The thermodynamic database (Thermochemie V10a.dat)[32] used by PFLOTRAN was expanded to include K_{sp} values from Gorman-Lewis et al.[24] and from Nipruk et al.[20] and includes the most recent update to U aqueous complexes, for example those presented in Rutsch et al.: $UO_2H_2AsO_4^+$, $UO_2(H_2AsO_4)_2$, and UO_2HAsO_4 (Table S4 in SI).[25, 33-36]

3.1.5. High-temperature oxide-melt calorimetry.

A Setaram Alexsys high-temperature oxide-melt calorimeter was used to measure drop solution enthalpies of NaUAs and KUAs. Calorimetric techniques and experimental details can be found in existing literature.[37-40] The calorimeter was calibrated using the heat content of Al_2O_3. The calorimeter was flushed with high purity O_2 for the duration of the experiment to remove moisture from the environment. The samples were initially ground and then pressed into ~5mg pellets and accurately weighed before the drop. The pellets were then dropped from room temperature into the calorimeter, which contained a sodium molybdate ($3Na_2O•4MO_3$) solvent that was equilibrated at 976 K. Each experiment was performed over the course of approximately 75 min, and the experiments for which the baseline stabilized after collection were used for data analysis. Enthalpy of the drop solution (ΔH°_{ds}) was obtained as an average of each experiment. Thermocycles were then used to calculate the enthalpy of formation of both the oxide and element species.

The calculated log K_{sp} value for each uranyl arsenate solid was used to determine the state Gibbs free energy of formation (ΔG°_f) starting with the standard state Gibbs free energy of reaction (ΔG°_r) for each dissolution reaction of interest (Table S3, Eqs. 9 and 10 in SI). Using the enthalpy

of formation from elements ($\Delta H°_{f-el}$) and $\Delta G°_f$, the standard-state entropy of formation ($\Delta S°_f$) can be calculated (Table S3, Eq. 11 in SI). The $\Delta S°_f$ was obtained using Table S3 Eqs. 9 and 10 in SI with the $\Delta H°_{f-el}$[22] and with the values obtained from Cox et al.[41] and Nordstrom et al.[42] that are: $\Delta G°_{f(H_2O)}$= -237.14; $\Delta G°_{f(UO_2^{2+})}$ = -952.55; $\Delta G°_{f(AsO_4^{3-})}$= -646.36; $\Delta G°_{f(Na^+)}$ = -261.95 in kJ mol^{-1}.

3.2. Results and discussion

3.2.1. Stoichiometry of NaUAs$_{(s)}$ and KUAs$_{(s)}$.

The p-XRD diffraction patterns of NaUAs and KUAs exhibit sharp profiles and all peaks are assignable to the target phase, confirming the identity of NaUAs and KUAs (Figure S1 in SI). The mass loss over 30-170°C of 9% was attributed to the water contained in each compound (Figure S2 in SI). The stoichiometries of NaUAs and KUAs were obtained integrating p-XRD, microprobe analyses, and acid digestions, yielding the following results for NaUAs and KUAs compositions:

NaUAs = $Na_{0.5}(H_3O)_{0.5}[(UO_2)(AsO_4)](H_2O)_{2.5(s)}$

KUAs = $K_{0.9}(H_3O)_{0.1}[(UO_2)(AsO_4)](H_2O)_{2.5(s)}$

Microprobe analyses indicate that NaUAs has an alkali cation deficiency with a ≈0.5:1 Na:U molecular ratio; a close to equimolar ratio between 1.1:1 to 1.2:1 for As:U was obtained for NaUAs and KUAs. Chemical analyses of acid digestions using ICP-OES (Table S5 in SI) confirm the stoichiometry of NaUAs. Close to equimolar ratio between ≈0.9:1:1 for K:U:As was obtained with microprobe analyses and p-XRD for KUAs (Table S5 in SI).

The chemical analyses and p-XRD indicate that a single phase of NaUAs and KUAs solid was obtained using the diffusion method described above. Single phase crystals of uranyl arsenates of

the meta-autunite group with mono and divalent cations have also been identified in previous studies after synthesis using the same method.[6, 28] The discrepancy between microprobe and acid digestion analyses for KUAs is attributed to instability of the compound during electron beam irradiation, as is typical for similar compounds under the microprobe beam.[43]

The chemical analysis of both compounds NaUAs and KUAs indicate substitution of H_3O^+ for K^+ or Na^+ in the interlayer region of the structures. Compounds like uranospinite and chernikovite are examples of this substitution. The hydronium-bearing analog of uranospinite, $(H_3O)_2[(UO_2)_2(AsO_4)_2](H_2O)_8$, has been documented.[46] Chernikovite is a well-characterized H_3O^+-bearing autunite-structure compound with composition $(H_3O)_2[(UO_2)_2(PO_4)_2](H_2O)_n$, and a hydronium-$K^+$ solid-solution series has been noted in this uranyl phosphate system.[44, 45] Hydronium substitution for various monovalent cations in autunite-type uranyl compounds has also been documented.[46-48] Furthermore, a reported single-crystal structure determination for KUAs assigned with the formula $K_{0.91}(H_3O)_{0.09}[(UO_2)(AsO_4)](H_2O)_3$,[28] similar to that derived in the current study.

3.2.2. Dissolution and precipitation experiments.

The results for the NaUAs and KUAs dissolution and precipitation experiments conducted in this study confirmed that equilibrium was reached within 2 d **(**Figures 1, and S3, S4 in SI), well under the 30 d duration of the experiments. The concentrations at equilibrium were obtained using average values calculated over a ± 10% interval (Table S2 in SI). The equilibrium concentrations of U and As obtained for all dissolution experiments with NaUAs and KUAs at pH ranging from 1.5 to 2 are close to equimolar (Figures 1a and 1e).

The molar ratios of U:As:Na 1:1:0.72 were measured after the dissolution of NaUAs in aqueous solutions with pH ranging from 1.5 to 2 (Figures 1a and S3a in SI). In contrast, in

precipitation experiments the molar ratios of U:As:Na were 1:1:1.15 in solutions with pH ranging from 1.5 to 2 (Figures 1b and S3b in SI). Both results are consistent with incorporation of H_3O^+ in NaUAs. X-ray diffraction analysis of residual solids in each case indicated NaUAs was the only phase present (Figure S5 in SI).

Upon dissolution of KUAs in aqueous solutions with pH ranging from 1.5 to 2, at equilibrium the molar ratios of U:As:K were 1:0.97:0.99 (Figures 1e and S4a in SI). However, precipitation reactions in solutions with pH ranging from 1.5 to 2 yielded an elevated K concentration relative to U and As (Figure 1f and Figure S4b in SI). Powder X-ray diffraction analyses of the recovered solids in this case revealed the presence of $(UO_2)(H_2AsO_4)_2(H_2O)_{(s)}$[26, 49] (Figure 2B). This observation suggests that the secondary phase of $(UO_2)(H_2AsO_4)_2(H_2O)_{(s)}$ could have caused lower concentrations of U and As compared to K in the precipitation experiments with KUAs. Additionally, this phase could have influenced the chemical equilibrium and kinetics of the reactions affecting KUAs solubility. More research is needed to better understand the influence of secondary phases on soluble U and As concentration in solution at acidic pH.

For both NaUAs and KUAs experiments in aqueous solution with pH in the range of 2.6 to 3, the concentrations of U and As in solution was up to 93% lower than observed in solutions with pH ranging from 1.5 to 2 (Figures 1a, 1c, 1e, 1g, and S3a, S3c, S4a, S4c in SI). The aqueous solutions in precipitation experiments at pH from 2.6 to 3 contained from 65 to 97% less soluble U and As as compared to experiments for pH ranging from 1.5 to 2 (Figures 1b, 1d, 1f, 1h, and S3b, S3d, S4b, S4d in SI). Under the conditions studied, KUAs was found to be less soluble than NaUAs. For example, the concentration of U and As in solution in contact with KUAs was 22.6% lower as compared to NaUAs in dissolution experiments at pH ranging from 1.5 to 2. Likewise, U and As concentrations in contact with KUAs were 15.38% and 86.3% lower, respectively,

compared to the NaUAs system in dissolution experiments at pH ranging 2.6 to 3 (Figures 1a, 1c, 1e, 1g, and S3a, S3c, S4a, S4c in SI).

The changes in soluble U and As concentration in solution as a function of pH could also be affected by the formation of secondary phases. The secondary phase trögerite $(UO_2)_3(AsO_4)_2 12H_2O_{(s)}$,[20, 50] was present in the solids recovered from dissolution and precipitation experiments with NaUAs in solutions with pH ranging from 2.6 to 3. This indicates that the solubility is not only controlled by NaUAs, but also by trögerite in these pH conditions (Figure 2A(a-d)). X-ray diffraction analysis of residual solids from dissolution and precipitation experiments in this pH confirmed that KUAs was the only phase present (Figure S6 in SI). The presence of $(UO_2)(H_2AsO_4)_2(H_2O)_{(s)}$ was not detected by p-XRD in these experiments. However, XRD is not a trace technique, therefore, the presence of this phase at a concentration below the detection of this instrument cannot be discarded.

Application of the species name trögerite is inconsistent in the literature. The International Mineralogical Association states its formula is $(H_3O)(UO_2)(AsO_4)\cdot 3H_2O$ and attributes this to a publication from 1871.[51] The same formula appears several times in the literature associated with the name trögerite over the years, and Locock and Burns listed trögerite with this formula along with autunite-group minerals, implying that it has the autunite-type structure.[52] Chernorukov et al. referred to the compound $(UO_2)_3(AsO_4)_2 12H_2O$ as trögerite and argued that this composition likely corresponds to the natural mineral.[50] It is likely that the name trögerite has been applied to more than one mineral species in the literature. Herein, we equate trögerite with $(UO_2)_3(AsO_4)_2 12H_2O$ according to Chernorukov et al.[50] Although the crystal structure of this phase has not been determined, it is clearly not an autunite-group mineral as the different U:As ratio mandates a different structural connectivity.

3.2.3. Solubility product measurements.

The log K_{sp} obtained using the concentrations at equilibrium from the solubility experiments in speciation calculations using PFLOTRAN ranged from -23.50 to -22.96 for NaUAs, and from -23.87 to -23.38 for KUAs. We based our calculations on the dissolution and precipitation experiments (Tables 1, and S6, S7 in SI). The obtained log K_{sp} for NaUAs and KUAs are within one order of magnitude and with a maximum difference of 3.4% between dissolution and precipitation experiments at pH ranging from 1.5 to 2 and 2.6 to 3. Thus, the log K_{sp} for NaUAs and KUAs is independent of pH within experimental error by both dissolution and precipitation experiments within experimental error (Table 1).

The solubility product obtained for NaUAs at pH ranging from 1.5 to 2 was within one order of magnitude compared to the pH ranging from 2.6 to 3 (Table 1). However, the solubility of U and As in dissolution and precipitation experiments at pH 2.6 to 3 was controlled by NaUAs and the secondary phase trögerite. We estimated a log K_{sp} for trögerite of -47.97 at dissolution and at pH ranging from 2.6 to 3, which is within two orders of magnitude of the value reported in a previous study of -45.93[20] (Table 1).

The solubility product obtained for KUAs at pH ranging from 1.5 to 2 was within one order of magnitude compared to the pH ranging from 2.6 to 3 (Table 1). However, the solubility of U and As in precipitation experiments at pH ranging from 1.5 to 2 was controlled by KUAs and the secondary phase $(UO_2)(H_2AsO_4)_2(H_2O)_{(s)}$. We also estimated a log K_{sp} for $(UO_2)(H_2AsO_4)_2(H_2O)_{(s)}$ of -46.97 (Table 1) for precipitation and for pH ranging from 1.5 to 2 which is within one order of magnitude of the log K_{sp} from trögerite reported in a previously indicated study.[20]

The log K_{sp} obtained for NaUAs was not sensitive to the deficiency of Na in the stoichiometry of this solid. For example, we varied the stoichiometry of Na to estimate the log K_{sp} for NaUAs using Na molarities of 0.25, 0.48, 0.7, and 1. The log K_{sp} values for varying Na stoichiometries were within 2.8% using the equilibrium concentrations in dissolution and precipitation experiments for pH ranging from 1.5 to 2 and 2.6 to 3 (Table S6 in SI).

The log K_{sp} values calculated with and without uranyl arsenate aqueous complexes for NaUAs and KUAs are within the same order of magnitude. For example, the corresponding log K_{sp} are within 2.66% for NaUAs and KUAs for the dissolution experiments with pH ranging from 1.5 to 2 and 2.6 to 3 (Tables 1, S6-S8 in SI). The uranyl arsenate complexes predominant at acidic pH are: $UO_2(H_2AsO_4)(H_2O)^{3+}$, $(UO_2)_3(AsO_4)_2{\cdot}4H_2O$, $(UO_2)_3(AsO_4)_2{\cdot}12H_2O$, $UO_2H_2AsO_4^+$, $UO_2(HAsO_4)$, and $UO_2(H_2AsO_4)_2$.[20, 25, 49] We considered all of these uranyl arsenate complexes in the PFLOTRAN simulations to estimate the log K_{sp} values reported in this study (Tables 1, and S6, S7 in SI). All the main input species considered for the PFLOTRAN simulations conducted in this study are reported in Table S4 in SI. The log K_{sp} values in this study that did not consider the aqueous uranyl arsenate complexes in the PFLOTRAN simulations are reported in Table S8 in SI. Our log K_{sp} values are within close range of those reported in previous studies in which the log K_{sp} for $NaAsUO_6{\cdot}3H_2O$ was -21.86 and for $KAsUO_6{\cdot}3H_2O$ was -22.65[21, 53, 54]. However, aqueous uranyl arsenate complexes were not considered in the determination of the log K_{sp} values reported in these studies.[21, 53, 54]

3.2.4. Standard-state enthalpy (ΔH°_f), Gibbs free energy (ΔG°_f), and entropy of formation (ΔS°_f).

High temperature oxide melt calorimetry was used to determine the enthalpy of formation for NaUAs and KUAs. The measured enthalpies of drop solution for each compound can be found in Table S9 in SI and the relevant calorimetric cycles are in Table 2 for NaUAs and KUAs. The

calculated standard enthalpies of formation from the oxides ($\Delta H°_{f-ox}$) are -305.4 ± 22.0 and -436.4 ± 28.0 kJ mol^{-1} for NaUAs, and KUAs, respectively. Calculated $\Delta H°_{f-el}$ are -3025 ± 22 and -3000 ± 28 kJ mol^{-1} for NaUAs and KUAs, respectively.

Dzik et al.[6] provided high-temperature calorimetric measurements for a series of uranyl arsenate phases with alkali, alkali-earth, and transition metal cations present in the interlayer. Their study suggested an overall stoichiometry for the KUAs phase of $K_{0.87}[(UO_2)(AsO_4)_{1.05}]\bullet 3H_2O$ with $\Delta H°_{f-ox}$ and $\Delta H°_{f-el}$ values of -363.7 ± 14.1 and -3089 ± 14 kJ mol^{-1}, respectively.[6] We note that in their study they assumed an overall formula $K[(UO_2)(AsO_4)_{1.05}]\bullet 3H_2O$, and did not include additional hydronium to charge-balance the structure. The previous work, from Dzik et al.,[6] evaluated the relationship between the $\Delta H°_{f-ox}$ and the acidity of the cation present in the interlayer (derived from the acidity value of the metal oxide) and found it to be linear (R^2 = 0.8571)[6]. With the data presented herein, we observe a similar relationship between the $\Delta H°_{f-ox}$ and the acidity, and an improved fit once additional hydronium is included (R^2 = 0.9549) (Figure S11 in SI). These data indicate that as the metal cation becomes more acidic, the enthalpy of formation for the uranyl arsenates becomes less exothermic. This relationship between the metal cation acidity and the enthalpy of formation has also been reported[40] for uranyl oxyhydroxide and uranyl silicate phases (Figure 3). The slopes for uranyl arsenates were steeper compared to the silicate and oxyhydroxide phases (Figure 3), suggesting a larger interaction between the uranyl arsenate sheet and the interstitial cations compared to that of the silicate and oxyhydroxide phases.

The modeled values for $\Delta G°_f$ NaUAs are -2456.8 kJ mol^{-1} at pH ranging from 1.5 to 2 and -2455 kJ mol^{-1} for pH ranging from 2.6 to 3. The modeled values for $\Delta G°_f$ KUAs are -2582 kJ mol^{-1} for pH ranging from 1.5 to 2 and -2581 kJ mol^{-1} for pH ranging from 2.6. to 3. The $\Delta S°_f$

NaUAs are -1907 J mol^{-1} K^{-1} at pH ranging from 1.5 to 2 and -1913 J mol^{-1} K^{-1} for pH ranging from 2.6 to 3. The $\Delta S°_f$ modeled values for KUAs are -1401 J mol^{-1} K^{-1} for pH ranging from 1.5 to 2 and -1407 J mol^{-1} K^{-1} for pH ranging from 2.6. to 3 (Table 3). Our results are similar to those found in a previous study for uranyl hydrogen phosphate.[22]

3.3. Insights about solubility of uranyl arsenate solids.

The solubility values indicate that lower concentrations of U and As were detected for the dissolution of KUAs relative to NaUAs at pH 1.5 to 3. Incorporation of K^+ in the interlayer of uranyl arsenates presumably reduces solubility relative to Na^+. Instead, the substitution of cations are known to impact the number of H_2O molecules in the interlayer of UAs.[21] Uranium and As form anionic two-dimensional layers of the type $[P(As)UO_6]^{n-}{}_{2\infty}$ known by an increased stability.[21] For instance, the role of hydronium in the UAs structure needs to be further understood.

The occurrence of hydronium $(H_3O)^+$ in the interlayer region of compounds containing uranyl phosphate and arsenate sheets with the autunite topology is lacking an understanding of the details of the substitution of hydronium for other monovalent cations in the interlayers of autunite-structure compounds. In the case of autunite-structure compounds, the importance of hydronium is well established. The structure of the hydronium endmember compound $(H_3O)[(UO_2)(PO_4)](H_2O)_3$ was reported by Morosin et al. and is a hydrogen ion solid electrolyte.[55] The structure of $(H_3O)[(UO_2)(AsO_4)](H_2O)_3$ was determined more recently, including the location of the H atoms corresponding to the hydronium ions.[56] Earlier determinations of the structures of autunite compounds containing monovalent cations also noted the presence of hydronium.[28] However, we are missing more information about the substitution of hydronium for monovalent cations in the interlayers of autunite-structure compounds, as hydronium is rare in mineral structures, and it is challenging to identify it.

The presence of hydronium is difficult to directly demonstrate by spectroscopy, and in the case of chemically well-characterized materials, its presence can be demonstrated by the electroneutrality principle. Locally in the interlayer region hydronium could substitute for a H_2O group or a monovalent cation, or the H atom may be largely mobile, which is consistent with the compound $(H_3O)[(UO_2)(PO_4)](H_2O)_3$ that exhibits rapid H^+ ion conductivity.[57] In the current case, the hydronium ion content was determined by establishing the composition of the compounds by chemical analyses, with hydronium assumed for charge-balance.

The presence of trögerite in the residual solids may relate to the role of H_3O^+ substitution in NaUAs used in the dissolution experiments at pH 2.6 to 3. Trögerite was also confirmed in precipitation experiments with NaUAs at pH 2.6 to 3. Formation of trögerite influences the soluble U and As concentration in solution and also the pH of the solution that has been found to be in the range of 3 as indicated in another study.[50]

The aqueous speciation of U, As, Na, and K influences the dissolution and precipitation reactions for the determination of the log K_{sp} of NaUAs and KUAs solids. For example, the formation of uranyl arsenate complexes has been reported in the literature and cannot be ignored in the determination of the solubility constants. According to the literature, at pH 2 and 3, U(VI) will be present as UO_2^{2+}, while As(V) at pH 2 and 3 could be present as 50% to 75% of H_3AsO_4 and $H_2AsO_4^{1-}$, and Na could be a free ion Na^{1+}.[58] However, we considered other aqueous complexes in the dissolution reactions with the PFLOTRAN modeling such as $UO_2H_2AsO_4^{+}{}_{(aq)}$, $UO_2HAsO_{4(aq)}$, and $UO_2(H_2AsO_4)_2$. [25, 49,] The log K_{sp} was not sensitive to these aqueous uranyl complexes as they differed only between 2.06 to 2.43%. Future research is necessary to determine how aqueous uranyl arsenate complexes influence aqueous speciation of U and As as a function of pH.

3.4. Environmental Implications.

The solubility and thermodynamic data obtained for NaUAs and KUAs in this study contribute new information that will underpin prediction of U and As dissolution using chemical equilibrium and reactive transport models. Additionally, our findings show that different charge-balancing cations between the uranyl arsenate sheets do not notoriously change the log K_{sp}. The thermodynamic variables obtained can be used in reactive transport models to interpret and predict the solubility of U and As. The findings from this study can be useful for risk assessment and risk reduction studies where anthropogenic activities such as mining and nuclear weapons development have resulted in contamination.

3.5. Acknowledgments

Funding for this research was provided by the National Science Foundation (CAREER Award 1652619, CREST Award 1914490) and the National Institute of Environmental Health Sciences (Superfund Research Program Award 1 P42 ES025589 and R01ES027145). PCB´s contribution to this work was funded by the Chemical Sciences, Geosciences and Biosciences Division, Office of Basic Energy Sciences, Office of Science, U.S. Department of Energy, Grant No. DE-FG02–07ER15880. Any opinions, findings, and conclusions or recommendations expressed in this publication are those of the author(s) and do not necessarily reflect the views of the National Science Foundation, the National Institutes of Health, or the U.S. Department of Energy. The TOC art was created with www.BioRender.com.

Supporting information.

Additional materials and methods (Text S1, S2, and S3), 9 tables (Table S1, S2, S3, S4, S4, S5, S6, S7, S8, and S9), and 7 figures (Figures S1, S2, S3, S4, S4, S5, S6, S7) are available in SI.

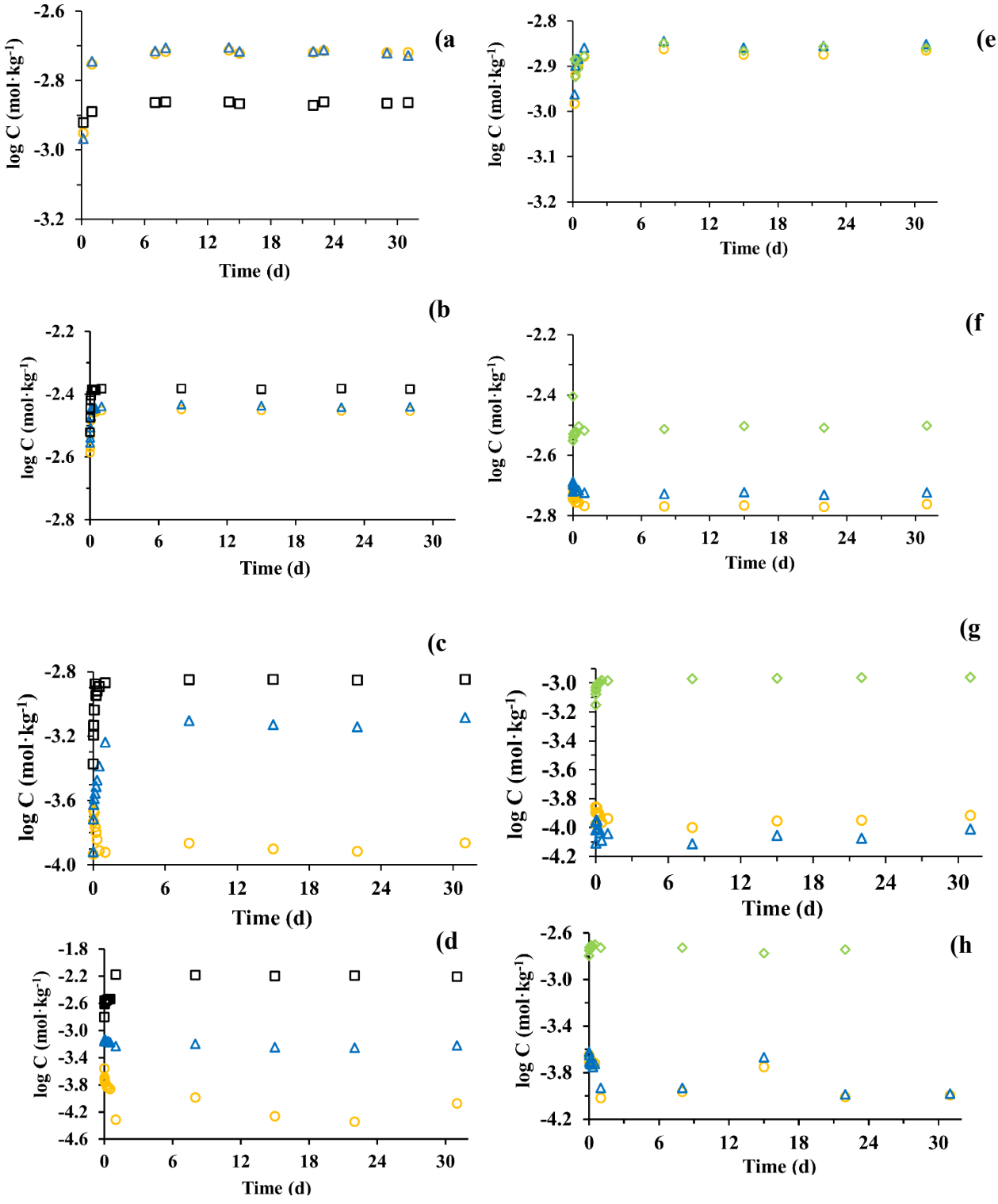

Figure 1. Experimental measurements of the dissolved concentrations of U (circles), As (triangles), Na (squares), and K (diamonds) as log mol·kg-1 against time for NaUAs for dissolution (a), precipitation (b) at pH 1.5 to 2, dissolution (c), precipitation experiments (d) at pH 2.6 to 3; for KUAs for dissolution (e), precipitation (f) at pH 1.5 to 2, dissolution (g), and precipitation experiments (h) at pH 2.6 to 3.

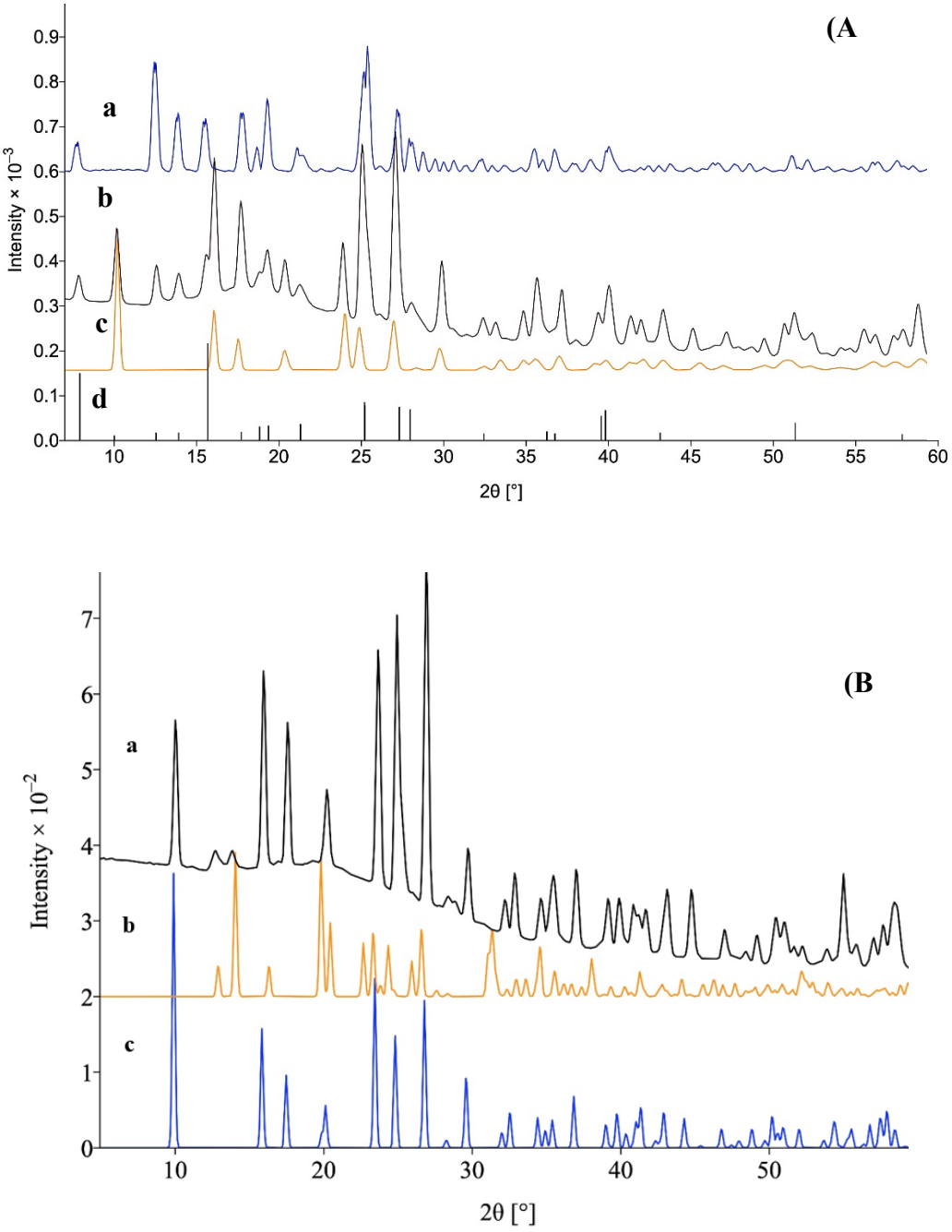

Figure 2. A) Powder X-ray diffraction patterns of synthetic $Na[(UO_2)(AsO_4)](H_2O)_3$ reacted material from dissolution (a) and precipitation experiments (b) pH range 2.7 to 3, compared to sodium uranyl arsenate (c) and trögerite (d). B) Powder X-ray diffraction patterns of KUAs reacted material (a) compared to $(UO_2)(H_2AsO_4)_2(H_2O)_{(s)}$ (b) and potassium uranyl arsenate (c).

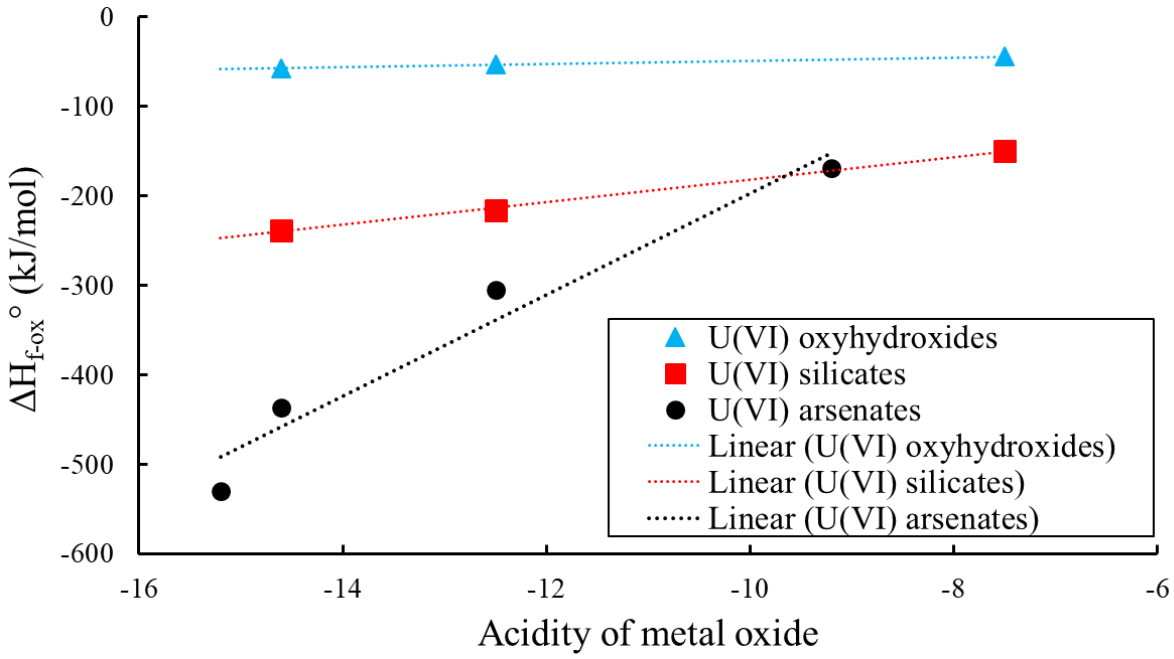

Figure 3. Plot of the standard enthalpy of formation from the oxides ($\Delta \boldsymbol{H}^{\circ}_{\boldsymbol{f-ox}}$) for uranyl oxyhydroxides, silicates, and arsenates versus the acidity of the alkali metal oxide. Data for the U(VI) oxyhydroxide and silicates taken from Shvareva *et al*.[40]

Table 1. Reaction Stoichiometry. All the calculations of log Ksp values consider uranyl-arsenate complexes.

Experimental pH range	Mineral phase	Mineral reaction	Mass action equations	Log K_{sp} at dissolution	Log K_{sp} at precipitation
1.5 to 2	**NaUAs**	$Na_{0.5}(H_3O)_{0.5}(UO_2)(AsO_4)(H_2O)_{2.5(s)} \leftrightarrow (AsO_4)^{3-}+(UO_2)^{2+}+0.5Na^{+}+0.5(H_3O)^{+}+2.5H_2O$	$\boldsymbol{K_{sp}}=\boldsymbol{a}(UO_2)^{2+}\cdot\boldsymbol{a}(AsO_4)^{3-}\cdot\boldsymbol{a}^{0.5}(H_3O)^{+}\cdot\boldsymbol{a}^{0.5}Na^{+}\cdot$	-23.50	-22.96
2.6 to 3	**NaUAs** +	$Na_{0.5}(H_3O)_{0.5}(UO_2)(AsO_4)(H_2O)_{2.5(s)} \leftrightarrow (AsO_4)^{3-}+(UO_2)^{2+}+0.5Na^{+}+0.5(H_3O)^{+}+2.5H_2O$		-23.15	-23.15
	Trögerite $(UO_2)_3(AsO_4)_2\cdot 12H_2O_{(s)}$	$(UO_2)_3(AsO_4)_2\cdot 12H_2O_{(s)} \leftrightarrow 2(AsO_4)^{3-}+3(UO_2)^{2+}+12H_2O$	$\boldsymbol{K_{sp}}=\boldsymbol{a}^{3}(UO_2)^{2+}\cdot\boldsymbol{a}^{2}(AsO_4)^{3-}$	-47.97 -45.33[a]	-48.85 --
1.5 to 2	**KUAs** +	$K_{0.9}(H_3O)_{0.1}(UO_2)(AsO_4)(H_2O)_{2.5(s)} \leftrightarrow (AsO_4)^{3-}+(UO_2)^{2+}+0.9K^{+}+0.1(H_3O)^{+}\,2.5H_2O$	$\boldsymbol{K_{sp}}=\boldsymbol{a}(UO_2)^{2+}\cdot\boldsymbol{a}(AsO_4)^{3-}\cdot\boldsymbol{a}^{0.1}(H_3O)^{+}\cdot\boldsymbol{a}^{0.9}K^{+}$	-23.87	-23.50
	$(UO_2)(H_2AsO_4)_2(H_2O)$	$(UO_2)(H_2AsO_4)_2(H_2O)(s) \leftrightarrow 2(AsO_4)^{3-}+(UO_2)^{2+}+H_2O+4H^{+}$	$\boldsymbol{K_{sp}}=\boldsymbol{a}(UO_2)^{2+}\cdot\boldsymbol{a}^{2}(AsO_4)^{3-}\cdot\boldsymbol{a}^{-4}H^{+}$	-47.19	-46.97
2.6 to 3	**KUAs**	$K_{0.9}(H_3O)_{0.1}(UO_2)(AsO_4)(H_2O)_{2.5(s)} \leftrightarrow (AsO_4)^{3-}+(UO_2)^{2+}+0.9K^{+}+0.1(H_3O)^{+}\,2.5H_2O$	$\boldsymbol{K_{sp}}=\boldsymbol{a}(UO_2)^{2+}\cdot\boldsymbol{a}(AsO_4)^{3-}\cdot\boldsymbol{a}^{0.1}(H_3O)^{+}\cdot\boldsymbol{a}^{0.9}K^{+}$	-23.57	-23.38

[a] log K_{sp} obtained by Chernorukov et al.[34]

Table 2. Thermochemical cycles for calculation of $(\Delta H°_{(f\text{-}ox)})$ and $(\Delta H°)_{(f\text{-}el)}$ for NaUAs and KUAs. [7-12]

Reaction	ΔH	KUAs ΔH (kJ/mol)	NaUAs ΔH (kJ/mol)
$Na_{0.5}(H_3O)_{0.5}[(UO_2)(AsO_4)] \cdot 2.5\ H_2O_{(s,\ 298K)} = 0.25\ Na_2O_{(soln,\ 976K)} + UO_{3\ (soln,\ 976K)} + 0.5\ As_2O_{5\ (s,\ 976K)} + 3.25\ H_2O_{(g,976K)}$	$\Delta H_1 = \Delta H_{ds}$		523.1 ± 21.7
$K_{0.9}(H_3O)_{0.1}[(UO_2)(AsO_4)] \cdot 2.5\ H_2O_{(xl,\ 298K)} = 0.45\ K_2O_{(soln,\ 976K)} + UO_{3\ (soln,\ 976K)} + 0.5\ As_2O_{5\ (soln,\ 976K)} + 2.65\ H_2O_{(g,\ 976K)}$	$\Delta H_1 = \Delta H_{ds}$	523.9 ± 27.8	
$As_2O_{5\ (xl,\ 298K)} = As_2O_{5\ (soln,\ 976K)}$	$\Delta H_2 = \Delta H_{ds}$	76.7 ± 0.8	76.7 ± 0.8
$UO_{3\ (xl,\ 298K)} = UO_{3\ (soln,\ 298K)}$	$\Delta H_3 = \Delta H_{ds}$	9.49 ± 1.53	9.49 ± 1.53
$Na_2O_{(s,\ 298K)} = Na_2O_{(976K)}$	$\Delta H_4 = \Delta H_{ds}$		-217.56 ± 4.25
$K_2O_{(298K)} = K_2O_{(soln,\ 976K)}$	$\Delta H_4 = \Delta H_{ds}$	-318.0 ± 3.1	
$H_2O_{(l,298K)} = H_2O_{(g,\ 976K)}$	$\Delta H_5 = \Delta H_{ds}$	69	69
$0.25\ Na_2O_{(xl,\ 298\ K)} + UO_{3\ (s,\ 298\ K)} + 3.25\ H_2O_{(g,\ 298\ K)} + 0.5\ As_2O_{5\ (s,\ 298\ K)} = Na_{0.5}(H_3O)_{0.5}[(UO_2)(AsO_4)] \cdot 2.5\ H_2O_{(xl,\ 298K)}$	$\Delta H_6 = \Delta H°_{f-ox} = -\Delta H_1 + 0.5\ \Delta H_2 + \Delta H_3 + 0.25\ \Delta H_4 + 3.25\ \Delta H_5$		**-305.4 ± 22.0**
$0.45\ K_2O_{(xl,\ 298K)} + UO_{3\ (xl,\ 298K)} + 2.65\ H_2O_{(g,\ 298K)} + 0.5\ As_2O_5 = K_{0.9}(H_3O)_{0.1}[(UO_2)(AsO_4)] \cdot 2.5\ (H_2O)_{(xl,\ 298K)}$	$\Delta H_6 = \Delta H°_{f-ox} = -\Delta H_1 + 0.5\ \Delta H_2 + \Delta H_3 + 0.45\ \Delta H_4 + 2.65\ \Delta H_5$	**-436.4 ± 28.0**	
$2As_{(s,\ 298K)} + 2.5\ O_{2\ (g,\ 298K)} = As_2O_{5\ (s,\ 298K)}$	$\Delta H_7 = \Delta H°_f$	-926	-926
$U_{(xl,\ 298K)} + 1.5\ O_{2\ (g,\ 298K)} = UO_{3\ (xl,\ 298K)}$	$\Delta H_8 = \Delta H°_f$	-1223.8 ± 0.8	-1223.8 ± 0.8
$2Na_{(298\ K)} + 0.5\ O_{2\ (298\ K)} = Na_2O_{(298\ K)}$	$\Delta H_9 = \Delta H°_f$		-414.8 ± 0.3
$2\ K_{(s,\ 298K)} + 0.5\ O_{2\ (g,\ 298K)} = K_2O_{(s,\ 298K)}$	$\Delta H_9 = \Delta H°_f$	-363.2 ± 2.1	
$H_{2\ (g,\ 298K)} + 0.5\ O_{2\ (g,\ 298K)} = H_2O_{(g,\ 298K)}$	$\Delta H_{10} = \Delta H°_f$	-285.8 ± 0.1	-285.8 ± 0.1
$0.5\ Na_{(xl,\ 298\ K)} + U_{(s,\ 298\ K)} + As_{(g,\ 298\ K)} + 4.5\ O_{2\ (g,\ 298\ K)} + 2.5\ H_{2\ (g,\ 298K)} = Na_{0.5}\ (H_3O)_{0.5}[(UO_2)(AsO_4)] \cdot 2.5\ H_2O_{(xl,\ 298K)}$	$\Delta H_{11} = \Delta H°_{f-el} = \Delta H_6 + 0.5\ \Delta H_7 + \Delta H_8 + 0.25\ \Delta H_9 + 2.5\ \Delta H_{10}$		**-3025 ± 22**
$0.9\ K_{(xl,\ 298K)} + U_{(xl,\ 298K)} + As_{(xl,\ 298K)} + 4.3\ O_{2\ (g,\ 298K)} + 2.65\ H_{2\ (g,298K)} = K_{0.9}(H_3O)_{0.1}[(UO_2)(AsO_4) \cdot 2.5\ H_2O_{(xl,\ 298K)}$	$\Delta H_{11} = \Delta H°_{f-el} = \Delta H_6 + 0.5\ \Delta H_7 + \Delta H_8 + 0.45\ \Delta H_9 + 2.65\ \Delta H_{10}$	**-3000 ± 28**	

Table 3. The calculated enthalpy ($\Delta H°_{(f\text{-}el)}$), Gibbs free energy ($\Delta G°_f$), and entropy ($\Delta S°_f$) for NaUAs and KUAs.

			$(\Delta H°_{f-el})$ (kJ mol^{-1})	$(\Delta G°_f)$ (kJ mol^{-1})	$(\Delta S°_f)$ (J mol^{-1} K^{-1})
1.5 to 2	**NaUAs**	$Na_{0.5}(H_3O)_{0.5}(UO_2)(AsO_4)(H_2O)_{2.5(s)} \leftrightarrow (AsO_4)^{3-}+UO_2^{2+}+0.5Na^{+}+0.5(H_3O)^{+}+2.5H_2O$	-3025 ± 22	-2455	-1907
2.6 to 3				-2455	-1913
1.5 to 2	**KUAs**	$K_{0.9}(H_3O)_{0.1}(UO_2)(AsO_4)(H_2O)_{2.5(s)} \leftrightarrow (AsO_4)^{3-}+(UO_2)^{2+}+0.9K^{+}+0.1(H_3O)^{+}\ 2.5H_2O$	-3000 ± 28	-2582	-1401
2.6 to 3				-2581	-1407

REFERENCES

1. Coyte, R. M.; Vengosh, A., Factors controlling the risks of co-occurrence of the redox-sensitive elements of arsenic, chromium, vanadium, and uranium in groundwater from the eastern United States. *Environ. Sci. Technol.* **2020,** *54*, (7), 4367-4375.

2. Das, N.; Das, A.; Sarma, K. P.; Kumar, M., Provenance, prevalence and health perspective of co-occurrences of arsenic, fluoride and uranium in the aquifers of the Brahmaputra River floodplain. *Chemosphere* **2018,** *194*, 755-772.

3. Yadav, S. K.; Ramanathan, A. L.; Kumar, M.; Chidambaram, S.; Gautam, Y. P.; Tiwari, C., Assessment of arsenic and uranium co-occurrences in groundwater of central Gangetic Plain, Uttar Pradesh, India. *Environ. Earth Sci.* **2020,** *79*, (6), 154.

4. Sobel, M.; Sanchez, T. R.; Zacher, T.; Mailloux, B.; Powers, M.; Yracheta, J.; Harvey, D.; Best, L. G.; Bear, A. B.; Hasan, K.; Thomas, E.; Morgan, C.; Aurand, D.; Ristau, S.; Olmedo, P.; Chen, R.; Rule, A.; O'Leary, M.; Navas-Acien, A.; George, C. M.; Bostick, B., Spatial relationship between well water arsenic and uranium in Northern Plains native lands. *Environ. Pollut.* **2021,** *287*, 117655.

5. Corkhill, C. L.; Crean, D. E.; Bailey, D. J.; Makepeace, C.; Stennett, M. C.; Tappero, R.; Grolimund, D.; Hyatt, N. C., Multi-scale investigation of uranium attenuation by arsenic at an abandoned uranium mine, South Terras. *NPJ Mater. Degrad.* **2017,** *1*, (1), 19.

6. Dzik, E. A.; Lobeck, H. L.; Zhang, L.; Burns, P. C., High-temperature calorimetric measurements of thermodynamic properties of uranyl arsenates of the meta-autunite group. *Chem. Geol.* **2018,** *493*, 353-358.

7. Hoover, J.; Gonzales, M.; Shuey, C.; Barney, Y.; Lewis, J., Elevated arsenic and uranium concentrations in unregulated water sources on the Navajo Nation, USA. *Expos. Health.* **2017,** *9*, (2), 113-124.

8. Hoover, J. H.; Coker, E.; Barney, Y.; Shuey, C.; Lewis, J., Spatial clustering of metal and metalloid mixtures in unregulated water sources on the Navajo Nation – Arizona, New Mexico, and Utah, USA. *Sci. Total Environ.* **2018,** *633*, 1667-1678.

9. Brockgreitens, J. W.; Heidari, F.; Abbas, A., Versatile process for the preparation of nanocomposite sorbents: phosphorus and arsenic removal. *Environ. Sci. Technol.* **2020,** *54*, (14), 9034-9043.

10. Dzik, E. A.; Lobeck, H. L.; Zhang, L.; Burns, P. C., Thermodynamic properties of phosphate members of the meta-autunite group: A high-temperature calorimetric study. *J. Chem. Thermodyn.* **2017,** *114*, 165-171.

11. Blake, J. M.; Avasarala, S.; Ali, A.-M. S.; Spilde, M.; Lezama-Pacheco, J. S.; Latta, D.; Artyushkova, K.; Ilgen, A. G.; Shuey, C.; Nez, C.; Cerrato, J. M., Reactivity of As and U co-occurring in mine wastes in northeastern Arizona. *Chem. Geol.* **2019,** *522*, 26-37.

12. Office, U. S. G. A.; Mittal, A. K., *Abandoned Mines: Information on the Number of Hardrock Mines, Cost of Cleanup, and Value of Financial Assurances: Testimony Before the Subcommittee on Energy and Mineral Resources, Committee on Natural Resources, House of Representativese*. US Government Accountability Office: 2011.

13. Blake, J. M.; Avasarala, S.; Artyushkova, K.; Ali, A.-M. S.; Brearley, A. J.; Shuey, C.; Robinson, W. P.; Nez, C.; Bill, S.; Lewis, J., Elevated concentrations of U and co-occurring metals in abandoned mine wastes in a northeastern Arizona Native American community. *Environ. Sci. Technol.* **2015,** *49*, (14), 8506-8514.

14. Finch, R. M., T., *Systematics and Paragenesis of Uranium Minerals*. Argonne National Laboratory. Mineralogical Institute University of Japan: Argonne National Laboratory. Mineralogical Institute-University of Japan, 1999; Vol. 1, p 87.

15. Miyawaki, R. Commission on new minerals, nomenclature and classification. http://cnmnc.main.jp/ (12/16/2021),

16. Frost, R. L.; Carmody, O.; Erickson, K. L.; Weier, M. L., Near-infrared spectroscopy to uranyl arsenates of the autunite and metaautunite group. *pectrochim. Acta A Mol. Biomol. Spectrosc.* **2005,** *61*, (8), 1923-1927.

17. Burns, P. C.; Sigmon, G. E., *Uranium: cradle to grave*. Mineralogical Association of Canada Winnipeg: 2013; Vol. 43.

18. Troyer, L. D.; Tang, Y.; Borch, T., Simultaneous reduction of arsenic(v) and uranium(vi) by mackinawite: role of uranyl arsenate precipitate formation. *Environ. Sci. Technol.* **2014,** *48*, (24), 14326-14334.

19. Liu, H.-K.; Ramachandran, E.; Chen, Y.-H.; Chang, W.-J.; Lii, K.-H., High-temperature, high-pressure hydrothermal synthesis, characterization, and structural relationships of layered uranyl arsenates. *Inorg. Chem.* **2014,** *53*, (17), 9065-9072.

20. Nipruk, O. V.; Chernorukov, N. G.; Pykhova, Y. P.; Godovanova, N. S.; Eremina, A. A., State of uranyl phosphates and arsenates in aqueous solutions. *Radiochemistry* **2011,** *53*, (5), 483.

21. Chernorukov, N. G.; Karyakin, N. V., The physical chemistry of the compounds $MIP(As)UO_6$ (MI=H, Li, Na, K, Rb, Cs) and their crystalline hydrates. *Russ. Chem. Rev.* **1995,** *64*, (10), 913-927.

22. Gorman-Lewis, D.; Shvareva, T.; Kubatko, K.-A.; Burns, P. C.; Wellman, D. M.; McNamara, B.; Szymanowski, J. E. S.; Navrotsky, A.; Fein, J. B., Thermodynamic properties of autunite, uranyl hydrogen phosphate, and uranyl orthophosphate from solubility and calorimetric measurements. *Environ. Sci. Technol.* **2009,** *43*, (19), 7416-7422.

23. Gorman-Lewis, D.; Fein, J. B.; Burns, P. C.; Szymanowski, J. E.; Converse, J., Solubility measurements of the uranyl oxide hydrate phases metaschoepite, compreignacite, Na–compreignacite, becquerelite, and clarkeite. *J. Chem. Thermodyn.* **2008,** *40*, (6), 980-990.

24. Gorman-Lewis, D.; Burns, P. C.; Fein, J. B., Review of uranyl mineral solubility measurements. *J. Chem. Thermodyn.* **2008,** *40*, (3), 335-352.

25. Rutsch, M.; Geipel, G.; Brendler, V.; Bernhard, G.; Nitsche, H., Interaction of uranium(VI) with arsenate(V) in aqueous solution studied by time-resolved laser-induced fluorescence spectroscopy (TRLFS). In *Radiochim. Acta*, 1999; Vol. 86, p 135.

26. Gezahegne, W. A.; Hennig, C.; Tsushima, S.; Planer-Friedrich, B.; Scheinost, A. C.; Merkel, B. J., EXAFS and DFT investigations of uranyl arsenate complexes in aqueous solution. *Environ. Sci. Technol.* **2012,** *46*, (4), 2228-2233.

27. Gonzalez-Estrella, J.; Meza, I.; Burns, A. J.; Ali, A.-M. S.; Lezama-Pacheco, J. S.; Lichtner, P.; Shaikh, N.; Fendorf, S.; Cerrato, J. M., Effect of bicarbonate, calcium, and pH on the reactivity of As(V) and U(VI) mixtures. *Environ. Sci. Technol.* **2020**.

28. Locock, A. J.; Burns, P. C.; Duke, M. J. M.; Flynn, T. M., Monovalent cations in structures of the meta-autunite group. *Can. Mineral.* **2004,** *42*, (4), 973-996.

29. Suleimanov, E. V.; Chernorukov, N. G.; Veridusova, V. V., Physical chemistry of magnesium and calcium uranophosphate and uranoarsenate $A^{II}(B^{V}UO_6)_2 \cdot nH_2O$. *Radiochemistry* **2006,** *48*, (2), 159-161.

30. Bureau of reclamation, D. o. I., *Ground Water Manual. A Water Resources Technical Publication from The Water Encyclopedia*. Third Edition ed.; 1997; p 480.

31. Lichtner, P. C.; Hammond, G. E.; Lu, C.; Karra, S.; Bisht, G.; Andre, B.; Mills, R.; Kumar, J. *PFLOTRAN User Manual: A Massively Parallel Reactive Flow and Transport Model for*

Describing Surface and Subsurface Processes; LA-UR-15-20403 United States 10.2172/1168703 LANL English; Los Alamos National Lab. (LANL): 2015; p Medium: ED; Size: 197 p.

32. I. Campos, E. C. A. ThermoChimie Technical report. Bibliography. https://www.thermochimie-tdb.com/pages/contact.php

33. Dong, W.; Brooks, S. C., Determination of the formation constants of ternary complexes of uranyl and carbonate with alkaline earth metals (Mg^{2+}, Ca^{2+}, Sr^{2+}, and Ba^{2+}) using anion exchange method. *Environ. Sci. Technol.* **2006,** *40*, (15), 4689-4695.

34. Dong, W.; Brooks, S. C., Formation of Aqueous $MgUO_2(CO_3)_3^{2-}$ Complex and Uranium Anion Exchange Mechanism onto an Exchange Resin. *Environmental Science & Technology* **2008,** *42*, (6), 1979-1983.

35. Guillaumont, R. G., Ingmar. Fuger, Jean. , *Updated on the chemical thermodynamics of Uranium, Plutonium, Americium, and Technetium.* . Organisation for economic co-operation and development: Paris, France., 2004.

36. Giffaut, E.; Grivé, M.; Blanc, P.; Vieillard, P.; Colàs, E.; Gailhanou, H.; Gaboreau, S.; Marty, N.; Madé, B.; Duro, L., Andra thermodynamic database for performance assessment: ThermoChimie. *J. Appl. Geochem.* **2014,** *49*, 225-236.

37. Navrotsky, A., Progress and New Directions in High-Temperature Calorimetry. *Phys. Chem. Miner.* **1977,** *2*, (1−2), 89.

38. Navrotsky, A., Progress and new directions in high temperature calorimetry revisited. *Phys. Chem. Miner.* **1997,** *24*, (3), 222.

39. Navrotsky, A., Progress and new directions in calorimetry: a 2014 perspective. *J. Am. Ceram. Soc.* **2014,** *97*, (11), 3349-3359.

40. Shvareva, T. Y.; Fein, J. B.; Navrotsky, A., Thermodynamic properties of uranyl minerals: constraints from calorimetry and solubility measurements. *Ind. Eng. Chem. Res.* **2012,** *51*, (2), 607-613.

41. Cox, J. D.; Wagman, D. D.; Medvedev, V. A., *CODATA Key Values for Thermodynamics*. 1989.

42. Nordstrom, D.; Archer, D., Arsenic thermodynamic data and environmental geochemistry. In 2003; pp 1-25.

43. Mills, S. J.; Birch, W. D.; Kolitsch, U.; Mumme, W. G.; Grey, I. E., Lakebogaite, $CaNaFe_2^{3+}H(UO_2)_2(PO_4)_4(OH)_2(H_2O)_8$, a new uranyl phosphate with a unique crystal structure from Victoria, Australia. *Am. Mineral.* **2008,** *93*, (4), 691-697.

44. Ondrus, P.; Veselovsky, F.; Skala, R.; Cisarova, I.; Hlousek, J.; Fryda, J.; Vavrin, I.; Cejka, J.; Gabasova, A., New naturally occurring phases of secondary origin from Jachymov (Joachimsthal). *J. Czech Geol. Soc.* **1997,** *42*, (4), 77-108.

45. Clavier, N.; Crétaz, F.; Szenknect, S.; Mesbah, A.; Poinssot, C.; Descostes, M.; Dacheux, N., Vibrational spectroscopy of synthetic analogues of ankoleite, chernikovite and intermediate solid solution. *Spectrochim. Acta B: At. Spectrosc.* **2016,** *156*, 143-150.

46. Ross, M.; Evans Jr, H., Studies of the torbernite minerals (III): role of the interlayer oxonium, potassium, and ammonium ions, and water molecules. *Am. Mineral.* **1965,** *50*, (1-2), 1-12.

47. Ross, M.; Evans Jr, H.; Appleman, D., Studies of the torbernite minerals (II): The crystal structure of meta-torbernite. *Am. Mineral.* **1964,** *49*, (11-12), 1603-1621.

48. Ross, M.; Evans Jr, H. T., Studies of the torbernite minerals (i): the crystal structure of abernathyite and the structurally related compounds $NH_4(UO_2AsO_4)\cdot 3H_2O$ and $K(H_3O)(UO_2AsO_4)_2\cdot 6H_2O$. *Am. Mineral.* **1964,** *49*, (11-12), 1578-1602.

49. He, M.; Liu, X.; Cheng, J.; Lu, X.; Zhang, C.; Wang, R., Uranyl arsenate complexes in aqueous solution: Insights from first-principles molecular dynamics simulations. *Inorg. Chem.* **2018,** *57*, (10), 5801-5809.

50. Chernorukov, N.; Nipruk, O.; Knyazev, A.; Pykhova, Y. P., Synthesis and study of uranyl arsenate $(UO_2)_3(AsO_4)_2\cdot 12H_2O$. *Russ. J. Inorg. Chem.* **2011,** *56*, (2), 163-167.

51. Weisbach, A., Vorläufige Mitteilung – Trögerit, Walpurgin. *Neues Jahrb. Mineral* . **1871**, 869–870.

52. Locock, A. J.; Burns, P. C., Structures and syntheses of layered and framework amine-bearing uranyl phosphate and uranyl arsenates. *J. Solid State Chem.* **2004,** *177*, (8), 2675-2684.

53. Chukhlantsev, V. G.; Sharova, A. K., Solubility products of uranyl arsenates. *Russ. J. Inorg. Chem.* **1956,** *1*, (1), 39-44.

54. Zhil'tsova, I. G.; Polupanova, L. I.; Shmariovich, E. M.; Perlina, S. A., Physico-chemical conditions of uranyl-arsenate mineralization. *Litologiya i Poleznye Iskopaemye* **1987**, (3), 44-54.

55. Morosin, B., Hydrogen uranyl phosphate tetrahydrate, a hydrogen ion solid electrolyte. *Acta Crystallographica - Section B: Structural Crystallography and Crystal Chemistry* **1978,** *34*, (12), 3732.

56. Ivanova, A. G.; Budantseva, N. A.; Fedoseev, A. M., Synthesis, crystal structure, and properties of new actinide(VI) arsenates $(H_3O)[(AnO_2)(AsO_4)]\cdot 3H_2O$ (An = U, Np, Pu). *Radiochemistry* **2017,** *59*, (2), 119-123.

57. Shilton, M. G.; Howe, A. T., Rapid H^+ conductivity in hydrogen uranyl phosphate-A solid H^+ electrolyte. *Materials Research Bulletin* **1977,** *12*, (7), 701-706.

58. Benjamin, M. M., *Water Chemistry*. Boston : McGraw-Hill, ©2002.: 2002.

59. Zhang, Y., Thermochemistry of rare-earth aluminate and aluminosilicate glasses. *J. Non. Cryst. Solids.* **2004,** *341*, (1-3), 141.

60. Forray, F. L., Synthesis, characterization and thermochemistry of synthetic PbAs, PbCu and PbZn jarosites. *Geochim. Cosmochim. Acta.* **2014,** *127*, 107.

61. Grenthe, I. F., Jean. Konings, Rudy. Lemire, Robert. Muller, Anthony. Nguyen-Trung Cregu, Chinh. Wanner, Hans., *Chemical thermodynamics of Uranium*. Nuclear Energy Agency, 1992.

62. Kubatko, K. A.; Helean, K. B.; Navrotsky, A.; Burns, P. C., Thermodynamics of uranyl minerals: Enthalpies of formation of rutherfordine, UO_2CO_3, andersonite, $Na_2CaUO_2(CO_3)_3(H_2O)_5$, and grimselite, $K_3NaUO_2(CO_3)_3H_2O$. *Am. Mineral.* **2005,** *90*, (8−9), 1284.

63. Robie, R. A., Hemingway, B.S., Fisher, J.R., Thermodynamic properties of minerals and related substances at 298.15K and 1 bar (10^5 pascals) pressure and at higher temperatures. In U.S. G.P.O.: 1978.

CHAPTER 4. KINETIC INVESTIGATION OF THE SOLUBILITY OF NA- AND K-URANYL ARSENATE SOLIDS

Isabel Meza,[1,2] Noah Jemison [1,2] Jorge Gonzalez-Estrella,[3] Peter C. Burns,[4] Virginia Rodriguez[4], Ginger E. Sigmon,[4] Jennifer E.S. Szymanowski,[4] Abdul-Mehdi S. Ali,[5] Kaelin Gagnon,[1,2] José M. Cerrato,[1,2] and Peter Lichtner.[2]*

*Corresponding email address: jcerrato@unm.edu, mameza@unm.edu

Telephone: (001) (505) 277-0870

Fax: (001) (505) 277-1918

[1] Department of Civil, Construction & Environmental Engineering, MSC01 1070, University of New Mexico, Albuquerque, New Mexico 87131, USA

[2] Center for Water and the Environment, UNM, Albuquerque, NM, USA

[3] School of Civil and Environmental Engineering, College of Engineering, Architecture, and Technology, Oklahoma State University, Stillwater, Oklahoma, USA

[4] Department of Civil and Environmental Engineering and Earth Sciences, University of Notre Dame, Notre Dame, Indiana 46556, USA and Department of Chemistry and Biochemistry, University of Notre Dame, Notre Dame, Indiana 46556, USA.

[5] Department of Earth and Planetary Sciences, MSC03 2040, University of New Mexico, Albuquerque, New Mexico 87131, USA

Abstract.

We integrated aqueous chemistry analyses with reactive transport modeling to interpret the influence of chemical equilibrium and kinetics on the solubility of uranium (U) and arsenic (As) in sodium (Na)- and potassium (K)- uranyl arsenate solids ($UAs_{(s)}$) reacted at acidic pH. Improving our understanding of how $UAs_{(s)}$ dissolve under acidic conditions is essential to predict the transport of U and As in water caused by natural and anthropogenic processes. At pH 2.0, the concentrations of U and As are controlled by the reaction rate of Na- and K- $UAs_{(s)}$, which are measured at 3.16×10^{-7} mol m^{-2} s^{-1} for both sodium uranyl arsenate ($NaUAs_{(s)}$) and potassium uranyl arsenate ($KUAs_{(s)}$). $NaUAs_{(s)}$ dissolves slightly slower (7.94×10^{-8} mol m^{-2} s^{-1}) at pH 3.0 over the first hour of reaction. Following the first hour, the secondary precipitation of trögerite controls U and As concentrations in a $NaUAs_{(s)}$ system. For $KUAs_{(s)}$ at pH 3.02, U and As dissolve rapidly with the concentrations of U and As controlled by the chemical equilibrium for $KUAs_{(s)}$. The results from this study help us understand kinetics and chemical equilibrium of $UAs_{(s)}$ which have relevant implications for risk assessment and remediation.

INTRODUCTION.

Understanding the kinetics of the dissolution of uranyl arsenates solids ($UAs_{(s)}$) in aqueous solutions is essential to gain fundamental knowledge of uranium (U) and arsenic (As) mobilization in environmentally relevant conditions. The toxicity of U and As has been well documented.[1-3] Acid mine drainage (AMD) is a common condition in sites affected by mining legacy, where metal sulfide minerals upon exposure to oxidizing conditions (water and oxygen) form acidic, sulfate-rich drainage, thus causing acidic pH conditions in source waters.[4] Further understanding the influence of chemical equilibrium and kinetics on the mobilization of U and As is necessary for improved interpretation and prediction of the fate and transport of these toxic elements in the environment and to develop risk assessment and remediation strategies.

Modeling and optimization of chemical equilibrium and kinetics require knowledge of thermodynamic properties for the range of uranyl arsenate minerals that can form under environmental conditions. Numerous studies have investigated the co-sorption of U and As onto various mineral surfaces,[5] however, only a few studies have measured the solubility products (log K_{sp}) of $UAs_{(s)}$ of environmental relevance.[6, 7, 8-11] Our mechanistic understanding of the dissolution of $UAs_{(s)}$ with respect to chemical equilibrium and kinetic processes influencing their solubility is still lacking.

In this study we investigated the mechanisms influencing the mobilization of U as uranyl $(UO_2)^{2+}$ and As as arsenate $(AsO_4)^{3-}$ in sodium uranyl arsenate $(Na_{0.5}(H_3O)_{0.5}[(UO_2)(AsO_4)](H_2O)_{2.5(s)}$ and potassium uranyl arsenate $K_{0.9}[(H_3O)_{0.1}(UO_2)(AsO_4)](H_2O)_{2.5(s)}$ reacted in aqueous solutions at acidic pH. Hereafter, we will refer to uranyl as U, arsenate as As, sodium uranyl arsenate as $NaUAs_{(s)}$ and potassium uranyl arsenate as $KUAs_{(s)}$. These data were modeled using the surface area and thermodynamic information from well synthesized and characterized uranyl arsenates

($NaUAs_{(s)}$ and $KUAs_{(s)}$), to obtain dissolution rates and gain further understanding of the factors influencing the release of U and As in water. The novelty of this study is the determination of dissolution rates for $NaUAs_{(s)}$ and $KUAs_{(s)}$ in aqueous solutions at a range of acidic pH conditions (pH range: 2-3) to interpret the influence of kinetic and chemical equilibrium processes on U and As mobilization. The outcomes from this study provide new insights about the solubility of $UAs_{(s)}$ at acidic pH conditions, which have implications for the use of reactive transport models for risk assessment and remediation applications

4.1. Materials and methods.

4.1.1. Synthesis and characterization of uranyl arsenate solids.

The $UAs_{(s)}$ were synthesized and characterized as reported in a previous publication of our group.[11] Briefly, $UAs_{(s)}$ (NaUAs and KUAs) were synthesized by the diffusion method and powder X-ray diffraction (p-XRD) was used for the characterization described by Meza et al. (2022).[11]

4.1.2. Dissolution experiments.

All dissolution experiments were conducted in batch reactors containing aqueous solutions at 25°C using Teflon Nalgene® bottles. A Thermo Orion Ross pH micro electrode that was calibrated daily with 3 NIST standards (pH 4, 7, and 10) was used for pH measurements. Dissolution experiments in triplicate (three separate reactors) were used for all experiments. Experiments used a ratio of 1.4 in terms of mass of each uranyl arsenate solid and mass of 18 MΩ H_2O (e.g., ~40 mg of NaUAs in 28 mL of water which can dissolve into ~690 mg L^{-1} of U and 217 mg L^{-1} of As). The conversion of volume of water to mass was conducted by assuming that the density of water was 997 g/L.[12]

Dissolution experiments were performed at pH 2.0 and 3.0 due to the chemical speciation of U and As is well-constrained at low pH. For example, chemical equilibrium modeling indicates

that UO_2^{2+} is the predominant species of U, while H_3AsO_4 and $H_2AsO_4^{1-}$ are the predominant species of As with limited influence of the carbonate system (i.e., carbonic acid is predominant at this acidic pH). Also, experiments were conducted at pH 2.0 and 3.0 due to As species buffering the pH with a pKa_1 of 2.24 for arsenic acid (H_3AsO_4).[13] To adjust the pH for experiments with pH 2, a small quantity of concentrated HNO_3 was used. The pH was monitored daily, and no adjustment of the pH was performed over the 31 d of the experiments with a slight increase in the pH throughout the $NaUAs_{(s)}$ and $KUAs_{(s)}$ experiments at both pH 2.0 and 3.0. Also, we decided to stay with pH 3, because while our initial objective was to raise the pH to 4.0, the pH stabilized close to 3.

The batch reactors were sealed and agitated at 60 rpm in an analog rotisserie tube rotator (Scologex MX-RL-E, Rocky Hill, CT, US) at room temperature. Aliquots of the solution were extracted at selected times (0 min, 15 min, 30 min, 60 min, 120 min, 4 h, 6 h, 8 h, 12 h, 24 h, 8 d, 15 d, 22 d, 31 d), filtered through 0.1 μm MilliporeSigma Millex filters, and diluted with 2% HNO_3 for ICP-OES analysis to determine dissolved concentrations of U, As, and Na or K. A control experiment, where non aliquots were taken from the batch reactors, was conducted and demonstrated that the withdrawal of aliquots did not change the dissolved concentrations of the elements.

4.1.3. Solution analyses.

The soluble concentrations of U, As, Na, and K in the aqueous solutions were measured using a PerkinElmer Optima 5300DV inductively coupled plasma optical emission spectrometry (ICP-OES) with an instrument detection limit of 0.5 mg L^{-1}. Trace element concentrations were measured with a PerkinElmer NexION 300D (Dynamic Reaction Cell) inductively coupled plasma mass spectrometry (ICP-MS) with a detection limit of 0.5 μg L^{-1}. Both instruments were calibrated

with Fischer Scientific Standards with a five-point calibration curve, and QA/QC measures were taken to ensure quality results.

We encountered challenges in the analyses for Na as the measured concentrations from ICP-OES were highly variable (Figure S1). A similar challenge has been reported in other studies.[14] Therefore, we decided to base our quantitative analyses for this study only on U and As concentrations as a function of pH. The solution chemistry with Na and K for the dissolution experiments can be found in the SI (Figures S1, S2, S3, and S4)

4.1.4. Reactive transport modeling.

We considered a reaction in a batch reactor, where the reaction rate is given by:

$$\boldsymbol{R}_{UAs_{(s)}} = \boldsymbol{k}_{\boldsymbol{eff}} * \left(1 - \frac{Q}{\mathrm{K_{eq}}}\right) \quad (1)$$

where R (mol m^{-3} s^{-1}) is the reaction rate, k_{eff} (mol m^{-3} s^{-1}) is effective rate constant, which is equal to r_n x a, where r_n (mol m^{-2} s^{-1}) is the rate constant and a (m^{-1}) is the surface area, Q (--) is the activity product, and K_{eq} (--) is the equilibrium constant.

If $Q = K_{eq}$, the system is in equilibrium, if $Q > K_{eq}$, precipitation occurs, and if $Q < K_{eq}$, dissolution occurs. This rate law is based of transition state theory where the rate is influenced by how far the system is from equilibrium.

Calculations were carried out using the open-source computer code CRUNCHFLOW[15] that runs on MacOSX and Windows.[16] The primary species used during modeling were UO_2^{2+}, AsO_4^{3-}, Na^+, HCO_3^-, and NO_3^-. These primary species were allowed to form secondary species using the equilibrium constants of these secondary species (Table S1). Initially, the model contained a trivial amount of each primary species, and the model allowed these concentrations to increase as the $UAs_{(s)}$ dissolved. The equilibrium constants used for the reaction rates of these minerals (Table 1)

have been previously measured[11]. In addition, the surface area of $NaUAs_{(s)}$ (1.46 ± 0.26 m^2 g^{-1}) and $KUAs_{(s)}$ (0.77 ± 0.37 m^2 g^{-1}) were previously determined using BET techniques in collaboration with Virginia Tech (Table 1).[11] The surface area of $UAs_{(s)}$ as well as the known mass of $UAs_{(s)}$ added to experimental solutions were used to calculate the total surface area of the $UAs_{(s)}$ used in the models.

Trögerite $[(UO_2)_3(AsO_4)_2(H_2O)_{12}]_{(s)}$, which formed during the $NaUAs_{(s)}$ experiment at pH 3 (see below), did not have a measured surface area, so we utilized the same surface area as measured for $NaUAs_{(s)}$. While this assumption may be incorrect, the rate constant of trögerite precipitation (which is not a focus of this study) may be changed to obtain the same effective reaction rate. The reaction rate of the $UAs_{(s)}$ was adjusted to best fit the U and As concentrations observed in the dissolution experiments.

4.2. Results and discussion

4.2.1. Determination of dissolution rates for NaUAs solids.

The reaction rates normalized to surface area (r_n) for $NaUAs_{(s)}$ in aqueous solutions at pH 2.0 and pH 3.0 were similar. The r_n for $NaUAs_{(s)}$ at pH 2.0 was calculated at 3.16 x 10^{-7} mol m^{-2} s^{-1} and 7.94 x 10^{-8} mol m^{-2} s^{-1} at pH 3 using an equilibrium constant (log K_{sp}) of -23.50 from our previous study.[11] These r_n′s at pH 2.0 and pH 3.0 are less than one-order of magnitude different with rates slightly faster at pH 2.0. Our results contrast with a study showing reaction rates for uranyl minerals increasing about one order-of-magnitude with increasing pH and increasing dissolved carbonate concentration at pH ~ 5 and 10.[17, 18] Even though, our rates agree with the same study that shows data below pH 5, where reaction rates obtained with Na-autunite ($Na_2[(UO_2)_2(PO_4)_2]3H_2O$) and Ca-autunite ($Ca[(UO_2)_2(PO_4)_2]$ $3H_2O$) present closer to two-orders of magnitude higher reaction rate at pH 2.0 than pH 3.0.[17]

Sodium uranyl arsenate ($NaUAs_{(s)}$) presents a congruent dissolution of U and As in water at pH 2.0. The experimental data obtained for the dissolution experiments agree with CRUNCHFLOW modeling. The concentrations of U and As obtained during the initial 15 min were ~0.5 mM, achieving steady state at an average of 1.7 mM from 24 h to the end of the experiment at 30 d resulting from the dissolution of the $NaUAs_{(s)}$ at pH 2.0 (Figure 1A). After this high initial release, the dissolution of $NaUAs_{(s)}$ at pH 2.0 into U and As were similar overall during 30 d. The pH increased from an initial value of 1.88 to 2.04 from 15 min until the end of the experiment (Figure 1B).

Trögerite $[(UO_2)_3(AsO_4)_2(H_2O)_{12}]_{(s)}$ precipitated as a secondary phase during the dissolution/precipitation experiments with $NaUAs_{(s)}$ at pH 3.0. The concentrations of U and As at pH 3 were controlled by dissolution kinetics of $NaUAs_{(s)}$ over the first 30 min (Figure 2A). Trögerite $[(UO_2)_3(AsO_4)_2(H_2O)_{12}]_{(s)}$ began to precipitate as a secondary phase after 60 min at a rate of 2.95 x 10^{-8} mol g^{-1} s^{-1}, also obtained from CRUNCHFLOW and using the same surface area than $NaUAs_{(s)}$. Uranium reached a steady state concentration of ~0.13 mM with As at a steady state concentration of ~0.73 mM. The particularly low U concentrations require a mineral that contains a greater mol fraction of U than As, which is consistent with trögerite ($[(UO_2)_3(AsO_4)_2(H_2O)_{12}]_{(s)}$).[19] [11] The precipitation of trögerite agrees with literature where it is mentioned as a secondary phase that controls the concentrations of U and As in time, at acidic pH, leading to a difference in the U and As concentrations by 1-2 orders of magnitude.[19] Furthermore, the precipitation of a secondary phase agrees with uranyl phosphate (uranyl arsenate analogue) literature where the dissolution rate of Na-autunite ($Na_2[(UO_2)_2(PO_4)_2]3H_2O$), the reaction rate was also influenced by the secondary formation of other phase like $(UO_2)_3(PO_4)_2 \cdot x\ H_2O$.[17]

The steady state concentrations of U and As from $NaUAs_{(s)}$ were lower at pH 3.0 than at pH 2.0. The concentration of U was ~0.13 mM and As ~0.73 mM at pH 3, compared to ~1.7 mM for both, U and As, at pH 2.0. These results suggest that besides $NaUAs_{(s)}$ solubility, U and As could precipitated with trögerite as well. Trögerite and $NaUAs_{(s)}$ could become a solid substrate that started heterogenous nucleation by adsorption or chemical bonding with metals, in this case U and As.[20-23]

4.2.2. Determination of dissolution rates for KUAs solids.

There is a reaction rate normalized to surface area (r_n) for $KUAs_{(s)}$ at pH 2.0 but for $KUAs_{(s)}$ we found chemical equilibrium at pH 3.0. The r_n for $KUAs_{(s)}$ at pH 2.0 was calculated at 3.16 x 10^{-7} mol m^{-2} s^{-1} using the equilibrium constant (log K_{sp}) of -23.87 from our previous study.[11] The congruent dissolution of U and As in aqueous solution reached 0.5 mM concentrations following 15 min of reaction, achieving steady state at 2.3 mM at 24 h for $KUAs_{(s)}$ at pH 2.0 (Figure 3A). The steady states concentrations for $KUAs_{(s)}$ at pH 3.0 for U were ~0.11 mM and for As were 0.09 mM, close to 20 times lower than at pH 2.0 (Figure 4A). Our results contrast with a study that showed reaction rates for uranyl minerals increasing about one order-of-magnitude with increasing pH and increasing dissolved carbonate concentration at pH ~ 5 and 10.[17, 18] However, no uranyl arsenates were mentioned in this study.[17, 18] The pH increased by 0.5 units after the first 15 min., but then it was adjusted back to 2.0 by addition of a couple µl of HNO_3, and stayed at pH 2.0 for 30 d for $KUAs_{(s)}$ at pH 2.0. (Figure 3B). The pH increased from 2.8 to 3.0 for $KUAs_{(s)}$ with experiments at pH 3.0 (Figure 4B).

The reaction rates and steady state U and As concentrations for $KUAs_{(s)}$ and $NaUAs_{(s)}$ in water at pH 2 are similar but are slightly faster than $NaUAs_{(s)}$ at pH 3.0. The reaction rates of both $KUAs_{(s)}$ and $NaUAs_{(s)}$ (3.16 x 10^{-7} mol m^{-2} s^{-1}) at pH 2.0 are faster than the reaction rate of

$NaUAs_{(s)}$ at pH 3 (7.94×10^{-8} mol m^{-2} s^{-1}). The concentrations of U and As were ~1.7 mM for $NaUAs_{(s)}$ at pH 2, ~2.3 mM for $KUAs_{(s)}$ at pH 2.0, but ~0.11 mM for $KUAs_{(s)}$ at pH 3.0 at 30 d, close to 20 times lower than pH 2.0. These results suggest that the reaction rates are pH dependent.[19] Furthermore, these results suggest that the precipitation of trögerite could have influenced the reaction rate and the U and As concentrations. The reacted solids from the dissolution experiments for $NaUAs_{(s)}$ and $KUAs_{(s)}$ at pH 2.0 did not show the formation of secondary phases, but $NaUAs_{(s)}$ at pH 3.0 precipitated trögerite. These also agree with previous literature in which the solubility of primary uranyl arsenate compounds is higher than secondary phases.[17-19]

4.3. Insights about kinetics and chemical equilibrium of uranyl arsenate solids.

The experiments in this study were conducted at acidic conditions, avoiding reactions with carbonate that would affect the formation of various secondary phases and aqueous complexes influencing the solubility of the minerals investigated here. The dissolution of $UAs_{(s)}$ at circumneutral pH could be enhanced by formation of strong aqueous uranyl-carbonate complexes.[24] Carbonate may lead to the dissolution of uranyl arsenate, uranyl phosphate, oxyhydroxide, and uranyl vanadate minerals as previously reported.[25-29] This study instead focused on the solubility of $UAs_{(s)}$ under acidic conditions, as found in AMD.[4]

Our findings indicate that at pH 2.0 the presence of $NaUAs_{(s)}$ and $KUAs_{(s)}$ control the aqueous concentrations of U and As through their dissolution kinetics over the first hour. At pH 3.0, $KUAs_{(s)}$ rapidly dissolves and reaches chemical equilibrium. These results agree with previous studies which found that U and As in solution can be removed at acidic pH, with the precipitation of U-As-bearing minerals.[30] As a whole, our study provides insights about U and As mobilization and information for possible remediation approaches.

Reaction rates for $NaUAs_{(s)}$ and for trögerite obtained from our dissolution experiments at pH 3 agree well with available literature for uranyl phosphates.[17, 18] Our calculated reaction rates also are comparable to other uranyl minerals but are typically 1 to 3-orders-of-magnitude faster. Monovalent cation uranyl phosphates K-ankoleite $KUPO_6(H_2O)_{3(S)}$ and Na-autunite $NaUO_2PO_4(H_2O)_{3(S)}$ dissolve at a rate of 4.67×10^{-10} and 1.12×10^{-9} mol m^{-2} s^{-1} respectively at a pH ranging from 7 to 8.2.[18] Wellman et al. obtained a U reaction rate from the divalent cation uranyl phosphate calcium meta-autunite $Ca[(UO_2(PO_4)]_2 \cdot 3H_2O$ of 1.33×10^{-10} mol m^{-2} s^{-1} at pH 2.0 and 3.13×10^{-14} mol m^{-2} s^{-1} at pH 5 in single pass flow experiments.[17] Another study reported reaction rates of 3.2×10^{-13} mol m^{-2} s^{-1} at pH 3.4 for a uranyl vanadate (carnotite $[K_2(UO_2)_2(VO_4)_2 \cdot {}_3H_2O])_{(s)}$[31] from abandoned uranium mine waste from flow through column experiments.[32]

The findings from this study can be useful for risk assessment and risk reduction studies where anthropogenic activities such as mining and nuclear weapons development have resulted in contamination.

4.4. Conclusions

The results obtained in this study revealed that the concentrations of U and As are controlled by the reaction rates of Na- and K- $UAs_{(s)}$ at pH 2.0 (3.16×10^{-7} mol m^{-2} s^{-1}). Even though, $NaUAs_{(s)}$ dissolves slightly slower (7.94×10^{-8} mol m^{-2} s^{-1}) at pH 3 over the first hour of reaction but has trögerite as a secondary precipitate that impacts U and As concentrations in an aqueous $NaUAs_{(s)}$ system. This difference indicates that reaction rates are pH dependent and the formation of secondary phases such as trögerite may decrease the reaction rate of $UAs_{(s)}$. For $KUAs_{(s)}$ at pH 3.0, U and As dissolve rapidly with the concentrations of U and As controlled by the chemical equilibrium for $KUAs_{(s)}$.

The kinetic data obtained for $NaUAs_{(s)}$ and $KUAs_{(s)}$ in this study contribute new information that will underpin prediction of U and As concentrations at chemical equilibrium and/or kinetics in reactive transport models.

4.5. Acknowledgments.

Funding for this research was provided by the National Science Foundation (CAREER Award 1652619, CREST Award 1914490) and the National Institute of Environmental Health Sciences (Superfund Research Program Award 1 P42 ES025589 and R01ES027145). Any opinions, findings, and conclusions or recommendations expressed in this publication are those of the author(s) and do not necessarily reflect the views of the National Science Foundation or the National Institutes of Health.

PCB´s contribution to this work was funded by the Chemical Sciences, Geosciences and Biosciences Division, Office of Basic Energy Sciences, Office of Science, U.S. Department of Energy, Grant No. DE-FG02–07ER15880.

Supporting information.

Additional 2 tables (Table S1 and S2) and 4 figures (Figures S1, S2, S3, and S4) are available in SI.

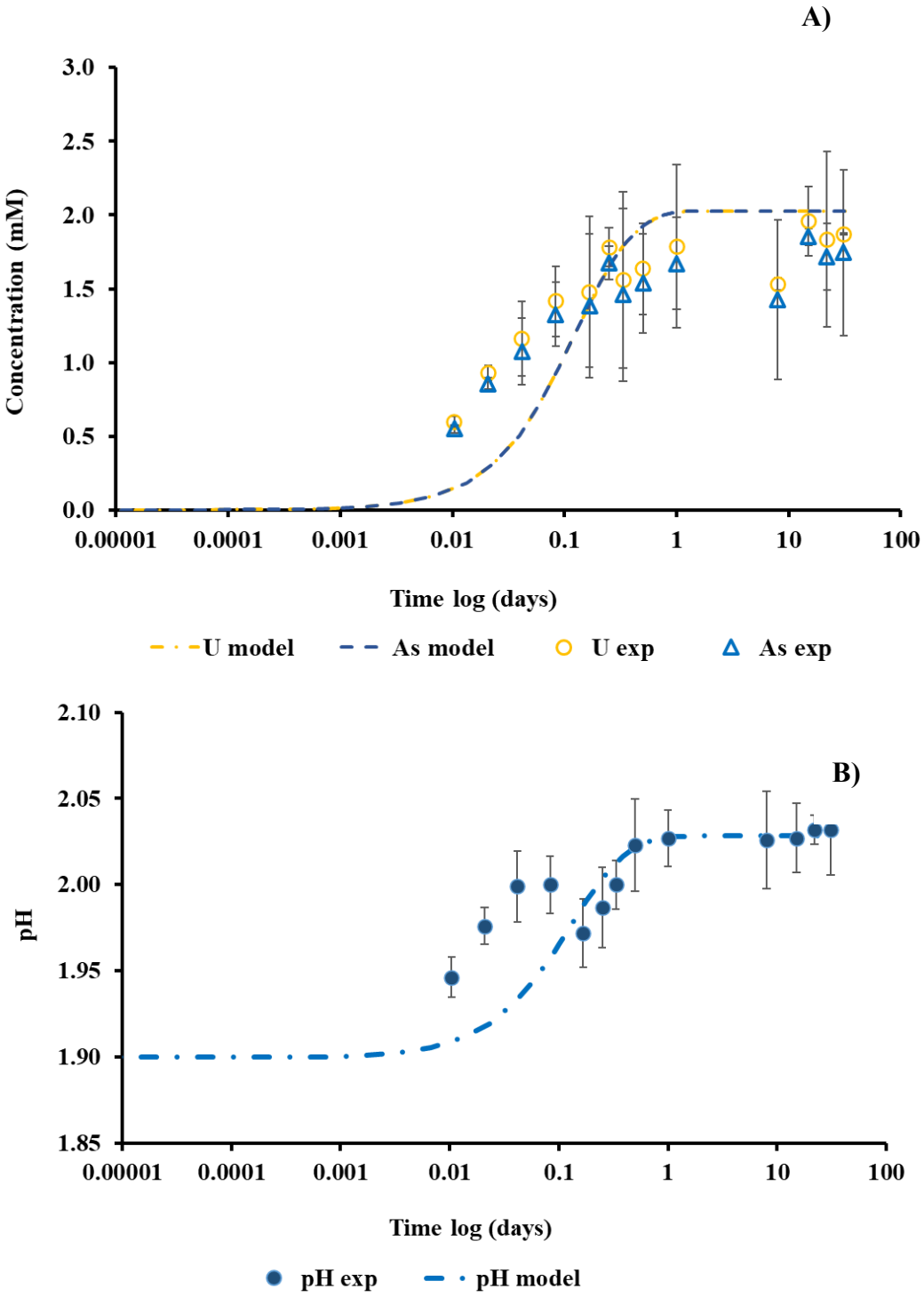

Figure 1. A) NaUAs dissolution experiments at pH 2.0 vs modeling with Crunchflow (continuous lines) presenting concentrations of U (open circles), and As (open triangles). B) pH of the NaUAs dissolution experiments vs modeling with Crunchflow in time.

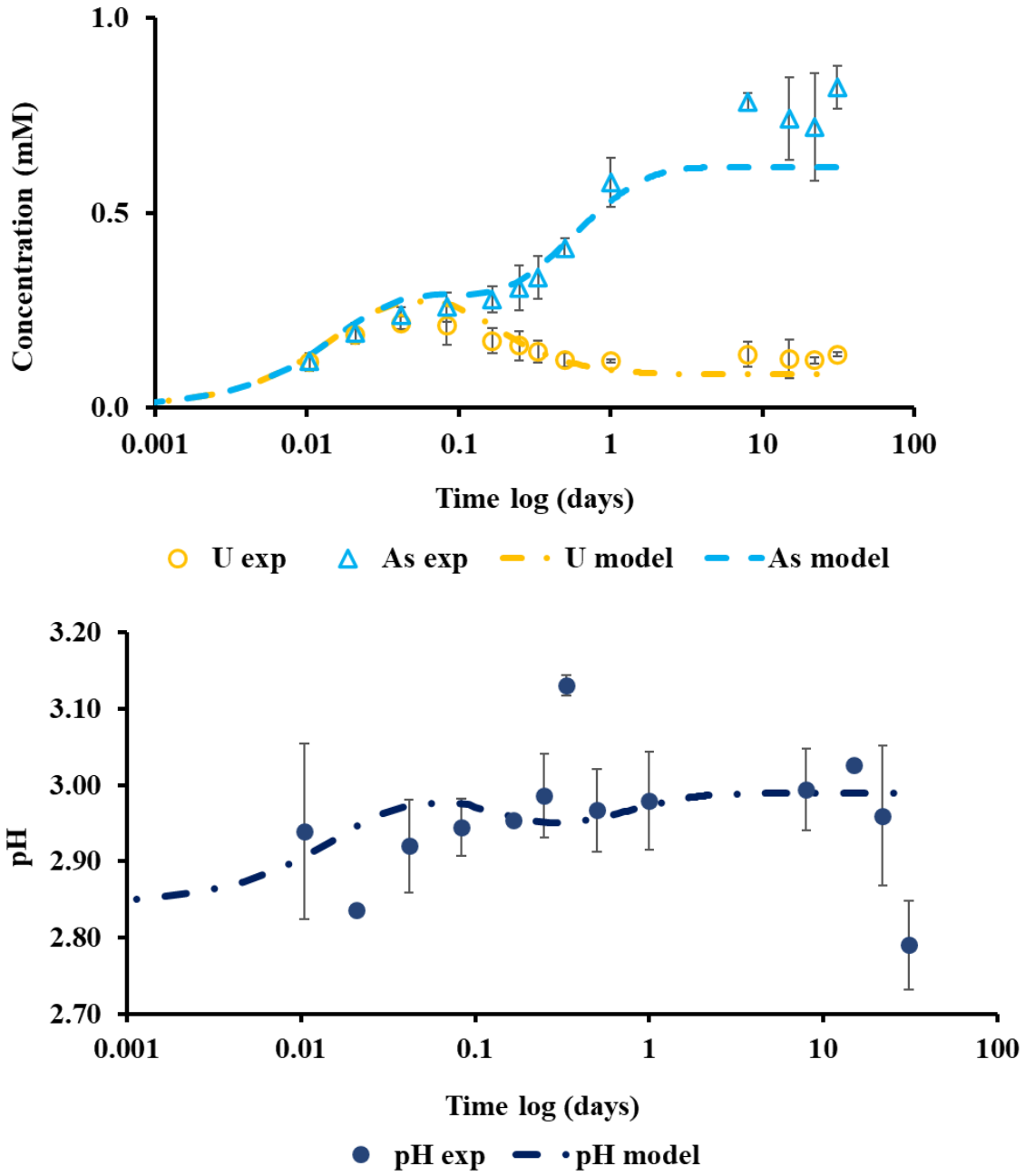

Figure 2. A) NaUAs dissolution experiments at pH 3.0 vs modeling with Crunchflow (continuous lines) presenting concentrations of U (open circles), and As (open triangles). B) pH of the NaUAs dissolution experiments vs modeling with Crunchflow in time.

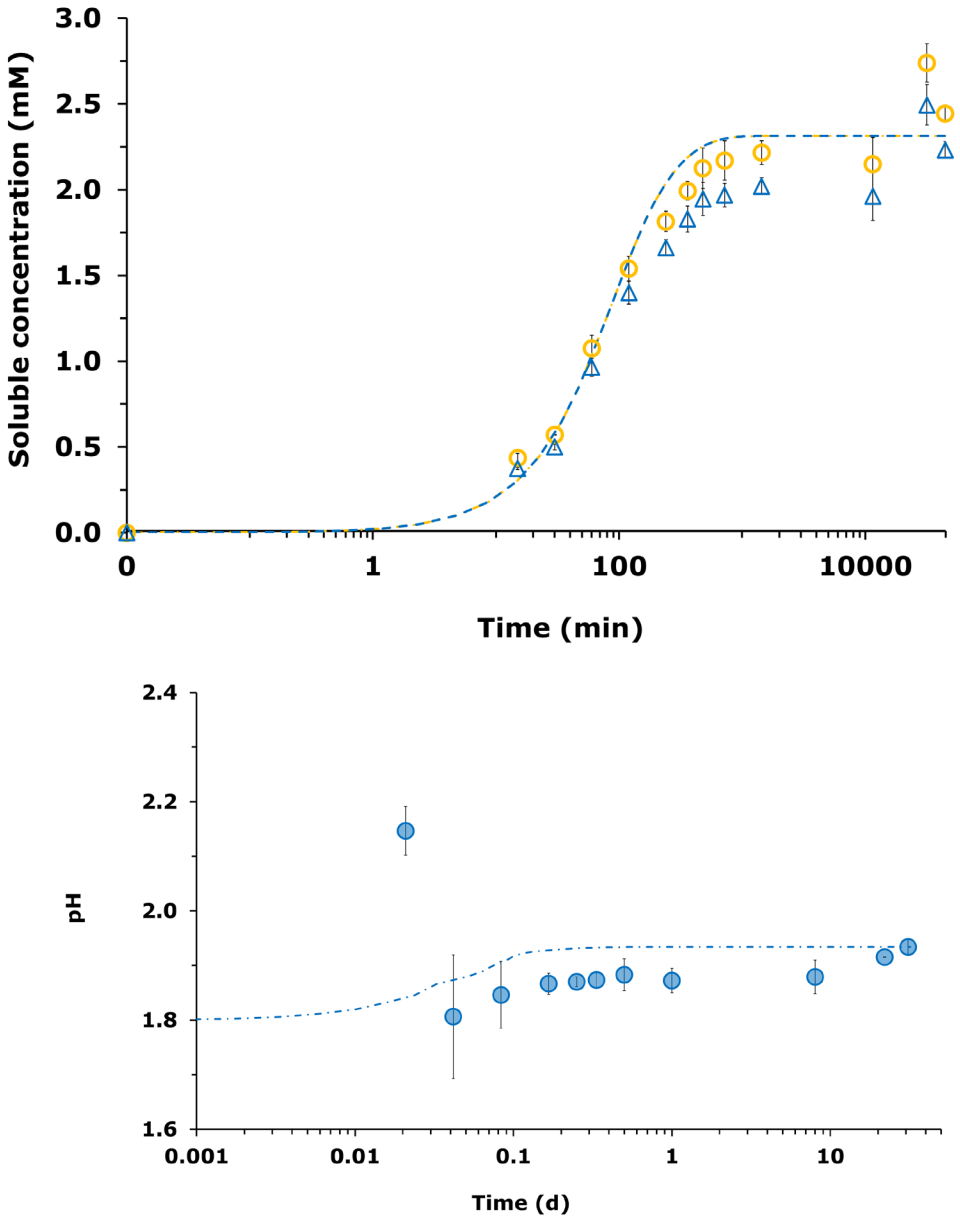

Figure 3. A) KUAs dissolution experiments at pH 2.0 vs modeling with Crunchflow (continuous lines) presenting concentrations of U (open circles), and As (open triangles). B) pH of the KUAs dissolution experiments vs modeling with Crunchflow in time (close circles).

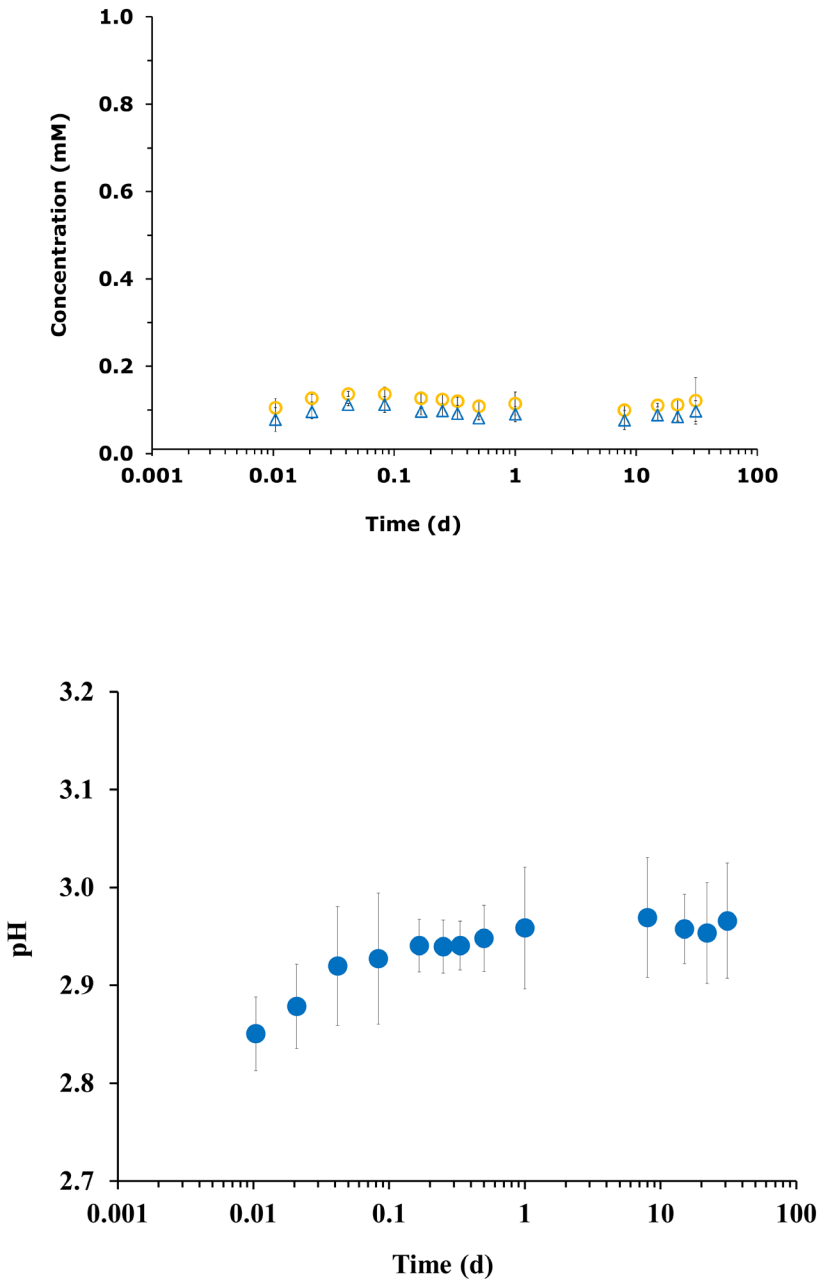

Figure 4. A) KUAs dissolution experiments at pH 3.0 presenting concentrations of U (open circles), and As (open triangles) in time. B) pH of the KUAs dissolution experiments in time.

Table 1. Modeled reaction rates normalized to Mass (r_m) and Surface area (r_n) obtained under various initial conditions.

Table 1. Modeled reaction rates normalized to Mass (r_m) and Surface area (r_n) obtained under various initial conditions.

Initial conditions					
Initial pH	**Equilibrium constant (log K_{sp})**	**Uranyl arsenate**	**a: Surface area BET (m^2g^{-1})**	**r_m (mol g^{-1} s^{-1})**	**r_n (mol m^{-2} s^{-1})**
2	-23.50	NaUAs [$Na_{0.48}H_{0.52}(UO_2)(AsO_4)(H_2O)_{2.5}$]	1.46	4.62×10^{-7}	3.16×10^{-7}
3	-23.50	NaUAs [$Na_{0.48}H_{0.52}(UO_2)(AsO_4)(H_2O)_{2.5}$]	1.46	1.16×10^{-7}	7.94×10^{-8}
	-45.63	Trögerite [$(UO_2)_3(AsO_4)_2(H_2O)_{12(s)}$] [a]		2.95×10^{-8}	2×10^{-8}
2	-23.87	KUAs [$K_{0.9}H_{0.1}(UO_2)(AsO_4)(H_2O)_{2.5}$]	0.77	2.46×10^{-7}	3.16×10^{-7}

a: log K_{sp} obtained by Chernorukov et al.[40]

REFERENCES.

1. Hoover, J. H.; Coker, E.; Barney, Y.; Shuey, C.; Lewis, J., Spatial clustering of metal and metalloid mixtures in unregulated water sources on the Navajo Nation – Arizona, New Mexico, and Utah, USA. *Sci. Total Environ.* **2018,** *633*, 1667-1678.

2. Brockgreitens, J. W.; Heidari, F.; Abbas, A., Versatile process for the preparation of nanocomposite sorbents: phosphorus and arsenic removal. *Environ. Sci. Technol.* **2020,** *54*, (14), 9034-9043.

3. Dzik, E. A.; Lobeck, H. L.; Zhang, L.; Burns, P. C., High-temperature calorimetric measurements of thermodynamic properties of uranyl arsenates of the meta-autunite group. *Chem. Geol.* **2018,** *493*, 353-358.

4. Akcil, A.; Koldas, S., Acid Mine Drainage (AMD): causes, treatment and case studies. *J. Clean. Prod.* **2006,** *14*, (12), 1139-1145.

5. Kipp, G. G.; Stone, J. J.; Stetler, L. D., Arsenic and uranium transport in sediments near abandoned uranium mines in Harding County, South Dakota. *J. Appl. Geochem.* **2009,** *24*, (12), 2246-2255.

6. Rutsch, M.; Geipel, G.; Brendler, V.; Bernhard, G.; Nitsche, H., Interaction of uranium(VI) with arsenate(V) in aqueous solution studied by time-resolved laser-induced fluorescence spectroscopy (TRLFS). In *Radiochim. Acta*, 1999; Vol. 86, p 135.

7. Gezahegne, W. A.; Hennig, C.; Tsushima, S.; Planer-Friedrich, B.; Scheinost, A. C.; Merkel, B. J., EXAFS and DFT investigations of uranyl arsenate complexes in aqueous solution. *Environ. Sci. Technol.* **2012,** *46*, (4), 2228-2233.

8. Moldovan, B. J.; Hendry, M. J., Characterizing and Quantifying Controls on Arsenic Solubility over a pH Range of 1−11 in a Uranium Mill-Scale Experiment. *Environ. Sci. Technol.* **2005,** *39*, (13), 4913-4920.

9. Meza. I.; Gonzalez-Estrella, J. B., P.C.; Rodriguez, V.; Velasco, C. A.; Sigmon, G. E.; Szymanowsky, J. E.S.; Forbes, T. Z.; Applegate, L. M.; Ali, A.M.; Lichtner, P.; Cerrato, J.M., Solubility and thermodynamic investigation of meta-autunite group uranyl arsenate solids with monovalent cations sodium (Na) and potassium (K) *Environ. Sci. Technol.* **2022 (Submitted)**.

10. Nipruk, O.; Chernorukov, N.; Pykhova, Y. P.; Godovanova, N.; Eremina, A., State of uranyl phosphates and arsenates in aqueous solutions. *Radiochemistry* **2011,** *53*, (5), 483-490.

11. He, M.; Liu, X.; Cheng, J.; Lu, X.; Zhang, C.; Wang, R., Uranyl arsenate complexes in aqueous solution: Insights from first-principles molecular dynamics simulations. *Inorg. Chem.* **2018,** *57*, (10), 5801-5809.

12. Bureau of reclamation, D. o. I., *Ground Water Manual. A Water Resources Technical Publication from The Water Encyclopedia*. Third Edition ed.; 1997; p 480.

13. Benjamin, M. M., *Water Chemistry*. Boston : McGraw-Hill, ©2002.: 2002.

14. Gorman-Lewis, D.; Fein, J. B.; Burns, P. C.; Szymanowski, J. E.; Converse, J., Solubility measurements of the uranyl oxide hydrate phases metaschoepite, compreignacite, Na–compreignacite, becquerelite, and clarkeite. *J. Chem. Thermodyn.* **2008,** *40*, (6), 980-990.

15. Steefel, C., CrunchFlow software for modeling multicomponent reactive flow and transport. User's manual. *Earth Sciences Division. Lawrence Berkeley, National Laboratory, Berkeley* **2009**, 12-91p.

16. Lichtner, P. C.; Hammond, G. E.; Lu, C.; Karra, S.; Bisht, G.; Andre, B.; Mills, R.; Kumar, J. *PFLOTRAN User Manual: A Massively Parallel Reactive Flow and Transport Model for Describing Surface and Subsurface Processes*; LA-UR-15-20403 United States 10.2172/1168703 LANL English; Los Alamos National Lab. (LANL): 2015; p Medium: ED; Size: 197 p.

17. Wellman, D. M.; Gunderson, K. M.; Icenhower, J. P.; Forrester, S. W., Dissolution kinetics of synthetic and natural meta-autunite minerals, $X_{3-n}^{(n)+}$ $[(UO_2)(PO_4)]_2 \cdot xH_2O$, under acidic conditions. *Geochem. Geophys. Geosyst.* **2007,** *8*, 1.

18. Reinoso-Maset, E.; Perdrial, N.; Steefel, C. I.; Um, W.; Chorover, J.; O'Day, P. A., Dissolved Carbonate and pH Control the Dissolution of Uranyl Phosphate Minerals in Flow-Through Porous Media. *Environ. Sci. & Technol.* **2020,** *54*, (10), 6031-6042.

19. Nipruk, O. V.; Chernorukov, N. G.; Elipasheva, E. V.; Klinshova, K. A.; Bakhmetev, M. O., State of uranyl arsenates $M^IAsUO_6 \cdot nH_2O$ (M^I–H^+, Li^+, Na^+, K^+, Rb^+, Cs^+, $NH4^+$) in aqueous solution. *J. Radioanal. Nucl. Chem.* **2020,** *324*, (1), 233-244.

20. Stumm, W.; Morgan, J. J., Aquatic Chemistry : Chemical Equilibria and Rates in Natural Waters. **2013**.

21. Lizama Allende, K.; Fletcher, T. D.; Sun, G., The effect of substrate media on the removal of arsenic, boron and iron from an acidic wastewater in planted column reactors. *Chem. Eng. J.* **2012,** *179*, 119-130.

22. Groudev, S.; Georgiev, P.; Spasova, I.; Nicolova, M., Bioremediation of acid mine drainage in a uranium deposit. *Hydrometallurgy* **2008,** *94*, (1), 93-99.

23. Ye, Z. H.; Lin, Z. Q.; Whiting, S. N.; de Souza, M. P.; Terry, N., Possible use of constructed wetland to remove selenocyanate, arsenic, and boron from electric utility wastewater. *Chemosphere* **2003,** *52*, (9), 1571-1579.

24. Ulrich, K.-U.; Ilton, E. S.; Veeramani, H.; Sharp, J. O.; Bernier-Latmani, R.; Schofield, E. J.; Bargar, J. R.; Giammar, D. E., Comparative dissolution kinetics of biogenic and chemogenic uraninite under oxidizing conditions in the presence of carbonate. *Geochim. Cosmochim. Acta* **2009,** *73*, (20), 6065-6083.

25. Avasarala, S.; Torres, C.; Ali, A.-M. S.; Thomson, B. M.; Spilde, M. N.; Peterson, E. J.; Artyushkova, K.; Dobrica, E.; Lezama-Pacheco, J. S.; Cerrato, J. M., Effect of bicarbonate and oxidizing conditions on U(IV) and U(VI) reactivity in mineralized deposits of New Mexico. *Chem. Geol.* **2019,** *524*, 345-355.

26. Blake, J. M.; Avasarala, S.; Ali, A.-M. S.; Spilde, M.; Lezama-Pacheco, J. S.; Latta, D.; Artyushkova, K.; Ilgen, A. G.; Shuey, C.; Nez, C.; Cerrato, J. M., Reactivity of As and U co-occurring in mine wastes in northeastern Arizona. *Chem. Geol.* **2019,** *522*, 26-37.

27. Reinoso-Maset, E., Rates and mechanisms of uranyl oxyhydroxide mineral dissolution. *Geochim. Cosmochim. Acta* **2017,** *207*, 298.

28. Avasarala, S.; Lichtner, P. C.; Ali, A.-M. S.; González-Pinzón, R.; Blake, J. M.; Cerrato, J. M., Reactive Transport of U and V from Abandoned Uranium Mine Wastes. *Environ. Sci. & Technol.* **2017,** *51*, (21), 12385-12393.

29. Blake, J. M.; Avasarala, S.; Artyushkova, K.; Ali, A.-M. S.; Brearley, A. J.; Shuey, C.; Robinson, W. P.; Nez, C.; Bill, S.; Lewis, J., Elevated concentrations of U and co-occurring metals in abandoned mine wastes in a northeastern Arizona Native American community. *Environ. Sci. Technol.* **2015,** *49*, (14), 8506-8514.

30. Gonzalez-Estrella, J.; Meza, I.; Burns, A. J.; Ali, A.-M. S.; Lezama-Pacheco, J. S.; Lichtner, P.; Shaikh, N.; Fendorf, S.; Cerrato, J. M., Effect of bicarbonate, calcium, and pH on the reactivity of As(V) and U(VI) mixtures. *Environ. Sci. Technol.* **2020**.

31. Tokunaga, T. K.; Kim, Y.; Wan, J.; Yang, L., Aqueous uranium (VI) concentrations controlled by calcium uranyl vanadate precipitates. *Environ. Sci. & Technol.* **2012,** *46*, (14), 7471-7477.

32. Chernorukov, N.; Nipruk, O.; Knyazev, A.; Pykhova, Y. P., Synthesis and study of uranyl arsenate $(UO_2)_3(AsO_4)_2 \cdot 12H_2O$. *Russ. J. Inorg. Chem.* **2011,** *56*, (2), 163-167.

CHAPTER 5. PRECIPITATION OF AQUEOUS URANYL AND ARSENATE WITH PHOSPHATE AND LIMESTONE

Isabel Meza,[1,2] Jorge Gonzalez-Estrella,[3] Annie Jane Burns, [1,2] Peter C. Burns,[4] Virginia Rodriguez,[4] Juan S Lezama-Pacheco,[5] Scott Fendorf,[5] Abdul-Mehdi S. Ali,[6] Peter Lichtner,[2] Kaelin Gagnon,[1,2] Han Hua,[1,2] and José M. Cerrato[1,2]*

*Corresponding email address: jcerrato@unm.edu, mameza@unm.edu

Telephone: (001) (505) 277-0870

Fax: (001) (505) 277-1918

[1] Department of Civil, Construction & Environmental Engineering, MSC01 1070, University of New Mexico, Albuquerque, NM, 87131, USA

[2] Center for Water and the Environment, UNM, Albuquerque, NM, 87131, USA

[3] School of Civil and Environmental Engineering, College of Engineering, Architecture, and Technology, Oklahoma State University, Stillwater, OK, 74078, USA

[4] Department of Civil and Environmental Engineering and Earth Sciences, University of Notre Dame, Notre Dame, Indiana 46556, USA and Department of Chemistry and Biochemistry, University of Notre Dame, Notre Dame, IN, 46556, USA

[5] Department of Environmental Earth System Science, Stanford University, Stanford, CA 94305, United States

[6] Department of Earth and Planetary Sciences, MSC03 2040, University of New Mexico, Albuquerque, NM, 87131, USA

Abstract.

We investigated the conditions that favor precipitation of uranyl [$(UO_2)^{2+}$] and arsenate [$(AsO_4)^{3-}$] from aqueous solutions with and without phosphate [$(PO_4)^{3-}$] and natural limestone in batch reactions with an initial pH of 3.0 or 7.0 using a combination of aqueous chemistry and solid analyses. The interaction of impacted waters containing dissolved $(UO_2)^{2+}$ and $(AsO_4)^{3-}$ with various minerals can retard their mobility by mechanisms including adsorption, precipitation, and ion exchange. Uranyl and $(AsO_4)^{3-}$ are known to adsorb and precipitate onto and with calcium phosphates. Batch reactions initiated at pH 3.0 in the presence of limestone resulted in a significant decrease in the aqueous concentrations of $(UO_2)^{2+}$ and $(AsO_4)^{3-}$ from 1.0 to 0.03 mM (>75%), and without limestone, from 1.0 to 0.25 mM (~75% for $(UO_2)^{2+}$ and ~60% of $(AsO_4)^{3-}$). In batch reactions initiated at pH 3.0 and 7.0 containing limestone and $(PO_4)^{3-}$, the aqueous concentration of $(UO_2)^{2+}$ was reduced from 0.05 to 1.7 x 10^{-7} mM (>98%) with initial concentrations of 0.05 for $(UO_2)^{2+}$ and $(AsO_4)^{3-}$ and 1.0 mM of $(PO_4)^{3-}$. Arsenate concentrations decreased ($(AsO_4)^{3-}$ ~15% and $(UO_2)^{2+}$ ~ 89%) in aqueous batch reactions with and without limestone when Ca was added with initial concentrations of 0.05 for $(UO_2)^{2+}$ and $(AsO_4)^{3-}$, 1.0 mM of $(PO_4)^{3-}$, and 2.0 mM of Ca at initial pH 3.0 and 7.0. In batch experiments in which substantial amounts of $(UO_2)^{2+}$ were removed from the aqueous solution uranyl arsenate or uranyl phosphate solids precipitated, but in the cases where uranyl phosphates formed, arsenate did not co-precipitate significantly. Addition of limestone to the aqueous systems enhanced $(UO_2)^{2+}$ removal because it neutralized the acidic systems to pH 7.0 thus minimizing the solubility of uranyl arsenate and uranyl phosphate solids, and because it provided Ca^{2+} cations needed to precipitate low-solubility uranyl arsenates and phosphates. The current results indicate that treatment of contaminated water with acidic or neutral pH with limestone amended with $(PO_4)^{3-}$ may be highly effective for removal of $(UO_2)^{2+}$ but less-so for removal of $(AsO_4)^{3-}$.

INTRODUCTION

Uranyl arsenate minerals have been reported from several Southwestern US mining sites.[1-3] During the uranium boom of the 1950s and 1960s that was driven by the Cold War, uranium was extensively mined in the U.S. Southwest. Much of the mining activity occurred on Native American land and has left a lasting legacy of contamination. In the Navajo Nation alone there are more than 500 abandoned uranium mine sites and remediation will cost billions of dollars.[4-11] Our previous work and studies by others have shown that waters on Southwest Native American lands impacting by mining can contain uranyl [$(UO_2)^{2+}$] concentrations 20 times higher than the maximum concentration limit (MCL) of 30 μg L^{-1} U set by the Environmental Protection Agency (EPA). Such waters have also been found to contain arsenate [$(AsO_4)^{3-}$] concentrations more than three times the EPA MCL (10 μg L^{-1} As).[12-16]

The aqueous speciation of $(UO_2)^{2+}$ is complicated owing to the numerous ligands that complex it and also a strong pH dependence. Under acidic conditions (pH<4) the $(UO_2)^{2+}$ ion is generally the dominant aqueous species, but the speciation is much more complex at circum-neutral and basic conditions in part due to the emergence of anionic uranyl carbonate complexes. In a vadose zone containing groundwater that is somewhat acidic, most mineral surfaces will be positively charged owing to protonation and thus the uranyl ion does not adsorb onto them. Under basic conditions, most mineral surfaces have a negative charge, but the uranyl speciation is dominated by anionic uranyl carbonates that also do not adsorb. As such, stable uranyl species in environmentally relevant conditions limit remediation approaches based on adsorption and precipitation with natural minerals. The formation of ternary uranyl aqueous complexes such as $Ca_2UO_2(CO_3)_3^0{}_{(aq)}$ increase U mobility. [2, 17] In our previous study we observed that uranyl arsenate solids are stable in aqueous solution at pH 3.0 but at pH 7.0 dissolution is enhanced by formation

of ternary Ca uranyl carbonate complexes.[18] Furthermore, the availability of environmentally relevant ions in solution, like bicarbonate and $(PO_4)^{3-}$, can release $(AsO_4)^{3-}$ through competitive ion displacement.[19] Nevertheless, research has also found that $(UO_2)^{2+}$ and $(AsO_4)^{3-}$ can decrease in concentration when amendments with $(PO_4)^{3-}$, and both limestone and apatite have been used in batch experiments at pH 3.0 and 7.0.[20, 21]

Interaction of aqueous solutions containing $(UO_2)^{2+}$ and $(AsO_4)^{3-}$ with naturally abundant minerals such as calcite and apatite can cause immobilization of these metals, and amendments with both have been considered as potential remediation pathways.[20-22] Uranyl and $(AsO_4)^{3-}$ can adsorb and precipitate onto and with calcium phosphate minerals including autunite, hydroxyapatite, and fluorapatite.[21-25] Uranyl and $(AsO_4)^{3-}$ immobilization may be the result of adsorption to apatite; formation of $(UO_2)^{2+}$ and $(AsO_4)^{3-}$-phosphate ternary surface complexes with strong sediment surface binding; and co-precipitation with calcium phosphate solids.[21, 25] However, the mechanisms involved in the sorption and coprecipitation of $(UO_2)^{2+}$ and $(AsO_4)^{3-}$ onto and with limestone and $(PO_4)^{3-}$ remain limited.

In the present study, we used spectroscopy, microscopy, and aqueous chemical analysis to investigate $(UO_2)^{2+}$ and $(AsO_4)^{3-}$ removal from aqueous solutions upon addition of natural limestone and $(PO_4)^{3-}$ in batch experiments initially at pH 3.0 and 7.0. Our study revealed the role of Ca in removal of $(UO_2)^{2+}$ and $(AsO_4)^{3-}$ in an aqueous system amended with $(PO_4)^{3-}$ and natural limestone. The information gained from this research is relevant for water remediation strategies and risk reduction strategies.

5.1. Materials and methods.

5.1.1. Limestone source and characterization.

Limestone collected from the Sandia Formation, Sandia Mountains, near Albuquerque, New Mexico was used in this study. The specimen was crushed and sieved to obtain a surface area of ~2 m^2 g^{-1}. X-ray fluorescence (XRF) and energy-dispersive X-ray (EDX) spectroscopies were used to study the composition of the limestone. Nitrogen (N_2) sorptometry (Micromeritics Gemini 2360 BET Surface Area Analyzer) was used to quantify the Brunauer, Emmett, and Teller (BET) specific surface area after samples were degasified at 80° C.[26] Zeta potential data were acquired with a Malvern Zetasizer Nano-ZS equipped with a He–Ne laser (633 nm) and non-invasive backscatter optics. All samples were suspended at 0.1 mg mL^{-1} concentration. Measurements were acquired at 25 °C. The zeta potential for all the samples was measured in triplicate according to the Smoluchowski theory. All reported values correspond to the average of three different samples measurements.

5.1.2. Batch Experiments.

Batch experiments were conducted in which aqueous solutions containing $(UO_2)^{2+}$ as uranyl acetate $[(UO_2)[CH_3COO)_2(H_2O)_2]$ and arsenate $(AsO_4)^{3-}$ as sodium arsenate $[Na_2HAsO_4(H_2O)_7]$ and they were adjusted to specific pH targets. In one set of experiments the aqueous solutions contained 1 mM of both $(UO_2)^{2+}$ and $(AsO_4)^{3-}$. The pH values of the initial solutions (prior to addition of limestone) were adjusted to 3.0 using hydrochloric acid (HCl) and 7.0 by adding sodium hydroxide (NaOH). Fifty mL centrifuge tubes with or without 50 mg of natural limestone (1000 mg L^{-1}) were used as the reactors. The batch reactions were done in triplicate including those without limestone. In the second and third sets of experiments we used aqueous solutions containing initially 0.05 mM for uranyl $(UO_2)^{2+}$ as uranyl nitrate

$[UO_2(NO_3)_2(H_2O)_6]$ and $(AsO_4)^{3-}$ as pentaoxide arsenic (As_2O_5) as these concentrations are more environmentally relevant than the higher concentrations used in the first set of experiments. The solutions were adjusted to initial pH values of 3.0 and 7.0 using nitric acid (HNO_3) and ammonium hydroxide (NH_4OH), respectively. For the second set of experiments we added 1.0 mM of $(PO_4)^{3-}$ as NH_6PO_4, and for the third set of experiments we added 2.0 mM of Ca as $CaCl_2$. Powdered limestone was added as 400 mg/L for set two experiments and 1000 mg/L for set three experiments. Otherwise, identical experiments lacking limestone additions were also conducted and all experiments are summarized in Table 1.

Liquid samples (0.5 – 2 mL) were taken from each batch reactor at 0, 0.25, 24, and 48 h for the first set of experiments, and 0, 15, 30, 60, 120, 480, 720, 1440, 21600, and 44640 minutes for the second and third sets of experiments. These samples were passed through 0.2 µm membranes, acidified by addition of 2% HNO_3, and refrigerated at 4 °C prior to subsequent analyses. The As, U, and Ca concentrations in the solutions were quantified by inductively coupled plasma optical emission spectroscopy (ICP-OES) as described below. The P concentrations were measure using an ion chromatography system (ICS). Where precipitates formed, they were collected for analyses.

5.1.3. Solid Analyses.

Solid samples were analyzed using powder X-ray diffraction (XRD), scanning electron microscopy (SEM), X-ray fluorescence (XRF), and X-ray absorption spectroscopy (XAS). The details of these analyses are described in the Supporting Information. Electron microprobe analyses were conducted using a JEOL JXA-8200 SuperProbe electron probe microanalyzer (EPMA) with wavelength dispersive X-ray spectroscopy (WDS) at an accelerating voltage of 15 kV with a 10 µm probe diameter and 10 nA probe current. The quantitative data was reduced using

the Phi-Rho-Z correction method in the Probe for EPMA software (Probe Software, Inc., Eugene, OR)

5.1.4. Solution analyses.

The metal concentration in each solution sample was measured using a PerkinElmer Optima 5300DV ICP-OES with a detection limit of 0.5 mg L^{-1}. Trace element concentrations were measured with a PerkinElmer NexION 300D (Dynamic Reaction Cell) ICP-MS with a detection limit of 0.5 μg L^{-1}. Both of these instruments were calibrated with a five-point calibration curve, and QA/QC measures were taken to ensure quality results. The P concentration was measured with an IC ThermoFisher/Dionex ICS 1100. Triplicates (three samples) were used for all the experiments.

5.1.5. Speciation Calculations.

Calculations were carried out using the open-source computer code PFLOTRAN that runs on MacOSX, linux, and Windows and Visual Minteq.[27] Speciation calculations were based on chemical equilibrium modeling using inputs from experimental conditions used in this study as a tool to gain insight into aqueous complexation and solid saturation state. PFLOTRAN can perform speciation calculations with options to input total and free ion concentrations, mineral and gas equilibrium constraints, and charge balance. The extended Debye-Hückel algorithm is used to compute activity.

5.2. Results and discussion

5.2.1. Limestone characterization.

Chemical and diffraction analysis confirmed that the natural limestone consists mostly of calcite ($CaCO_3$) with lesser quartz (SiO_2) in an approximately 5:1 molar ratio. Also, using the microprobe, the backscatter electron image suggested high concentrations of Ca, Si, Na, Mg, and

K. (Table S2). Limestone typically forms due to the precipitation of calcite during evaporation of an inland sea and detrital minerals such as quartz are typical. Minor elements detected include Fe (~1.5 wt.%), Al (~0.73 wt.%), Mg (~0.65 wt.%), K (~0.25 wt.%), and others (<0.08 wt.%).

Zeta potential analyses indicated the limestone used in this study is negatively charged from pH 2.0 to 9.0 at 25°C (Figure S1). These results agree with the available literature that presents quartz, albite, and calcite negative charged as well.[28-30]

5.2.2. Effect of uranyl and arsenate removal from aqueous solution with and without added limestone. The aqueous concentration of $(UO_2)^{2+}$ and $(AsO_4)^{3-}$ overall decreased by in all batch reactions performed starting with an initial pH of 3.0 in both the presence and absence of limestone (Figure 1A). Note that addition of limestone to these aqueous solutions causes the pH to increase to roughly 7 (Figure S3). Although these experiments with and without limestone were all initially at pH 3.0, the ending pH values are quite different with and without limestone. In batch reactions with an initial pH of 3.0, the concentration of $(UO_2)^{2+}$ and $(AsO_4)^{3-}$ decreased from 1.0 to 0.03 mM (>96%) in the presence of limestone, and from 1.0 to 0.25 mM (~75% for $(UO_2)^{2+}$ and ~40% of $(AsO_4)^{3-}$) without limestone. These results agree with an earlier study that showed the concentration of $(UO_2)^{2+}$ and $(AsO_4)^{3-}$ decreased >75% from initial concentrations of 1.0 mM of $(UO_2)^{2+}$ and $(AsO_4)^{3-}$ in an aqueous solution to which 10.0 mM of Ca was added at pH 3.0 owing to formation of precipitates and/or various complexes such as $UO_2AsH_2AsO_4^+$ at pH's ranging between 1.0 and 3.0, with a negative complex forming at neutral pH. [18,31]

In batch reactions of aqueous solutions of uranyl and arsenate with an initial pH of 7.0 with and without limestone considerably less $(UO_2)^{2+}$ and $(AsO_4)^{3-}$ were removed from solution than for experiments starting at pH 3.0 (removal values ranged from 25 to 6%). Trögerite is not likely to form under neutral pH conditions, and the extent of limestone dissolution in this batch

experiment would be modest. The pH was raised from an initial value 7.0 to 9.0 in batch reactions including limestone and to 8.0 in batch reactions without limestone (Figure S3). This pH raised could be due to the pK_{a3} of the As speciation, which is 11.60 and could have increased the pH in the whole U and As system.[32]

Precipitates rich in U and As were detected with limestone recovered from batch reactions with an initial pH of 3.0 and 7.0. These results indicate a heterogeneous distribution consistent with precipitation of U-rich compounds rather than removal by sorption onto limestone grains. The solids were examined in an SEM using EDS to characterize compositions (Figure 2A and 2B). These results agree with our PFLOTRAN modeling, where we found precipitation of $Na_{0.5}(H_3O)_{0.5}[(UO_2)(AsO_4)](H_2O)_{2.5(s)}$ using the equilibrium constant found in our previous study.[33] However, addition of limestone to these solutions causes a further decrease of the concentration of $(UO_2)^{2+}$ and $(AsO_4)^{3-}$. It is likely that a uranyl arsenate phase such as trögerite $[(UO_2)(H_2AsO_4)_2(H_2O)]$ precipitates in the limestone-free system. Addition of limestone that partially dissolved upon contact with the pH 3.0 solution potentially resulted in precipitation of uranospinite $[Ca(UO_2)_2(AsO_4)_2.10H_2O]$ owing to the addition of Ca. Whereas the solubility of this phase has not been studied, related uranyl phosphate and uranyl vanadate minerals are generally least soluble in aqueous solutions with pH in the range of 6-7[34] and the lower $(UO_2)^{2+}$ and $(AsO_4)^{3-}$ contents subsequent to addition of limestone may reflect simply the solubility of the precipitate formed. Addition of limestone also potentially provides sites for sorption and formation of co-precipitates. Limestone as a solid substrate can trigger heterogenous nucleation by adsorption or chemical bonding with metals.[35-38]

5.2.3. Effect of uranyl and arsenate removal from aqueous solution with added limestone and phosphate.

In all experiments carried out with an aqueous solution at an initial pH of 3.0 and supplied with 0.05 mM of $(UO_2)^{2+}$ and $(AsO_4)^{3-}$ and 1.0 mM of $(PO_4)^{3-}$, $(UO_2)^{2+}$ was largely removed from solution (>96%) both in the presence and absence of limestone (Figure C and D). Experiments carried out with an aqueous solution at an initial pH of 7.0 and supplied with 0.05 mM of $(UO_2)^{2+}$ and $(AsO_4)^{3-}$ and 1.0 mM of $(PO_4)^{3-}$ in the absence of limestone (Figure D) retained most of the $(UO_2)^{2+}$ (from ~0.05 to 0.04 mM (~25%) U) and $(AsO_4)^{3-}$ in solution. This is presumably due to the lack of a counter cation needed for precipitation of an autunite-type compound, whereas $(H_3O)^{+}$ was available at pH 3.0. Addition of limestone to an otherwise identical batch reaction caused a dramatic reduction of $(UO_2)^{2+}$ in solution from ~0.05 to 3.7 x 10^{-4} mM (>99%), although $(AsO_4)^{3-}$ was unaffected (Figure D). It is likely that Ca released by the dissolution of limestone triggered precipitation of autunite.

Uranium and P was found in the precipitates with limestone recovered from batch experiments with an initial pH of 3.0 and 7.0 as expected. SEM examination revealed the presence of grains containing both. U and P. It was not possible to confirm the presence of Ca in these phases owing to the abundance of limestone contained within the sample. Very little As was detected in these samples, which is consistent with the observation that it largely remained in the aqueous solution (Figure 2C and 2D). An earlier study utilizing an aqueous batch reaction at pH 4.0 with initial concentrations of 100 μM $(UO_2)^{2+}$ and 1000 μM $(PO_4)^{3-}$ observed that chernikovite $[H_3O(UO_2)(PO_4).3H_2O]$ precipitated in the absence of additional cations.[39] Given that our concentrations of $(UO_2)^{2+}$ and $(PO_4)^{3-}$ were higher, it is very likely that chernikovite precipitation in the batch experiment without limestone at pH 3.0 is the mechanism of $(UO_2)^{2+}$ removal. This is also consistent with the lack of removal of $(AsO_4)^{3-}$ in the same experiment. Addition of limestone

to an otherwise identical batch reaction caused the pH to move to 7.0 (Figure S4) and added dissolved Ca cations as the limestone partially dissolved. This likely caused precipitation of autunite [$Ca(UO_2)_2(PO_4)_2.11H_2O$] that is very insoluble in neutral pH conditions and was also found in Minteq´s modelling, or uramphite [$(NH_4)UO_2PO_4.3H_2O$].[40-42]

It is particularly notable that over the range of our batch reactions containing $(PO_4)^{3-}$, $(AsO_4)^{3-}$ did not co-precipitate into the uranyl phosphate phases that were responsible for removal of $(UO_2)^{2+}$ from solution. This is the case despite the close similarities between the crystal structures of many uranyl arsenates and uranyl phosphates and reflects the lower solubility of uranyl phosphates as compared to uranyl arsenates. It is also notable that formation of a ternary calcium uranyl carbonate species that are highly soluble at circumneutral pH[18, 43] did not occur owing to the presence of $(PO_4)^{3-}$ that caused precipitation of the U.

5.2.4. Effect of uranyl and arsenate removal from aqueous solution with limestone, $(PO_4)^{3-}$, and Ca.

Batch reactions were also conducted for aqueous systems initially containing 0.05 mM $(UO_2)^{2+}$, 0.04 mM $(AsO_4)^{3-}$, 1.0 mM $(PO_4)^{3-}$, and 2.0 mM of Ca both with and without added limestone with initial pH values of 3.0 and 7.0 (Figures E and F). In the batch reaction at an initial pH of 3.0 and with no added limestone, the concentration of $(UO_2)^{2+}$ was reduced to ~0.005 M and $(AsO_4)^{3-}$ decreased from 0.04 to 0.02 mM (~50%). In an earlier study, a batch reaction of 100 μM $(UO_2)^{2+}$ and 1000 μM $(PO_4)^{3-}$ with 5.0 mM Ca at pH 4.0 precipitated autunite[39], which is likely also the case here. Addition of limestone to an otherwise identical batch reaction with an initial pH of 3.0 caused the further removal of $(UO_2)^{2+}$ to ~0.001 M. This is likely because the pH rose to about 7 and autunite is less soluble at pH 7 than 3.[40] In the same experiments, the $(AsO_4)^{3-}$

concentration in solution decreased from 0.04 mM to ~0.02 mM in the absence of limestone, and to ~0.038 mM in the presence of limestone.

In batch reactions with an initial pH of 7.0, the $(UO_2)^{2+}$ concentration in solution was reduced from 0.05 to 1 x 10^{-4} mM with or without the addition of limestone. This is consistent with precipitation of autunite in both cases and is in contrast to the experiment at pH 7.0 that excluded Ca and limestone in which most of the $(UO_2)^{2+}$ remained in solution (Figure D). In these batch reactions the removal of $(AsO_4)^{3-}$ from solution was modest.

. Uranium and P was also found in the precipitates with limestone recovered from batch experiments with an initial pH of 3.0 and 7.0, very similar to the previous experiment without Ca. (Figures 2E). It is possible that some of these solids contain U and P and could also be associated with Ca (Figure 2E). However, as the experiment only with $(PO_4)^{3-}$, due to the abundance of Ca in limestone, it was challenging to determine the association of Ca with U and P. Arsenic was not found according to EDS and SEM analyses (Figure 2E).

These data suggests that U can be removed from water with precipitates like that contain Ca and PO_4. Research has found that U can be removed from water up to 74.4% using fluorapatite ($Ca_{10}(PO_4)_6F_2$), apatite, calcite ($CaCO_3$) or hydroxyapatite at pH 3.[22, 44] The U and As low concentrations also agree with literature found when hydroxyapatite or apatite was used for remediation and concentrations of U were nearly complete removed (>99.5%), by surface complexation between HA and U, and crystalline uranium(VI) phosphate solid phases like chernikovite and autunite can be precipitated.[44-46] These results also agree with the literature when using higher Ca:(P+As) ratio, As was removed more efficiently and pH variation (from 4.5 to 11.5) did not have a significant effect on As removal.[47]

5.5. Environmental Implications.

Reaction of phosphate in solution can increase U uptake through heterogenous precipitation through the formation of uranyl phosphate secondary phases. Reaction of 2 mM Ca and 1mM PO_4 in the initial phase of the reaction of U and As with limestone, results in chemical precipitation which also results in the decrease to 20-30% As. When U and As concentrations reach the saturation limit (at initial concentrations of 1 mM) the reaction with limestone enhances precipitation. However, at pH 7 most of the U and As remain in solution due to stability of uranyl-Ca-CO_3 aqueous complexes or low solubility of the solids. These results have relevant implications for the development of remediation strategies in contaminated sites making use of natural constituents such as limestone, Ca, and PO_4. The use of these natural constituents can be beneficial for the development of feasible remediation approaches that can be accessible to underserved communities affected mining legacy and other anthropogenic processes.

Batch reactions reported herein have demonstrated the effectiveness of a limestone and phosphate amendment for removal of uranyl ions from acidic and neutral pH water. In both cases the limestone provides Ca cations needed to form the very insoluble autunite-type uranyl phosphate compounds. In the case of an initially acidic water, the limestone neutralizes the pH into the range of minimum solubility for Ca uranyl phosphate minerals. Although some of the As in our batch reactions was removed from solution, amendments with limestone and phosphate were much less effective at removing As than U. This is a somewhat unexpected observation as we had initially hypothesized that $(AsO_4)^{3-}$ would co-precipitate in the target uranyl phosphate phases, but this was not the case perhaps owing to the significantly lower aqueous solubility of uranyl phosphates as compared to uranyl arsenates.

5.6. Acknowledgments.

Funding for this research was provided by the National Science Foundation (CAREER Award 1652619, CREST Award 1914490) and the National Institute of Environmental Health Sciences (Superfund Research Program Award 1 P42 ES025589 and R01ES027145). PCB´s contribution to this work was funded by the Chemical Sciences, Geosciences and Biosciences Division, Office of Basic Energy Sciences, Office of Science, U.S. Department of Energy, Grant No. DE-FG02–07ER15880. Any opinions, findings, and conclusions or recommendations expressed in this publication are those of the author(s) and do not necessarily reflect the views of the National Science Foundation, the National Institutes of Health, or the U.S. Department of Energy. Electron microprobe and scanning transmission electron microscopy were performed in the Electron Microbeam Analysis Facility, Department of Earth and Planetary Sciences and Institute of Meteoritics, University of New Mexico, a facility supported by the State of New Mexico, National Aeronautics and Space Administration (NASA), and the National Science Foundation. The TOC art was created with www.BioRender.com.

Supporting information.

Additional 1 table1 (Table S1) and 5 figures (Figures S1, S2, S3, S4, and S5) are available in SI.

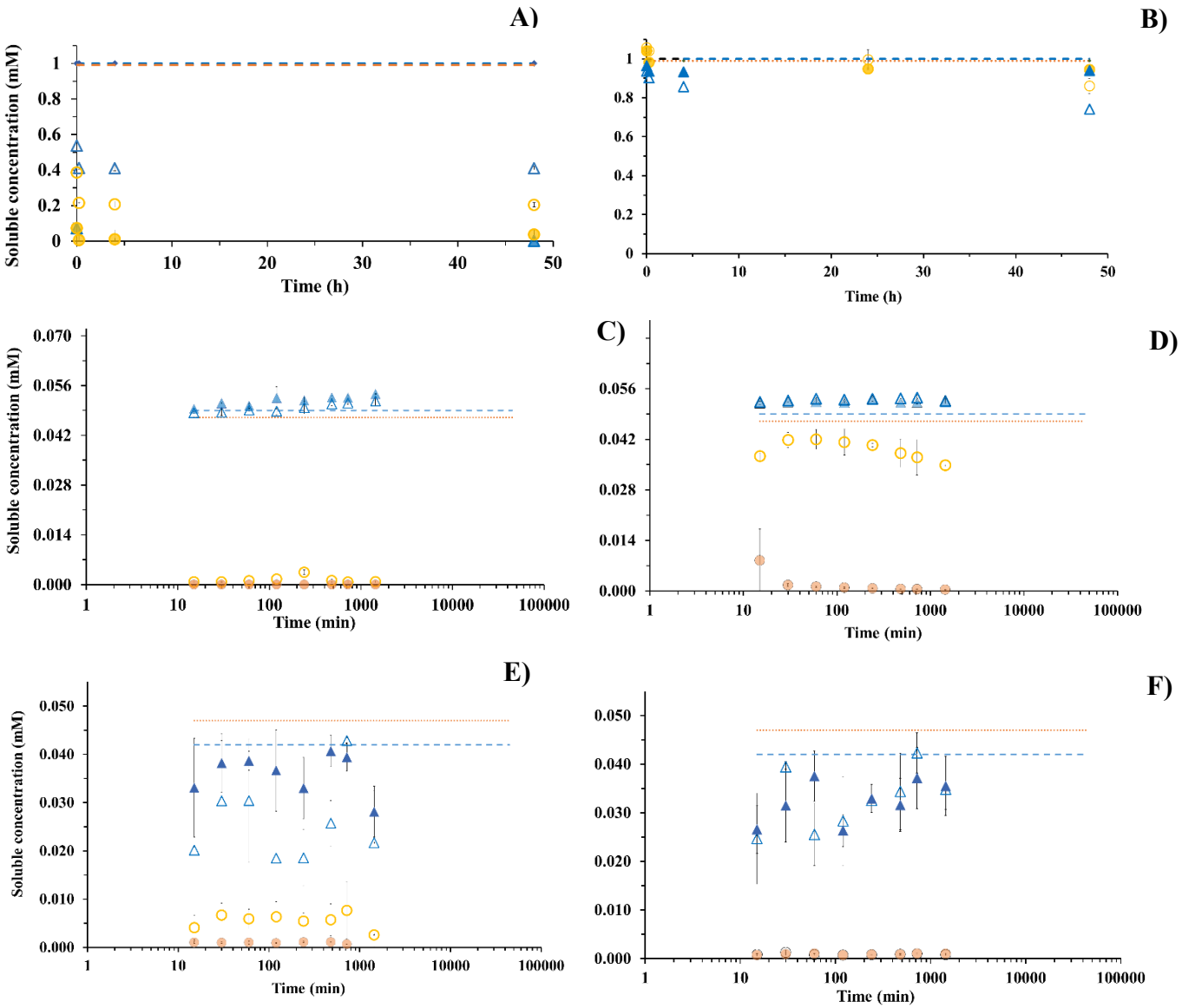
A)
B)
C)
D)
E)
F)
Soluble concentration (mM)
Time (h)
Time (min)

Figure 1. Time course concentration of U (circles) and As (triangles). Batch experiments supplied with limestone and U are represented with filled circles (●) and with limestone and As are represented with filled triangles (▲). Control experiments without limestone are represented with open circles (○) for U and open triangles (△) for As. Straight lines represent the stock solutions of U (···)and As (——) A) Experiments supplied with 1mM of U and As, 1000 mg L^{-1} of limestone carried out at pH 3 B) Experiments supplied with 1mM of U and As, 1000 mg L^{-1} of limestone carried out at pH 7, C) Experiments supplied with 0.05 mM of U and As, 400 mg L^{-1} of limestone, and 1 mM of PO_4 carried out at pH 3, D) Experiments supplied with 0.05 mM of U and As, 400 mg L^{-1} of limestone, and 1 mM of PO_4 carried out at pH 7, E) Experiments supplied with 0.05 mM of U and As, 1000 mg L^{-1} of limestone, 1 mM of PO_4 and 2 mM of Ca carried out at pH 3, F) Experiments supplied with 0.05 mM of U and As, 1000 mg L^{-1} of limestone, 1 mM of PO_4 and 2 mM of Ca carried out at pH 7.

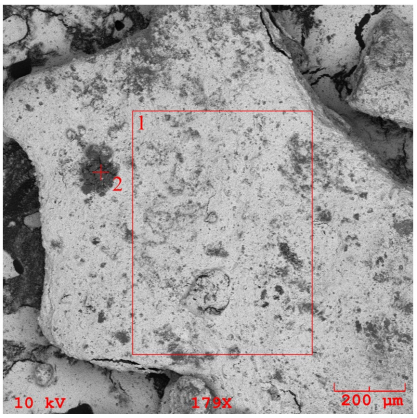
1
2
10 kV
179X
200 µm

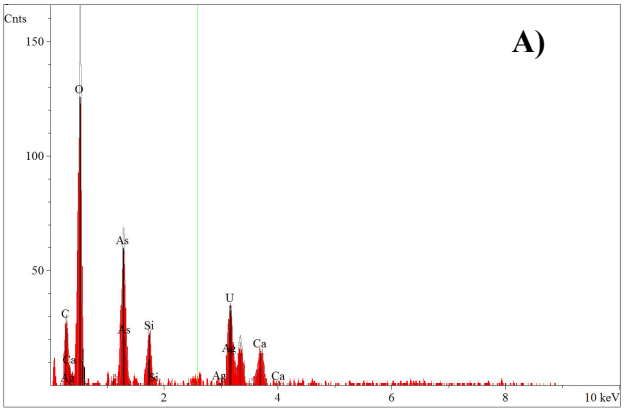
A)
Cnts
150
100
50
O
As
C
Si
U
Ca
2
4
6
8
10 keV

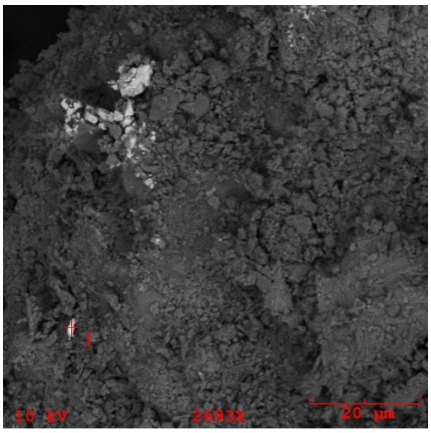
1
2
10 kV
2693X
20 µm

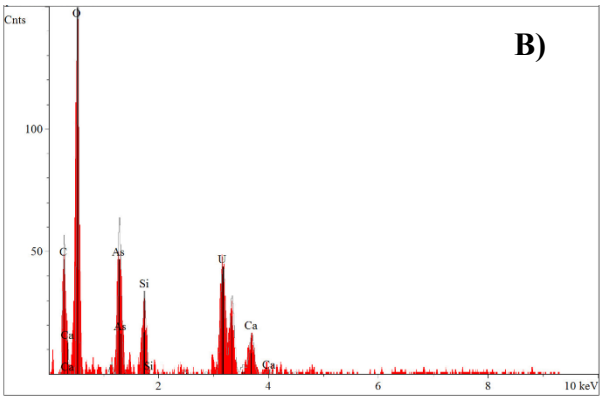
B)
Cnts
100
50
O
C
As
Si
U
Ca
2
4
6
8
10 keV

C)

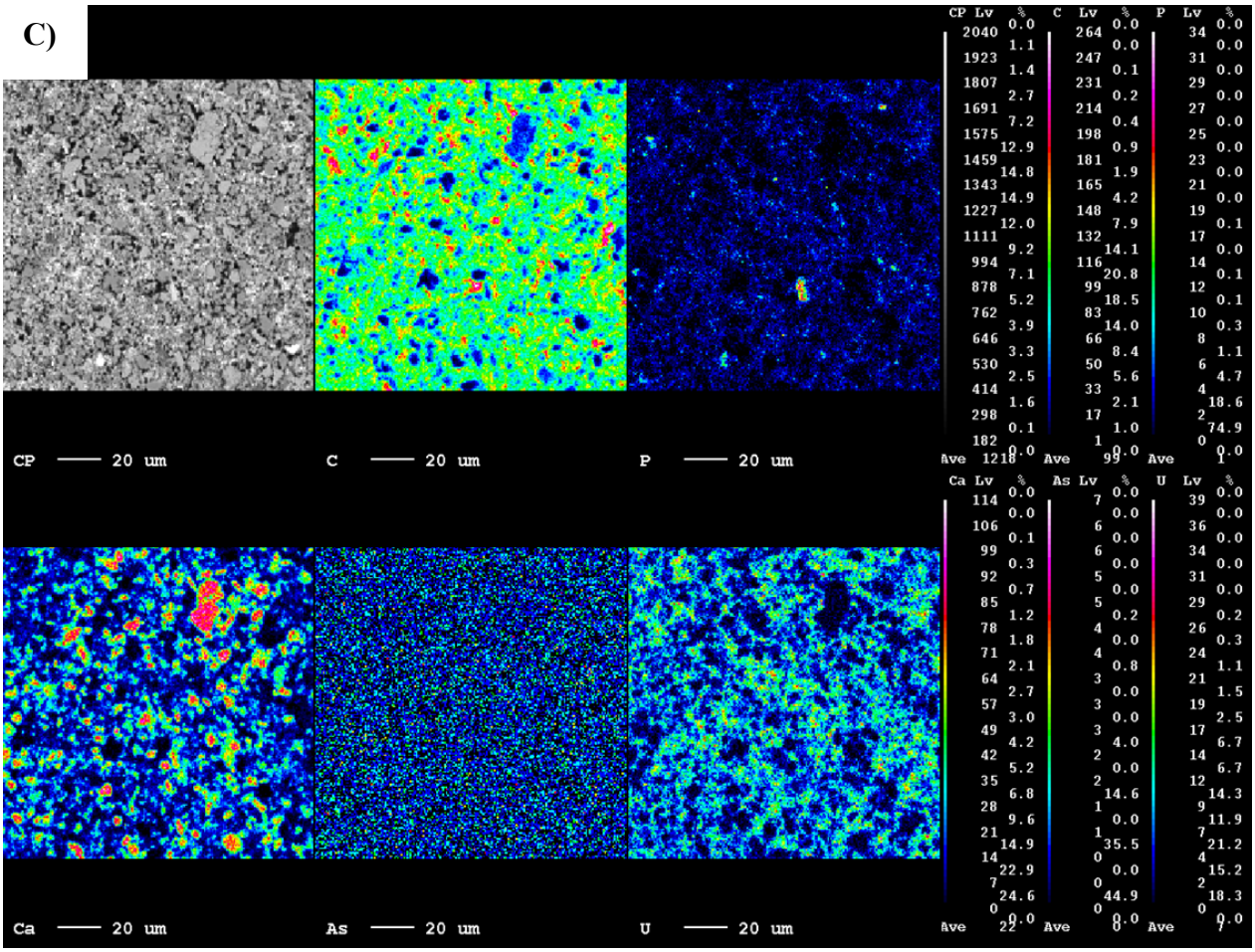
CP 20 um
C 20 um
P 20 um
Ca 20 um
As 20 um
U 20 um
CP Lv %
C Lv %
P Lv %
Ca Lv %
As Lv %
U Lv %
Ave
Ave
Ave
Ave
Ave
Ave

D)

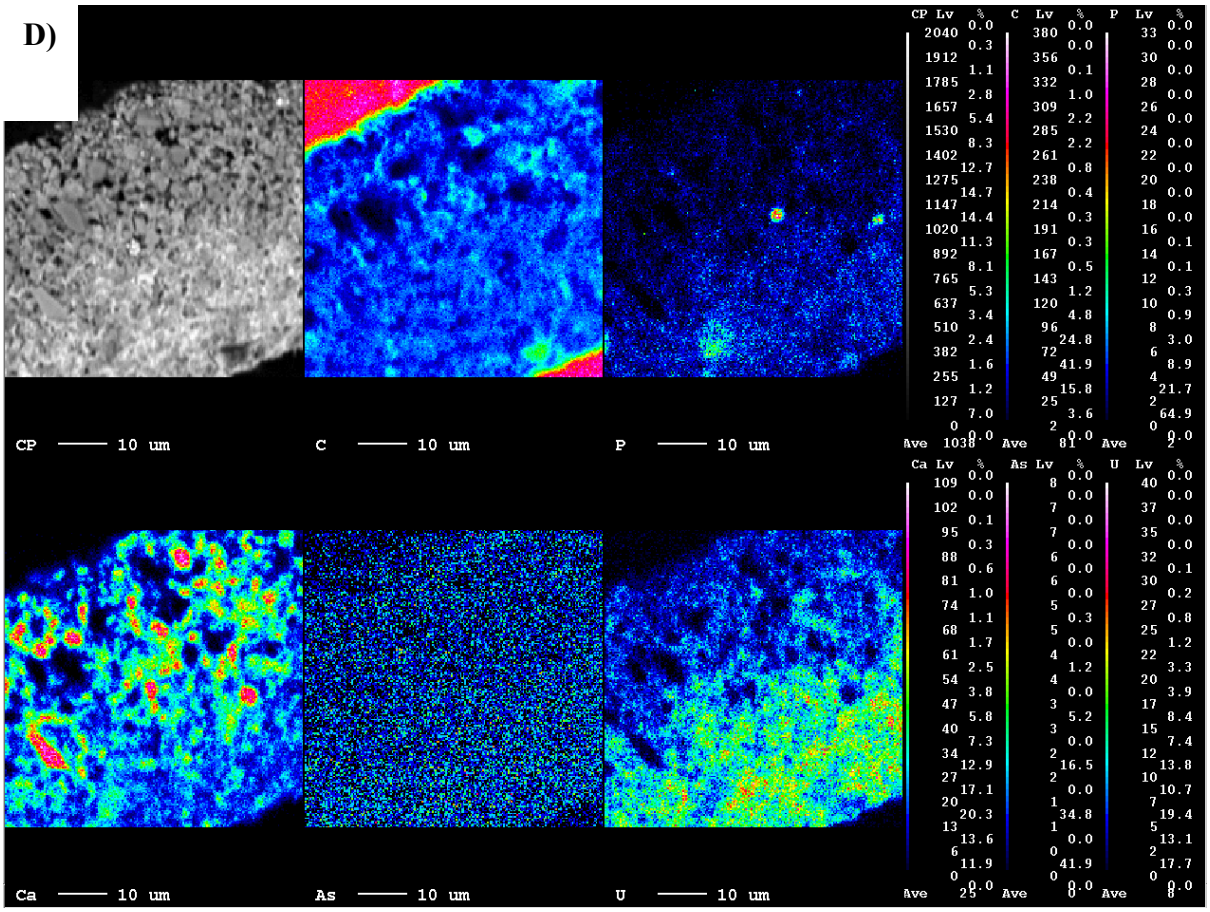
CP 10 um
C 10 um
P 10 um
Ca 10 um
As 10 um
U 10 um
CP Lv
C Lv
P Lv
Ca Lv
As Lv
U Lv
Ave 1038
Ave 81
Ave 2
Ave 25
Ave 0
Ave 8

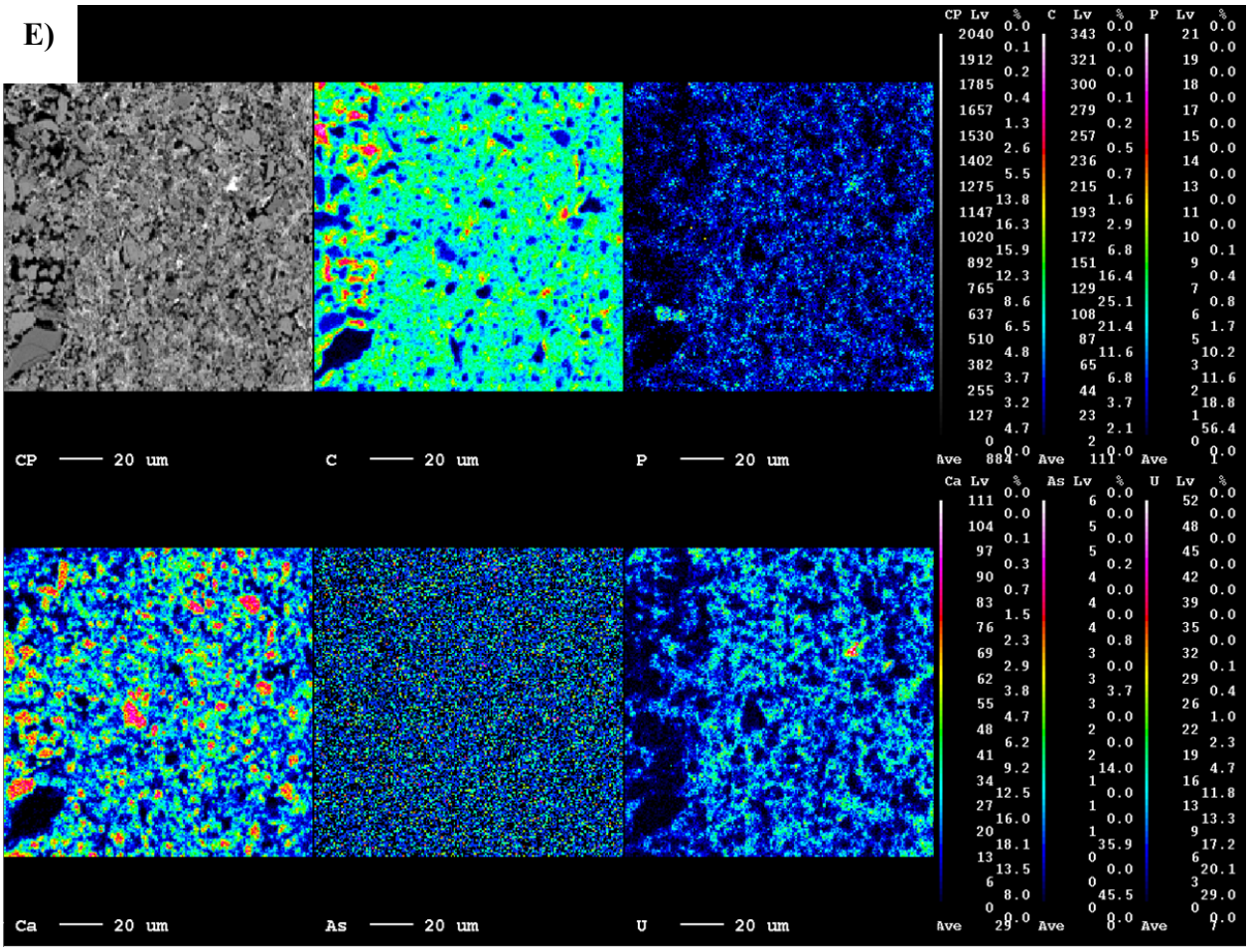

Figure 2. SEM/EDS analyses of precipitates recovered from experiments initiated with: A) 1 mM U and As, 1000 mg L^{-1} of limestone at pH 3, B) 1 mM U and As, 1000 mg L^{-1} of limestone at pH 7, EPMA maps of C) 0.05 mM U and As, 1 mM PO_4, 400 mgL^{-1} of limestone at pH 3, D) 0.05 mM U and As, 1 mM PO_4, 400 mg L^{-1} of limestone at pH 7, E) 0.05 mM U and As, 1 mM PO_4, 2 mM of Ca, 1000 mg L^{-1} of limestone at pH 7.

Table 1. Experimental set up

Treatment (label)	Reagents used as As and U source	Initial pH	Limestone (mg L^{-1})	PO_4 (mM)	Ca (mM)	As (mM)	U (mM)
1. U-As-L	$[Na_2HAsO_4(H_2O)_7]$ $(UO_2)[CH_3COO)_2(H_2O)_2]$	3 or 7	1000	0	0	1	1
2. U-As-PO_4-L	(As_2O_5) $[UO_2(NO_3)_2(H_2O)_6]$	3 or 7	400	1	0	0.05	0.05
3. U-As-Ca-PO_4-L	(As_2O_5) $[UO_2(NO_3)_2(H_2O)_6]$	3 or 7	1000	1	3	0.05	0.05
1. U-As-L-C	$[Na_2HAsO_4(H_2O)_7]$ $(UO_2)[CH_3COO)_2(H_2O)_2]$	3 or 7	0	0	0	1	1
2. U-As-PO_4-L-C	(As_2O_5) $[UO_2(NO_3)_2(H_2O)_6]$	3 or 7	0	1	0	0.05	0.05
3. U-As-Ca-PO_4-L-C	(As_2O_5) $[UO_2(NO_3)_2(H_2O)_6]$	3 or 7	0	1	3	0.05	0.05

REFERENCES

1. Dzik, E. A.; Lobeck, H. L.; Zhang, L.; Burns, P. C., Thermodynamic properties of phosphate members of the meta-autunite group: A high-temperature calorimetric study. *J. Chem. Thermodyn.* **2017,** *114*, 165-171.

2. Blake, J. M.; Avasarala, S.; Ali, A.-M. S.; Spilde, M.; Lezama-Pacheco, J. S.; Latta, D.; Artyushkova, K.; Ilgen, A. G.; Shuey, C.; Nez, C.; Cerrato, J. M., Reactivity of As and U co-occurring in mine wastes in northeastern Arizona. *Chem. Geol.* **2019,** *522*, 26-37.

3. Corkhill, C. L.; Crean, D. E.; Bailey, D. J.; Makepeace, C.; Stennett, M. C.; Tappero, R.; Grolimund, D.; Hyatt, N. C., Multi-scale investigation of uranium attenuation by arsenic at an abandoned uranium mine, South Terras. *NPJ Mater. Degrad.* **2017,** *1*, (1), 19.

4. Crowley, K. D., Managing the Environmental Legacy of US Nuclear-Weapons Production: Although the waste from America's arms buildup will never be" cleaned up," human and environmental risks can be reduced and managed. *Am. Sci.* **2002,** *90*, (6), 514.

5. USEPA, Federal Actions to Address Impacts of Uranium Contamination in the Navajo Nation Five-Year Plan Summary Report. In US Environmental Protection Agency: Pacific Southwest, Region 9: San Francisco CA, 2013.

6. NRC, *Uranium mining in Virginia: scientific, technical, environmental, human health and safety, and regulatory aspects of uranium mining and processing in Virginia*. National Research Council. National Academies Press: 2012.

7. Hund, L.; Bedrick, E. J.; Miller, C.; Huerta, G.; Nez, T.; Ramone, S.; Shuey, C.; Cajero, M.; Lewis, J., A Bayesian framework for estimating disease risk due to exposure to uranium mine and mill waste on the Navajo Nation. *J. R. Stat. Soc. Ser. A-Stat. Soc.* **2015,** *178*, (4), 1069-1091.

8. Schmoker, J. W.; Krystinik, K. B.; Halley, R. B., Selected characteristics of limestone and dolomite reservoirs in the United-States. *Aapg Bulletin-American Association of Petroleum Geologists* **1985,** *69*, (5), 733-741.

9. Allan, R. J., Impact of Mining Activities on the Terrestrial and Aquatic Environment with Emphasis on Mitigation and Remedial Measures. In *Heavy Metals: Problems and Solutions*, Förstner, U.; Salomons, W.; Mader, P., Eds. Springer Berlin Heidelberg: Berlin, Heidelberg, 1995; pp 119-140.

10. Wufuer, R.; Wei, Y.; Lin, Q.; Wang, H.; Song, W.; Liu, W.; Zhang, D.; Pan, X.; Gadd, G. M., Chapter Four - Uranium Bioreduction and Biomineralization. In *Adv. Appl. Microbiol*, Sariaslani, S.; Gadd, G. M., Eds. Academic Press: 2017; Vol. 101, pp 137-168.

11. Kapaj, S.; Peterson, H.; Liber, K.; Bhattacharya, P., Human Health Effects From Chronic Arsenic Poisoning–A Review. *J. Environ. Sci, Part A* **2006,** *41*, (10), 2399-2428.

12. Agency, E. P., National Primary Drinking Water Regulations. In Regulations, N. P. D. W., Ed. Environmental Protection Agency, 2019.

13. Roccaro, P.; Vagliasindi, F. G. A., Coprecipitation of vanadium with iron(III) in drinking water: a pilot-scale study. *Desalination Water Treat.* **2015,** *55*, (3), 799-809.

14. USEPA, Addressing uranium contamination on the Navajo Nation. U.S. . In Environmental Protection Agency, P acific Southwest, Region 9.: San Francisco, CA,, 2015.

15. Avasarala, S.; Lichtner, P. C.; Ali, A.-M. S.; González-Pinzón, R.; Blake, J. M.; Cerrato, J. M., Reactive Transport of U and V from Abandoned Uranium Mine Wastes. *Environ. Sci. & Technol.* **2017,** *51*, (21), 12385-12393.

16. Blake, J. M.; Avasarala, S.; Artyushkova, K.; Ali, A.-M. S.; Brearley, A. J.; Shuey, C.; Robinson, W. P.; Nez, C.; Bill, S.; Lewis, J., Elevated concentrations of U and co-occurring metals

in abandoned mine wastes in a northeastern Arizona Native American community. *Environ. Sci. Technol.* **2015,** *49*, (14), 8506-8514.

17. Dong, W.; Ball, W. P.; Liu, C.; Wang, Z.; Stone, A. T.; Bai, J.; Zachara, J. M., Influence of calcite and dissolved calcium on uranium(VI) sorption to a Hanford subsurface sediment. *Environ. Sci. Technol.* **2005,** *39*, (20), 7949-7955.

18. Gonzalez-Estrella, J.; Meza, I.; Burns, A. J.; Ali, A.-M. S.; Lezama-Pacheco, J. S.; Lichtner, P.; Shaikh, N.; Fendorf, S.; Cerrato, J. M., Effect of bicarbonate, calcium, and pH on the reactivity of As(V) and U(VI) mixtures. *Environ. Sci. Technol.* **2020**.

19. DeVore, C.; Freire, L. R.; Gonzalez-Estrella, J.; Villa, N.; Ali, A. M.; Ducheneaux, C.; Artyushkova, K.; Cerrato, J., Investigation of the effect of microbial processes on arsenic stability in sediments from Cheyenne River, South Dakota, USA. *Abstr. Pap. Am. Chem. Soc.* **2019,** *257*, 1.

20. Lizama-Allende, K.; Henry-Pinilla, D.; Diaz-Droguett, D. E. J. W., Air,; Pollution, S., Removal of Arsenic and Iron from Acidic Water Using Zeolite and Limestone: Batch and Column Studies. *Water Air Soil Pollut.* **2017,** *228*, (8), 275.

21. Moore, R. C.; Szecsody, J.; Rigali, M. J.; Vermuel, V.; Leullen, J. *Assessment of a Hydroxyapatite Permeable Reactive Barrier to Remediate Uranium at the Old Rifle Site Colorado*; United States, 2016; p 9.

22. Rakovan, J.; Reeder, R. J.; Elzinga, E. J.; Cherniak, D. J.; Tait, C. D.; Morris, D. E., Structural Characterization of U(VI) in Apatite by X-ray Absorption Spectroscopy. *Environ. Sci. Technol.* **2002,** *36*, (14), 3114-3117.

23. DeVore, C. L.; El Hayek, E.; Busch, T.; Long, B.; Mann, M.; Rudgers, J. A.; Ali, A.-M. S.; Howard, T.; Spilde, M. N.; Brearley, A.; Ducheneaux, C.; Cerrato, J. M., Arsenic Accumulation

in Hydroponically Grown Schizachyrium scoparium (Little Bluestem) Amended with Root-Colonizing Endophytes. *ACS Earth Space Chem.* **2021,** *5*, (6), 1278-1287.

24. Pan, Z.; Giammar, D. E.; Mehta, V.; Troyer, L. D.; Catalano, J. G.; Wang, Z., Phosphate-Induced Immobilization of Uranium in Hanford Sediments. *Environ. Sci. Technol.* **2016,** *50*, (24), 13486-13494.

25. Wen Hang, H.; Pan, Z.; Giammar, D.; Li, L., Enhanced uranium immobilization by phosphate amendment under variable geochemical and flow conditions: insights from reactive transport modeling. *Environ. Sci. Technol.* **2018,** *52*, (10), 5841-5850.

26. Brunauer, S., Adsorption of gases in multimolecular layers. *J. Am. Chem. Soc.* **1938,** *60*, (2), 309.

27. Lichtner, P. C.; Hammond, G. E.; Lu, C.; Karra, S.; Bisht, G.; Andre, B.; Mills, R.; Kumar, J. *PFLOTRAN User Manual: A Massively Parallel Reactive Flow and Transport Model for Describing Surface and Subsurface Processes*; LA-UR-15-20403 United States 10.2172/1168703 LANL English; Los Alamos National Lab. (LANL): 2015; p Medium: ED; Size: 197 p.

28. Kaya, A.; Yukselen, Y., Zeta potential of clay minerals and quartz contaminated by heavy metals. *Can. Geotech. J.* **2005,** *42*, (5), 1280-1289.

29. Alroudhan, A.; Vinogradov, J.; Jackson, M. D., Zeta potential of intact natural limestone: Impact of potential-determining ions Ca, Mg and SO4. *Colloids Surf. A: Physicochem. Eng. Asp.* **2016,** *493*, 83-98.

30. Jie, Z.; Weiqing, W.; Jing, L.; Yang, H.; Qiming, F.; Hong, Z., Fe(III) as an activator for the flotation of spodumene, albite, and quartz minerals. *Miner. Eng.* **2014,** *61*, 16-22.

31. Gezahegne, W. A.; Hennig, C.; Geipel, G.; Planer-Friedrich, B.; Merkel, B. J., Challenges in Detection, Structural Characterization and Determination of Complex Formation Constants of

Uranyl-Arsenate Complexes in Aqueous Solutions. In *The New Uranium Mining Boom: Challenge and Lessons learned*, Merkel, B.; Schipek, M., Eds. Springer Berlin Heidelberg: Berlin, Heidelberg, 2012; pp 607-616.

32. Benjamin, M. M., *Water Chemistry*. Boston : McGraw-Hill, ©2002.: 2002.

33. Meza. I.; Gonzalez-Estrella, J. B., P.C.; Rodriguez, V.; Velasco, C. A.; Sigmon, G. E.; Szymanowsky, J. E.S.; Forbes, T. Z.; Applegate, L. M.; Ali, A.M.; Lichtner, P.; Cerrato, J.M., Solubility and thermodynamic investigation of meta-autunite group uranyl arsenate solids with monovalent cations sodium (Na) and potassium (K) *Environ. Sci. Technol.* **2022 (Submitted)**.

34. Tokunaga, T. K.; Kim, Y.; Wan, J., Potential Remediation Approach for Uranium-Contaminated Groundwaters Through Potassium Uranyl Vanadate Precipitation. *Environmental Science & Technology* **2009,** *43*, (14), 5467-5471.

35. Stumm, W.; Morgan, J. J., Aquatic Chemistry : Chemical Equilibria and Rates in Natural Waters. **2013**.

36. Lizama Allende, K.; Fletcher, T. D.; Sun, G., The effect of substrate media on the removal of arsenic, boron and iron from an acidic wastewater in planted column reactors. *Chem. Eng. J.* **2012,** *179*, 119-130.

37. Groudev, S.; Georgiev, P.; Spasova, I.; Nicolova, M., Bioremediation of acid mine drainage in a uranium deposit. *Hydrometallurgy* **2008,** *94*, (1), 93-99.

38. Ye, Z. H.; Lin, Z. Q.; Whiting, S. N.; de Souza, M. P.; Terry, N., Possible use of constructed wetland to remove selenocyanate, arsenic, and boron from electric utility wastewater. *Chemosphere* **2003,** *52*, (9), 1571-1579.

39. Mehta, V. S.; Maillot, F.; Wang, Z.; Catalano, J. G.; Giammar, D. E., Effect of co-solutes on the products and solubility of uranium(VI) precipitated with phosphate. *Chem. Geol.* **2014,** *364*, 66-75.

40. Gorman-Lewis, D.; Shvareva, T.; Kubatko, K.-A.; Burns, P. C.; Wellman, D. M.; McNamara, B.; Szymanowski, J. E. S.; Navrotsky, A.; Fein, J. B., Thermodynamic properties of autunite, uranyl hydrogen phosphate, and uranyl orthophosphate from solubility and calorimetric measurements. *Environ. Sci. Technol.* **2009,** *43*, (19), 7416-7422.

41. Gustafsson, J. P. *Visual Minteq. 3 v. 3*, e; Jon Petter Gustafsson at KTH: Stockholm, Sweden, 2012.

42. Foster, R. I.; Kim, K.-W.; Lee, K., Uranyl phosphate (MUO2PO4, M = Na+, K+, NH4+) precipitation for uranium sequestering: formation and physicochemical characterisation. *Journal of Radioanalytical and Nuclear Chemistry* **2020,** *324*, (3), 1265-1273.

43. Dong, W.; Brooks, S. C., Determination of the formation constants of ternary complexes of uranyl and carbonate with alkaline earth metals (Mg^{2+}, Ca^{2+}, Sr^{2+}, and Ba^{2+}) using anion exchange method. *Environ. Sci. Technol.* **2006,** *40*, (15), 4689-4695.

44. Fuller, C. C.; Bargar, J. R.; Davis, J. A.; Piana, M. J., Mechanisms of Uranium Interactions with Hydroxyapatite: Implications for Groundwater Remediation. *Environ. Sci. Technol.* **2002,** *36*, (2), 158-165.

45. Arey, J. S.; Seaman, J. C.; Bertsch, P. M., Immobilization of Uranium in Contaminated Sediments by Hydroxyapatite Addition. *Environ. Sci. Technol.* **1999,** *33*, (2), 337-342.

46. Alexandratos, V. G.; Elzinga, E. J.; Reeder, R. J., Arsenate uptake by calcite: Macroscopic and spectroscopic characterization of adsorption and incorporation mechanisms. *Geochim. Cosmochim. Acta* **2007,** *71*, (17), 4172-4187.

47. Dungkaew, W.; Haller, K. J.; Flood, A. E.; Scamehorn, J. F., Arsenic Removal by Precipitation with Calcium Phosphate Hydroxyapatite. *Adv. Mat. Res.* **2012,** *506*, 413-416.

CHAPTER 6. IMPLICATIONS AND RECOMMENDATIONS FOR FUTURE RESEARCH

The concentrations of U and As that have exceeded the maximum contaminant levels (MCL) in surface waters neighboring U mineral deposits is a concern for nearby communities. This study investigated the mechanisms affecting the reaction of metal mixtures such as U, As, and other co-occurring elements in natural waters with minerals such as limestone for remediation applications.

This work is significant given that the reactions studied here may occur in remediation processes of U and As (or $UAs_{(s)}$) such as treatment of acid mine drainage solutions (acid conditions with pH between 2 and 4) and natural waters (circumneutral pH ~7). Knowing the thermodynamics from $UAs_{(s)}$ and understanding changes in functional chemistry at pH 3 and pH 7 is environmentally relevant due to the influence on chemical reactions that could impact U and As mobility and transport from the U mineralized deposits to surface waters and plants. This work highlights the importance of fundamental knowledge from $UAs_{(s)}$, and the application of natural minerals that affect surface complexation, precipitation, and solubilization reactions that should be consider in reactive transport models for risk assessment.

The results from this investigation advance understanding of the solubility, thermodynamics, and kinetics of U and As in conditions relevant for remediation applications. Furthermore, our results suggest that treatment of contaminated water with acidic or neutral pH with limestone amended with $(PO_4)^{3-}$ may be highly effective for removal of U but less-so for removal of As.

The findings reported in this Ph.D. dissertation also identify the need for further investigations with dissolution experiments at higher pH, not acidic, to see the effect of the

carbonate and hydroxide thermodynamics and kinetics of $UAs_{(s)}$. Especially, evaluating the influence of uranyl carbonate and oxyhydroxide secondary phases on soluble U and As concentrations in solutions. Also, given the significant amount of Ca in limestone, $UAs_{(s)}$ with Ca might form, so dissolution and precipitation experiments with synthesized uranospinite could be insightful on U and As mobilization in water. Lastly, comparing limestone from different places could be used in future experiments to see the effect of U and As removal.

APPENDIX A. SUPPORTING INFORMATION: SOLUBILITY AND THERMODYNAMIC INVESTIGATION OF META-AUTUNITE GROUP URANYL ARSENATE SOLIDS WITH MONOVALENT CATIONS SODIUM (NA) AND POTASSIUM (K)

Synthesis. 0.5 M aqueous solutions of uranyl nitrate [$UO_2(NO_3)_2$] and arsenic pentoxide (As_2O_5) were diffused into 0.05 M aqueous solutions of sodium nitrate ($NaNO_3$) and potassium nitrate (KNO_3), cation-containing (Na^+ or K^+) barrier solutions (Table S1). A Fisher Scientific, Accumet pH probe was used to measure the pH of the barrier solutions. The pH of the barrier solution was initially adjusted as described in Dzik et al.[11] and crystallization of solid occurred over 15 d. After enough crystals had formed on the lips of the vials, the barrier solution was decanted, and the crystals were harvested using vacuum filtration. All reagents, unless stated otherwise, were analytical grade. $NaNO_3$ (≥99.9%, Fisher) and KNO_3 (≥99.0%, VWR Analytical) were used to prepare the barrier solutions. Aqueous [$UO_2(NO_3)_2$] (98-102%, IBI Labs) and aqueous As_2O_5 (98%, Aldrich) were used to create saturated solutions. A few drops of 15.8 M nitric acid (HNO_3) were used to adjust the pH of the barrier solution.

Solid analyses. When sufficient sample was available, a conventional powder diffractometer was used to provide the highest possible resolution. When sample quantity was limited, as was the case for samples of solids collected after solubility experiments, a single-crystal diffractometer was used to collect powder diffraction data using a transmission geometry. Conventional diffraction patterns were collected using a Bruker D8 Advance DaVinci diffractometer with Bragg-Brentano geometry and CuKα radiation. Samples were ground dry in a mortar and pestle, and then placed onto a zero-background quartz slide. Data were collected over the 2Θ range of 5 to 60° with a step size of 0.01° and counting time of 1s/step. The sample was rotated about the normal to the slide

during data collection. Owing to the (001) platy morphology of the compounds, the diffraction intensities reflect a strong preferred orientation.

In the cases where sample quantity was very limited, a small amount of powder was mixed with epoxy and mounted on a glass fiber. The sample was then placed on a four-circle Rigaku XtaLAB Synergy X-ray diffractometer with a PhotonJet micro-focus sealed X-ray tube producing CuKα radiation and a HyPix-6000HE detector. During exposure the goniometer was used to move the sample in a Gandolfi-like fashion to randomize sample orientation. This methodology yielded a powder diffraction pattern reflecting a much-reduced amount of preferred orientation as compared to the conventional diffractometer.

All diffractograms were analyzed with the ICCD PDF-4+ software and CrystalDiffract was used to prepare illustrations. Note that diffraction patterns for a given compound collected using the two different methods described above are expected to differ in the relative intensities of reflections owing to the differing amounts of preferred orientation of crystallites.

Crystals of uranyl arsenate solids of the meta-autunite group can have variable hydration states. Thermogravimetric analyses (TGA) were performed using a TA Instruments Q50. Approximately 20 mg of each sample was placed in an alumina crucible and the solid material was heated from ambient to 800°C at a rate of 5°C/min under constant N_2 flow. The measured weight losses were used to calculate the water content in each sample.

Chemical analyses of the solid phases were conducted using a Cameca SX-100 electron microprobe. An accelerating voltage of 15 KV was used, with a beam size up to 10 μm and a beam current of 25 nA. The beam was rastered to minimize damage to the extent that the sample size allowed. Standards of uranium dioxide (UO_2), arsenic metal (As), microcline (K), and Amelia

Albite (Na) were used for quantification procedures. Uncertainties (2σ mean) are based on counting statistics and are ≤ 2% for Na, K, As and U, whereas oxygen (O) was calculated stoichiometrically. For all samples, spots analyzed were homogeneous in relation to their major element composition (75 μm diameter or larger) based on backscatter electron images that were also collected on the electron microprobe. During analysis damage caused by the electron beam was evident, especially in the absence of beam rastering. Sensitivity to the electron beam is typical of alkali-cation bearing hydrous uranyl compounds and most likely corresponds to loss of water and migration of the alkali cations during irradiation.

Solution analyses. The soluble molar concentrations of U, As, Na, and K were measured using a PerkinElmer Optima 5300DV ICP-OES with a detection limit of 0.5 mg L^{-1}. Trace element concentrations were measured with a PerkinElmer NexION 300D (Dynamic Reaction Cell) ICP-MS with a detection limit of 0.5 μg L^{-1}. Both ICPs were calibrated with Fischer Scientific Standards with a five-point calibration curve, and QA/QC measures were taken to ensure quality results. Triplicates were used for all the experiments.

Table S1. Experimental description for the synthesis of uranyl arsenate solids.

Sample name	Vial 1	Vial 2	Barrier solution	pH of barrier solution
NaUAs	0.5 M $UO_2(NO_3)_2(H_2O)_{6(aq)}$	0.5 M As_2O_5	0.05 M $NaNO_3$	5.83
KUAs	0.5 M $UO_2(NO_3)_2(H_2O)_{6(aq)}$	0.5 M As_2O_5	0.05 M KNO_3	5.66

Table S2. Equilibrium concentrations of dissolved species and pH measurements used in solubility calculations of NaUAs and KUAs.

pH range	Experiment	U (mM)	As (mM)	Na (mM)	K (mM)	Final pH
1.5 to 2	Dissolution NaUAs	1.81	1.81	1.30	--	1.98
	Precipitation NaUAs	3.61	3.62	4.2	--	1.96
	Dissolution KUAs	1.40	1.40	--	1.41	1.96
	Precipitation KUAs	1.90	1.90	--	3.0	1.94
2.6 to 3	Dissolution NaUAs	0.13	0.73	1.4	--	3.01
	Precipitation NaUAs	0.07	0.59	6.5	--	2.98
	Dissolution KUAs	0.11	0.10	--	1.07	3.03
	Precipitation KUAs	0.12	0.13	--	1.81	3.00

Table S3. Speciation equations and thermodynamic relations.

Term	Equation	Units
1. Mineral reaction	$M \leftrightarrow \sum \nu_j A_j$	NA
2. Activity product (Q)	$Q = \prod_j (\gamma_j C_j)^{\nu_j}$	(--)
3. Total concontration of primary species in solution	$C_j^{tot} = C_j + \sum_i \nu_{ji} * C_i$	Molal
4. Law of mass action for aqueous complexes	$C_i = \frac{K_i}{\gamma_i} \prod_j (\gamma_j C_j)^{\nu_{ji}}$	Molal
5. Ionic strength	$I = \frac{1}{2} \sum_{l = \text{all ions}} C_l z_l^2$	Molal
6. Debye-Hückel	$\log \gamma_l = \frac{-A z_l^2 \sqrt{I}}{1 + å_l B \sqrt{I}} + bI$ $A = 0.51$ $B = 0.33$ $å_l$ = ion size parameter for Na^+ or K^+ = 4 or 3, for $(AsO_4)^{3-}$ = 4, for $(UO_2)^{2+}$ = 5	L mol^{-1}
7. Solubility product	$K_{sp} = \frac{\prod_j (\gamma_j C_j).^{\nu_j}}{a_M}, \quad a_M = 1$	Unitless
8. Saturation Index	$SI = log\left(\frac{Q}{K_{sp}}\right)$	Unitless
9. Gibbs Free Energy of reaction	$\Delta G°_r = -2.303RT\ x\ Log\ K_{sp}$	kJ mol^{-1}
10. Gibbs Free Energy of formation	$\Delta G°_{f(NaUAs)} = 3\Delta G°_{f(H_2O)} + \Delta G°_{f(UO_2)^{2+}} + \Delta G°_{f(AsO_4)^{3-}} + \Delta G°_{f(Na^+)} - \Delta G°_r$	kJ mol^{-1}
11. Entropy of formation	$\Delta S°_f = \frac{\Delta H°_f - \Delta G°_f}{T}$	kJ mol^{-1} K^{-1}
12. Dissolution/precipitation reaction NaUAs	$NaUO_2AsO_4 \cdot 3H_2O_{(s)} \leftrightarrow Na^+ + (UO_2)^{2+} + (AsO_4)^{3-} + 3(H_2O)$	(--)
13. Dissolution reaction KUAs	$KUO_2AsO_4 \cdot 3H_2O_{(s)} \leftrightarrow K^+ + (UO_2)^{2+} + (AsO_4)^{3-} + 3(H_2O)$	(--)

ν_j = Stoichiometric coefficients, A_j = Symbol for jth primary species, M = Mineral: KUAs or NaUAs, ν_{ji} = Stoichiometric coefficients for aqueous complexing reactions, j = primary species (e.g. $(UO_2)^{2+}$, $(AsO_4)^{3-}$, K^+, H^+ ...), C_j^{eq} = Concentration of jth species in equilibrium, Total concentration of jth primary species, a = activity, i = Secondary species [aqueous complexes] (e.g. $(OH)^-$, $(H_2AsO_4)^-$), K_i = Equilibrium constant, γi = activity coefficient, C_i = free ion concentration of i ($\frac{mol}{L}$), z_i = charge on species i (--), T = Temperature (K).

Table S4. Primary species and thermodynamic equilibrium constants (at T = 25°C) for aqueous complexes used in the reactive transport model (PFLOTRAN).[67]

Primary species and reaction aqueous complexes	
Primary species	
H^+	
AsO_4^{3-}	
UO_2^{2+}	
Na^+	
K^+	
CO_2	
NO_3^-	
Uranyl arsenate aqueous complexes	**Log K_{eq}**
$UO_2^{2+} + AsO_4^{3-} + H^+ \leftrightarrow UO_2HAsO_4^0$	**18.76**
$UO_2^{2+} + AsO_4^{3-} + 2H^+ \leftrightarrow UO_2H_2AsO_4^+$	**21.95**
$UO_2^{2+} + 2AsO_4^{3-} + 4H^+ \leftrightarrow UO_2(H_2AsO_4)_2^0$	**41.53**
Aqueous complexes	
$H_3AsO_4 \leftrightarrow AsO_4^{3-} + 3H^+$	**20.63**
$H_2AsO_4^- \leftrightarrow AsO_4^{3-} + 2H^+$	**18.37**
$HAsO_4^{2-} \leftrightarrow AsO_4^{3-} + H^+$	**11.6**
$UO_2NO_3^+ \leftrightarrow NO_3^- + UO_2^{2+}$	**-0.10**
$NaNO_3 \leftrightarrow NO_3^- + Na^+$	**0.40**
$KNO_3 \leftrightarrow NO_3^- + K^+$	**0.15**
$NaNO_3 \leftrightarrow NO_3^- + Na^+$	**-0.4**
$UO_2OH^+ + H^+ \leftrightarrow H_2O + UO_2^{2+}$	**-5.25**
$(UO_2)_2(OH)^{3+} + H^+ \leftrightarrow H_2O + 2UO_2^{2+}$	**-2.70**
$(UO_2)_2(OH)_2^{2+} + 2H^+ \leftrightarrow 2H_2O + 2UO_2^{2+}$	**-5.62**
$HCO_3^- + H^+ \leftrightarrow H_2O + CO_2$	**6.35**
$UO_2CO_3 + 2H^+ \leftrightarrow H_2O + UO_2^{2+} + CO_2$	**6.74**
$UO_2(OH)_2 + 2H^+ \leftrightarrow 2H_2O + UO_2^{2+}$	**12.15**
$H_2O \leftrightarrow OH^- + H^+$	**-14.00**
$(UO_2)_3(OH)_4^{2+} + 5H+ \leftrightarrow 5H_2O + 3UO_2^{2+}$	**-11.90**
$(UO_2)_3(OH)_5^+ + 5H^+ \leftrightarrow 5H_2O + 3UO_2^{2+}$	**-15.55**
$NaOH + H^+ \leftrightarrow H_2O + Na^+$	**14.75**
$KOH + H^+ \leftrightarrow H_2O + K^+$	**14.46**
$UO_2(OH)^{3-} + 3H^+ \leftrightarrow 3H_2O + UO_2^{2+}$	**20.25**
$CO_3^{2-} 2H+ \leftrightarrow H_2O + UO_2^{2+} + CO_2$	**16.68**
$(UO_2)_2(CO_3)(OH)^{3-} + 5H^+ \leftrightarrow 4H_2O + 2UO_2^{2+} + CO_2$	**17.54**
$NaHCO_3 + H^+ \leftrightarrow H_2O + Na^+ + CO_2$	**6.6**
$NaCO_3^- + 2H^+ \leftrightarrow H_2O + Na^+ + CO_2$	**15.41**

Table S5. Elemental characterization of uranyl arsenate solids NaUAs and KUAs.

Primary species		ICP-OES			µProbe	
		Concentration (mM)	Concentration (%)	SD (mM)	Molecular ratio (avg)	Molecular ratio (SD)
NaUAs	As	5.54	13.81	0.04	0.24	0.03
	Na	2.61	2.00	0.01	0.11	0.09
	U	5.36	47.15	0.02	0.21	0.01
KUAs	As	4.92	18.23	0.10	0.24	0.02
	K	2.56	4.96	0.05	0.21	0.02
	U	4.63	54.47	0.09	0.21	0.01

Table S6. Solubility product with different Na molarities for NaUAs at pH ranges from 1.5 to 2 to 2.6 to 3, and for KUAs equimolar. Dissolution vs precipitation.

Experimental pH range	Mineral phase	Molar ratios (U:As:Na:H)	Dissolution reactions	Mass action equations	Log K_{sp} dissolution	Log K_{sp} precipitation
1.5 to 2	NaUAs	1:1:1:0	$Na_{0.5}(H_3O)_{0.5}(UO_2)(AsO_4)(H_2O)_{2.5(s)} \leftrightarrow (AsO_4)^{3-}+(UO_2)^{2+}+0.5Na^{+}+0.5(H_3O)^{+}+2.5H_2O$	$K_{sp}=a(UO_2)^{2+} \cdot a(AsO_4)^{3-} \cdot a^{0.5}Na^{+} \cdot a^{0.5}(H_3O)^{+}$	-23.98	-23.19
		1:1:0.7:0.3			-23.70	-23.06
		1:1:0.5:0.5			-23.50	-22.95
		1:1:0.25:0.75			-23.29	-22.85
2.6 to 3		1:1:1:0			-23.09	-22.75
		1:1:0.7:0.3			-23.13	-22.98
		1:1:0.5:0.5			-23.15	-23.15
		1:1:0.25:0.75			-23.18	-23.33
1.5 to 2	KUAs	1:1:0.9:0.1	$K_{0.9}(UO_2)(H_3O)_{0.1}(AsO_4)(H_2O)_{2.5(s)} \leftrightarrow (AsO_4)^{3-}+(UO_2)^{2+}+0.9K^{+}+0.1(H_3O)^{+}+2.5H_2O$	$K_{sp}= a(UO_2)^{2+} \cdot a(AsO_4)^{3-} \cdot a^{0.9}K^{+} \cdot a^{0.1}(H_3O)^{+}$	-23.87	-23.50
2.6 to 3					-23.57	-23.38

Table S7. Saturation index with different Na molarities for NaUAs at pH ranges from 1.5 to 2 to 2.6 to 3, and for KUAs equimolar, using the log K_{sp} from the dissolution experiments.

Experimental pH range	Mineral phase	Molar ratios (U:As:Na/K:H)	Dissolution reactions	Mass action equations	Log Saturation Index (SI)
1.5 to 2	**NaUAs**	1:1:1:0	$Na_{0.5}(H_3O)_{0.5}(UO_2)(AsO_4)(H_2O)_{2.5(s)} \leftrightarrow (AsO_4)^{3-}+(UO_2)^{2+}+0.5Na^{+}+0.5(H_3O)^{+}+2.5H_2O$	$K_{sp}=a(UO_2)^{2+} \cdot a(AsO_4)^{3-} \cdot a^{0.5}Na^{+} \cdot a^{0.5}(H_3O)^{+}$	0.79
		1:1:0.7:0.3			0.65
		1:1:0.48:0.52			0.54
		1:1:0.25:0.75			0.44
2.6 to 3		1:1:1:0			0.35
		1:1:0.7:0.3			0.14
		1:1:0.48:0.52			0.00
		1:1:0.25:0.75			0.15
1.5 to 2	**KUAs**	1:1:0.9:0.1	$K_{0.9}(UO_2)(H_3O)_{0.1}(AsO_4)(H_2O)_{2.5(s)} \leftrightarrow (AsO_4)^{3-}+(UO_2)^{2+}+0.9K^{+}+0.1(H_3O)^{+}+2.5H_2O$	$K_{sp}= a(UO_2)^{2+} \cdot a(AsO_4)^{3-} \cdot a^{0.9}K^{+} \cdot a^{0.1}(H_3O)^{+}$	0.37
2.6 to 3					0.19

Table S8. Solubility product without aqueous uranyl-arsenate complexes with different Na molarities for NaUAs at pH ranges from 1.5 to 2 to 2.6 to 3, and for KUAs equimolar, without aqueous uranyl-arsenate complexes.

Experimental pH range	Mineral phase	Molar ratios (U:As:Na:H)	Dissolution reactions	Mass action equations	Log K_{sp}
1.5 to 2	**NaUAs**	1:1:1:0	$Na_{0.5}(H_3O)_{0.5}(UO_2)(AsO_4)(H_2O)_{2.5(s)} \leftrightarrow (AsO_4)^{3-}+(UO_2)^{2+}+0.5Na^{+}+0.5(H_3O)^{+}+2.5H_2O$	$K_{sp}=a(UO_2)^{2+} \cdot a(AsO_4)^{3-} \cdot a^{0.5}Na^{+} \cdot a^{0.5}(H_3O)^{+}$	-23.41
		1:1:0.7:0.3			-23.13
		1:1:0.48:0.52			-22.93
		1:1:0.25:0.75			-22.72
2.6 to 3		1:1:1:0			-22.47
		1:1:0.7:0.3			-22.51
		1:1:0.48:0.52			-22.53
		1:1:0.25:0.75			-22.56
1.5 to 2	**KUAs**	1:1:0.9:0.1	$K_{0.9}(UO_2)(H_3O)_{0.1}(AsO_4)(H_2O)_{2.5(s)} \leftrightarrow (AsO_4)^{3-}+(UO_2)^{2+}+0.9K^{+}+0.1(H_3O)^{+}+2.5H_2O$	$K_{sp}= a(UO_2)^{2+} \cdot a(AsO_4)^{3-} \cdot a^{0.9}K^{+} \cdot a^{0.1}(H_3O)^{+}$	-23.41
2.6 to 3					-23.34

Table S9. Enthalpy of drop solution $\Delta H°_{ds}$ (kJ mol^{-1}) for NaUAs and KUAs in sodium molybdate solvent at 975 K. The average value and associated error (two standard deviations from the mean) is also provided.

NaUAs		**KUAs**	
(mg)	(kJ mol^{-1})	(mg)	(kJ mol^{-1})
4.69	585.1	7.46	550.22
4.63	545.8	6.30	591.78
6.06	511.8	4.84	563.83
5.11	513.8	5.52	498.23
4.41	515.6	5.32	501.49
5.86	496.6	6.17	485.37
5.19	487.8	5.59	491.78
4.42	528.4	5.39	508.89
	523.1 ± 21.7		**524.0 ± 27.8**

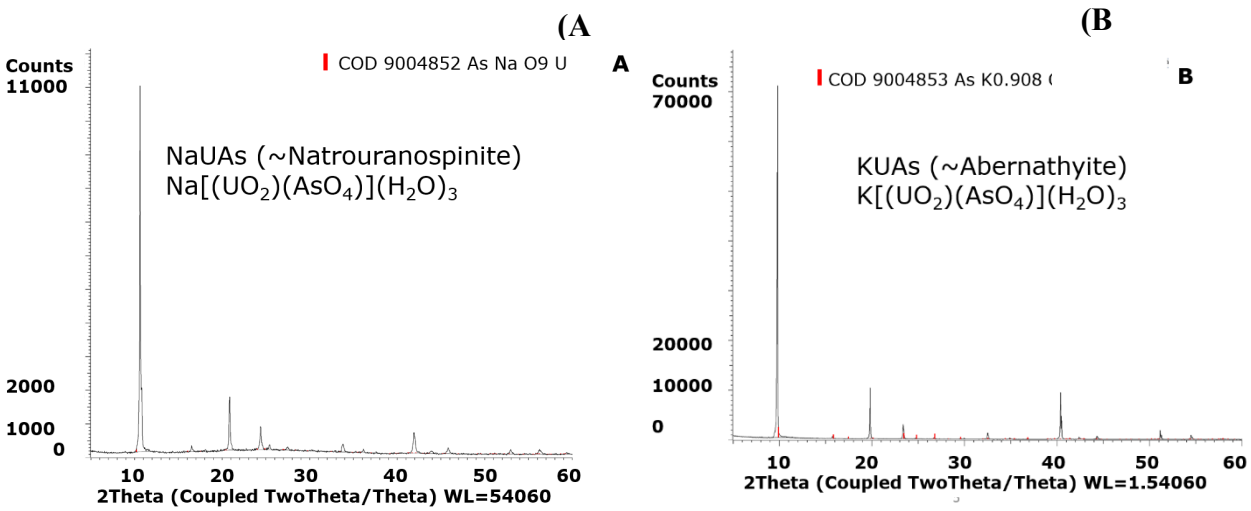

Figure S1. Powder X-ray diffraction patterns of synthetic A) $Na[(UO_2)(AsO_4)](H_2O)_3$ and B) $K[(UO_2)(AsO_4)](H_2O)_3$ starting material.

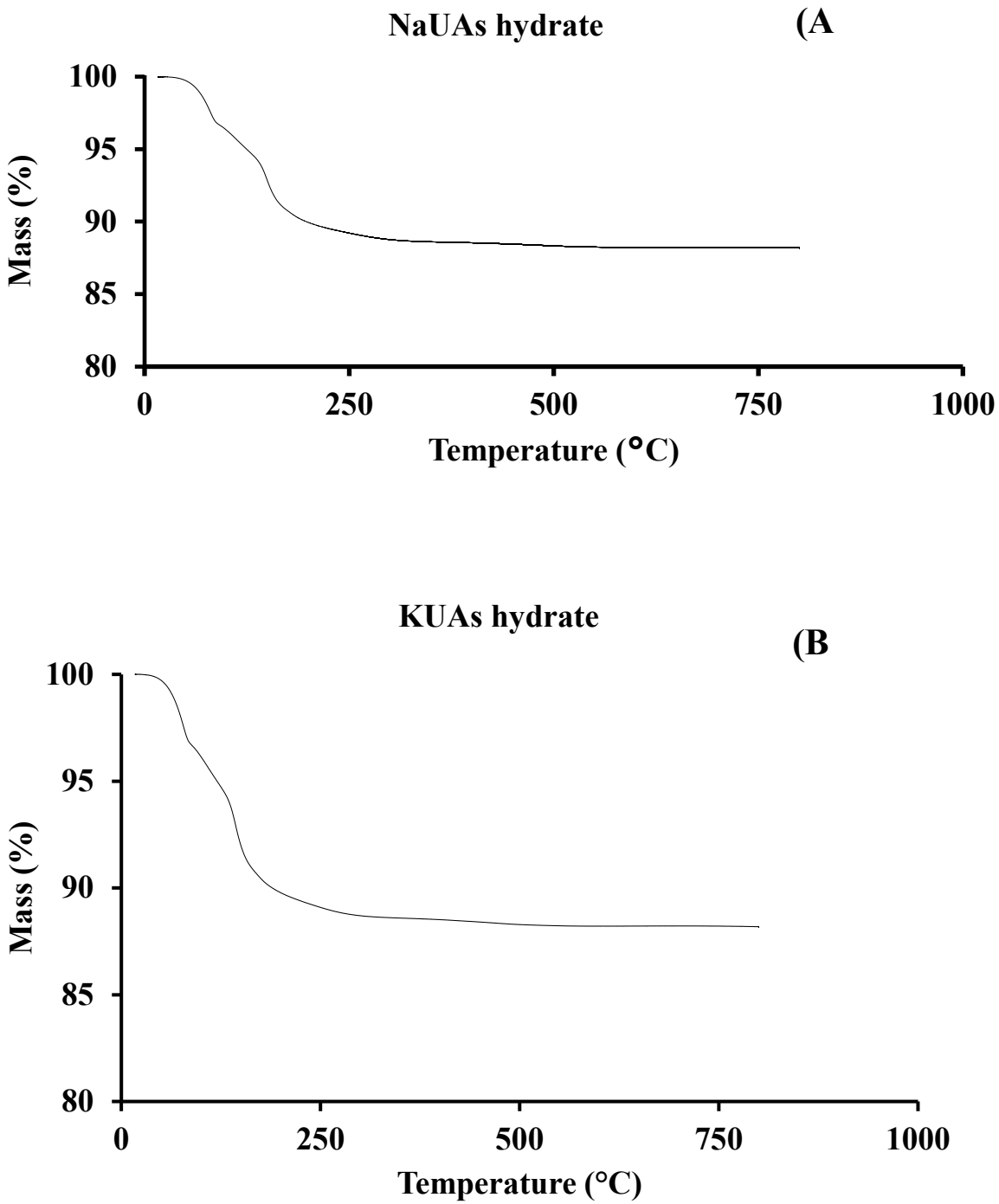

Figure S2. TGA (weight-%mass) curves of A) NaUAs and B) KUAs.

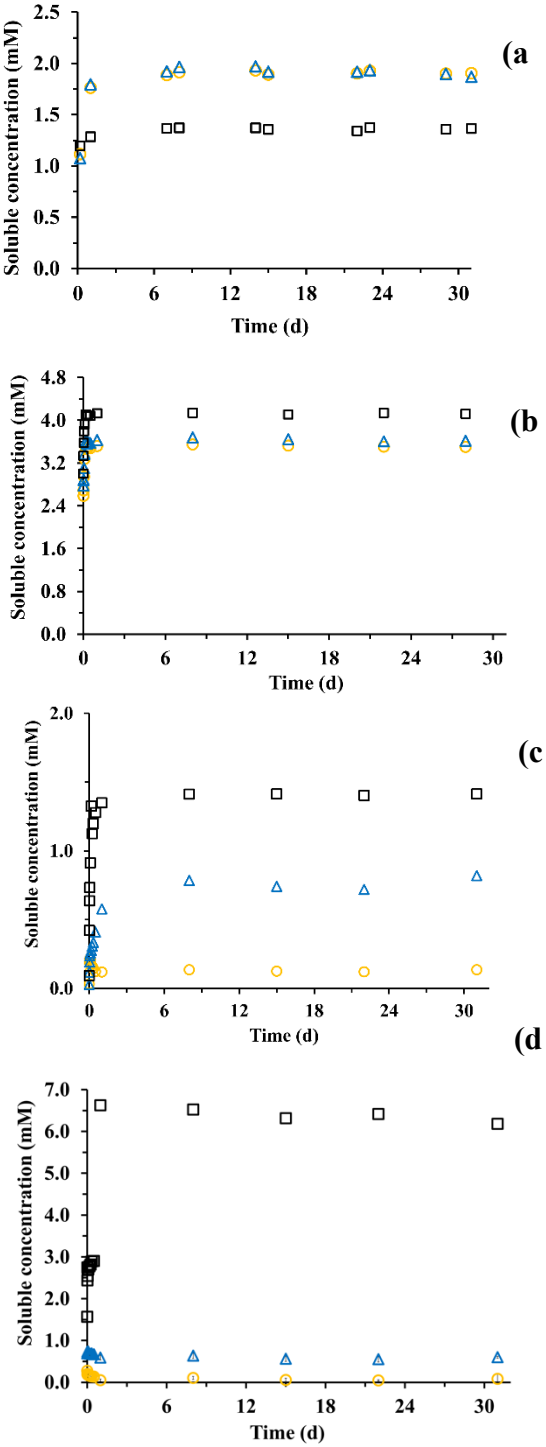

Figure S3. Experimental measurements of the dissolved concentrations of U (circles), As (triangles), and Na (squares) in mM against time for NaUAs for dissolution (a) and precipitation experiments (b) at pH 1.5 to 2 and dissolution (c) and precipitation experiments (d) at pH 2.6 to 3.

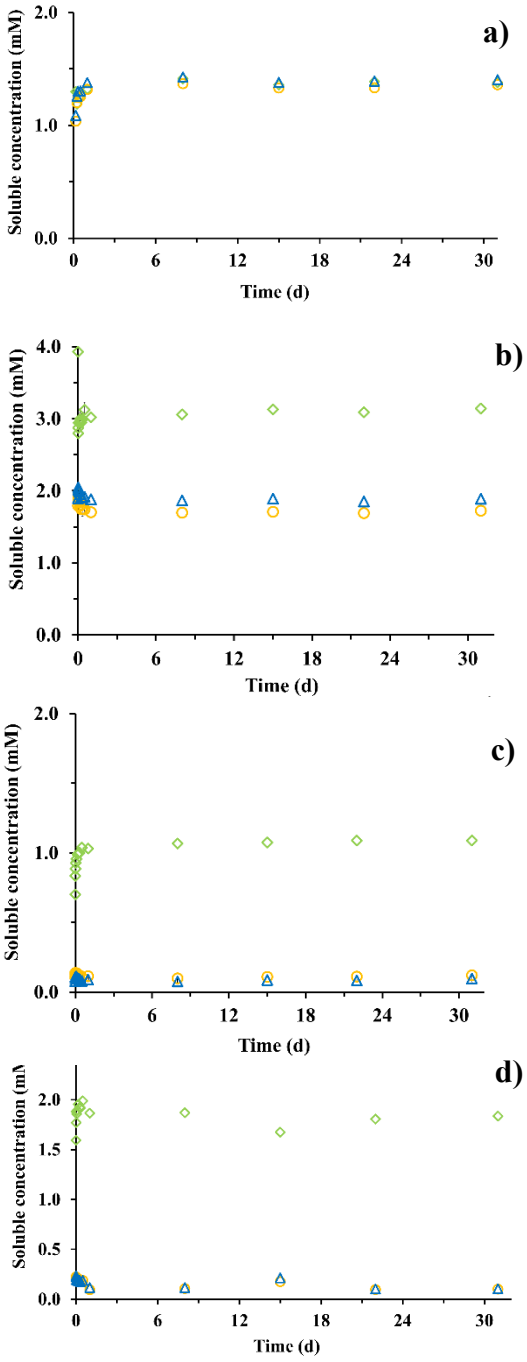

Figure S4. Experimental measurements of the dissolved concentrations of U (circles), As (triangles), and K (diamonds) in mM against time for KUAs for dissolution (a) and precipitation experiments (b) at pH 1.5 to 2 and dissolution (c) and precipitation experiments (d) at pH 2.6 to 3.

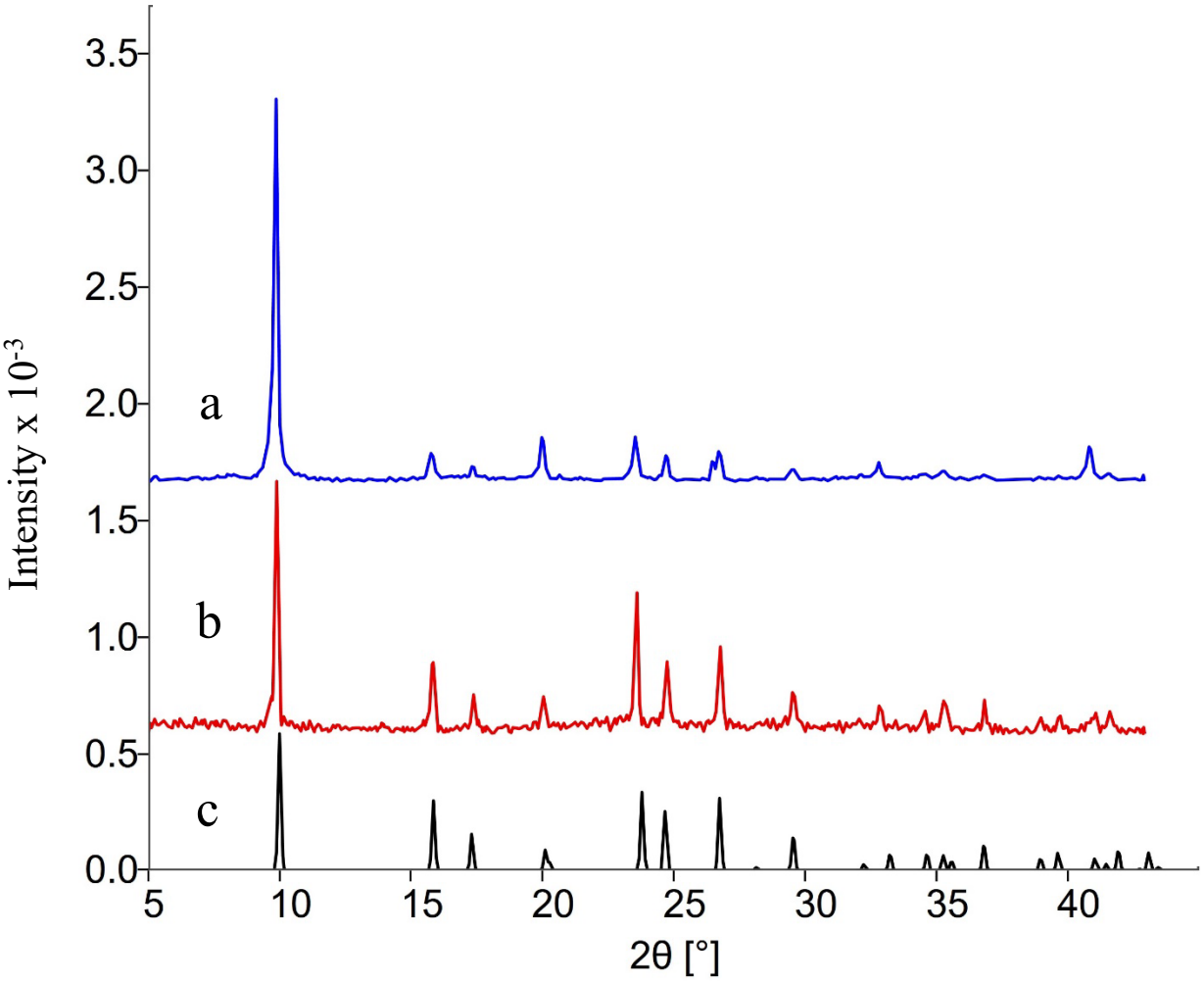

Figure S5. Powder X-ray diffraction patterns of reacted NaUAs dissolution (a) and precipitation (b) experiments at pH ranging from 1.5 to 2 compared to $Na[(UO_2)(AsO_4)](H_2O)_3$ (c).

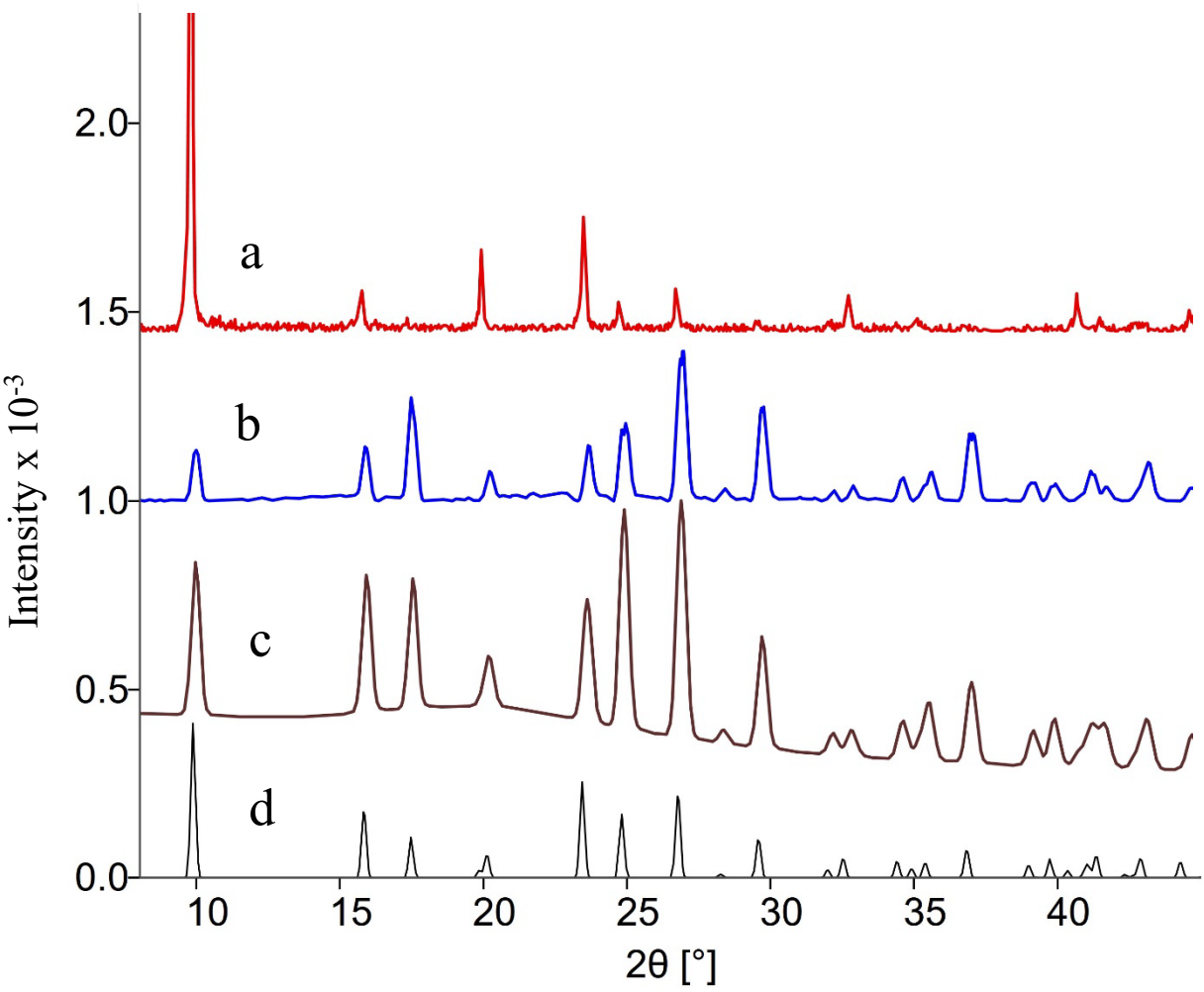

Figure S6. Powder X-ray diffraction patterns of reacted KUAs dissolution experiments at pH ranging from 1.5 to 2 (a), dissolution (b) and precipitation (c) experiments at pH ranging from 2.6 to 3 compared to $K[(UO_2)(AsO_4)](H_2O)_3$ (d).

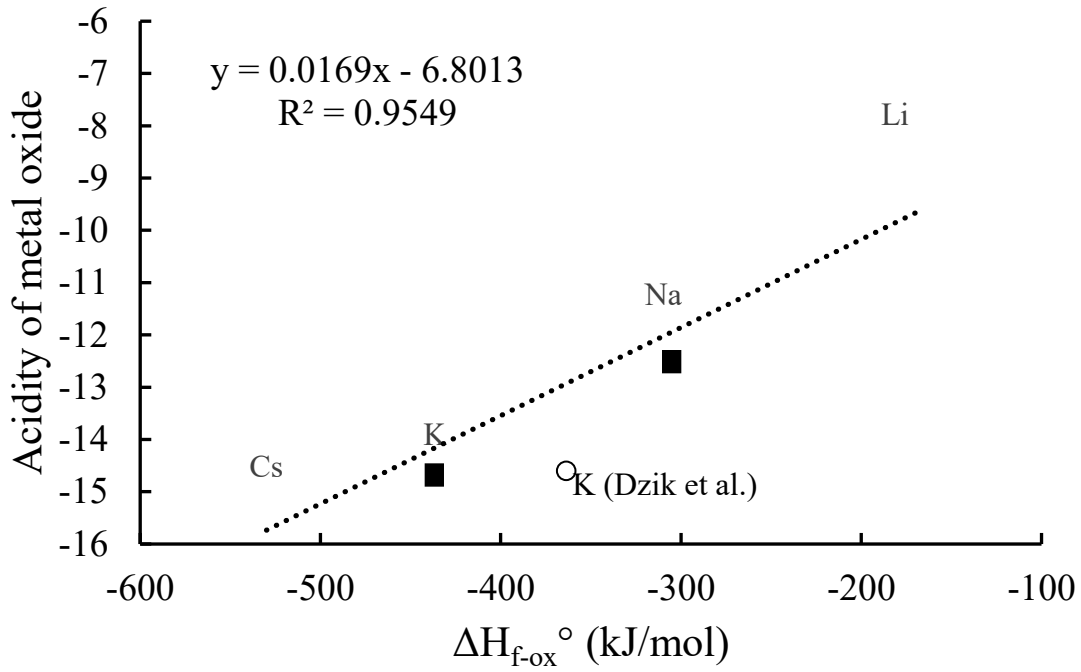

Figure S7. ΔH_f from oxides for uranyl arsenates plotted against the Smith scale (acidity of metal oxide) with a linear regression. The close squares represent the ΔH_{f-ox} for the NaUAs and KUAs phases from this work. The open circle represents the ΔH_{f-ox} for the potassium uranyl arsenate phase, the open squares represent the LiUAs and CsUAs, all of them determined by Dzik et al.[11]

References

1. Dzik Ewa, A. E., High-temperature calorimetric measurements of thermodynamic properties of uranyl arsenates of the meta-autunite group. *Chem. Geol.* **2018,** *493*, 353.

2. I. Campos, E. C. A. ThermoChimie Technical report. Bibliography. https://www.thermochimie-tdb.com/pages/contact.php

APPENDIX B. SUPPORTING INFORMATION: SOLUBILITY OF NA- AND K- URANYL ARSENATE SOLIDS: CHEMICAL EQUILIBRIUM OR KINETIC CONTROLS?

Table S1. Primary species and thermodynamic equilibrium constants (at T = 25°C) for aqueous complexes used in the reactive transport model (CRUNCHFLOW).[93]

Primary species and reaction aqueous complexes	
Primary species	
H^+	
AsO_4^{3-}	
UO_2^{2+}	
Na^+	
K^+	
CO_2	
NO_3^-	
Uranyl arsenate aqueous complexes	**Log K_{eq}**
$UO_2^{2+} + AsO_4^{3-} + H^+ \leftrightarrow UO_2HAsO_4^0$	**18.76**
$UO_2^{2+} + AsO_4^{3-} + 2H^+ \leftrightarrow UO_2H_2AsO_4^+$	**21.95**
$UO_2^{2+} + 2AsO_4^{3-} + 4H^+ \leftrightarrow UO_2(H_2AsO_4)_2^0$	**41.53**
Aqueous complexes	
$H_3AsO_4 \leftrightarrow AsO_4^{3-} + 3H^+$	**20.63**
$H_2AsO_4^- \leftrightarrow AsO_4^{3-} + 2H^+$	**18.37**
$HAsO_4^{2-} \leftrightarrow AsO_4^{3-} + H^+$	**11.6**
$UO_2NO_3^+ \leftrightarrow NO_3^- + UO_2^{2+}$	**-0.10**
$NaNO_3 \leftrightarrow NO_3^- + Na^+$	**0.40**
$KNO_3 \leftrightarrow NO_3^- + K^+$	**0.15**
$NaNO_3 \leftrightarrow NO_3^- + Na^+$	**-0.4**
$UO_2OH^+ + H^+ \leftrightarrow H_2O + UO_2^{2+}$	**-5.25**
$(UO_2)_2(OH)^{3+} + H^+ \leftrightarrow H_2O + 2UO_2^{2+}$	**-2.70**
$(UO_2)_2(OH)_2^{2+} + 2H^+ \leftrightarrow 2H_2O + 2UO_2^{2+}$	**-5.62**
$HCO_3^- + H^+ \leftrightarrow H_2O + CO_2$	**6.35**
$UO_2CO_3 + 2H^+ \leftrightarrow H_2O + UO_2^{2+} + CO_2$	**6.74**
$UO_2(OH)_2 + 2H^+ \leftrightarrow 2H_2O + UO_2^{2+}$	**12.15**
$H_2O \leftrightarrow OH^- + H^+$	**-14.00**
$(UO_2)_3(OH)_4^{2+} + 5H+ \leftrightarrow 5H_2O + 3UO_2^{2+}$	**-11.90**
$(UO_2)_3(OH)_5^+ + 5H^+ \leftrightarrow 5H_2O + 3UO_2^{2+}$	**-15.55**
$NaOH + H^+ \leftrightarrow H_2O + Na^+$	**14.75**
$KOH + H^+ \leftrightarrow H_2O + K^+$	**14.46**
$UO_2(OH)^{3-} + 3H^+ \leftrightarrow 3H_2O + UO_2^{2+}$	**20.25**
$CO_3^{2-} 2H+ \leftrightarrow H_2O + UO_2^{2+} + CO_2$	**16.68**
$(UO_2)_2(CO_3)(OH)^{3-} + 5H^+ \leftrightarrow 4H_2O + 2UO_2^{2+} + CO_2$	**17.54**
$NaHCO_3 + H^+ \leftrightarrow H_2O + Na^+ + CO_2$	**6.6**
$NaCO_3^- + 2H^+ \leftrightarrow H_2O + Na^+ + CO_2$	**15.41**

Table S2. Equilibrium concentrations of dissolved species and pH measurements of NaUAs and KUAs.

pH range	Experiment	U (mM)	As (mM)	Na (mM)	K (mM)	Final pH
2	Dissolution NaUAs	1.71	1.71	1.30	--	1.98
	Dissolution KUAs	2.30	2.30	--	1.41	1.96
3	Dissolution NaUAs	0.13	0.73	1.4	--	3.01
	Dissolution KUAs	0.11	0.10	--	1.07	3.03

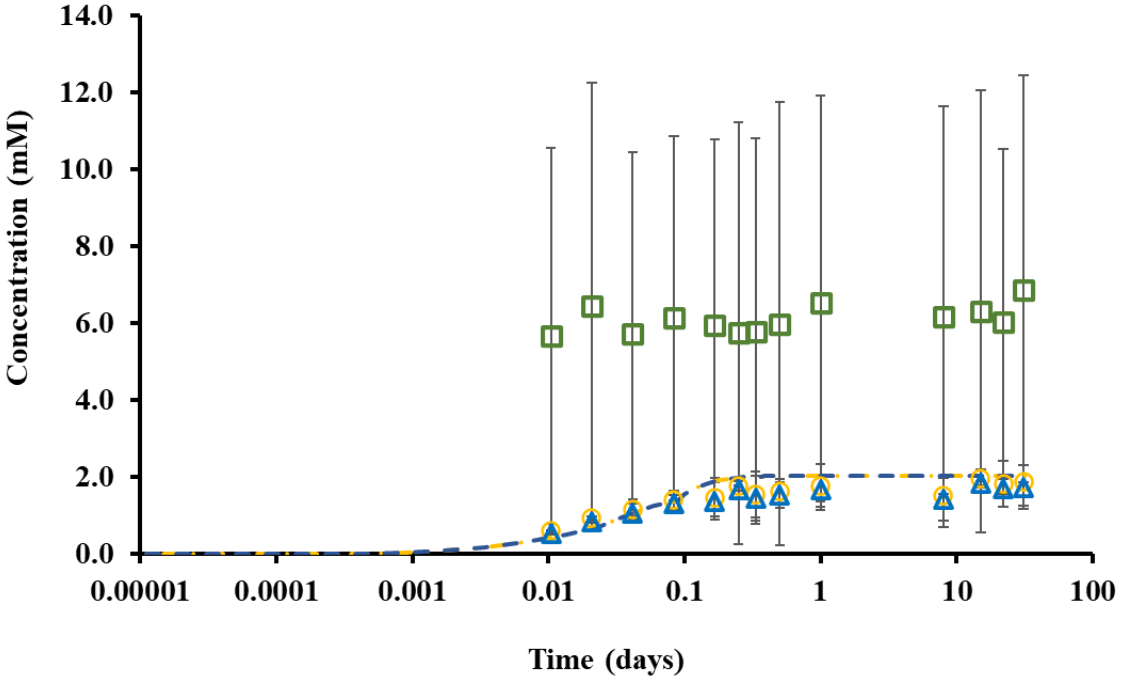

Figure S1. NaUAs dissolution experiments at pH 2 vs modeling with Crunchflow (continuous lines) presenting concentrations of U (open circles), As (open triangles), and Na (open squares).

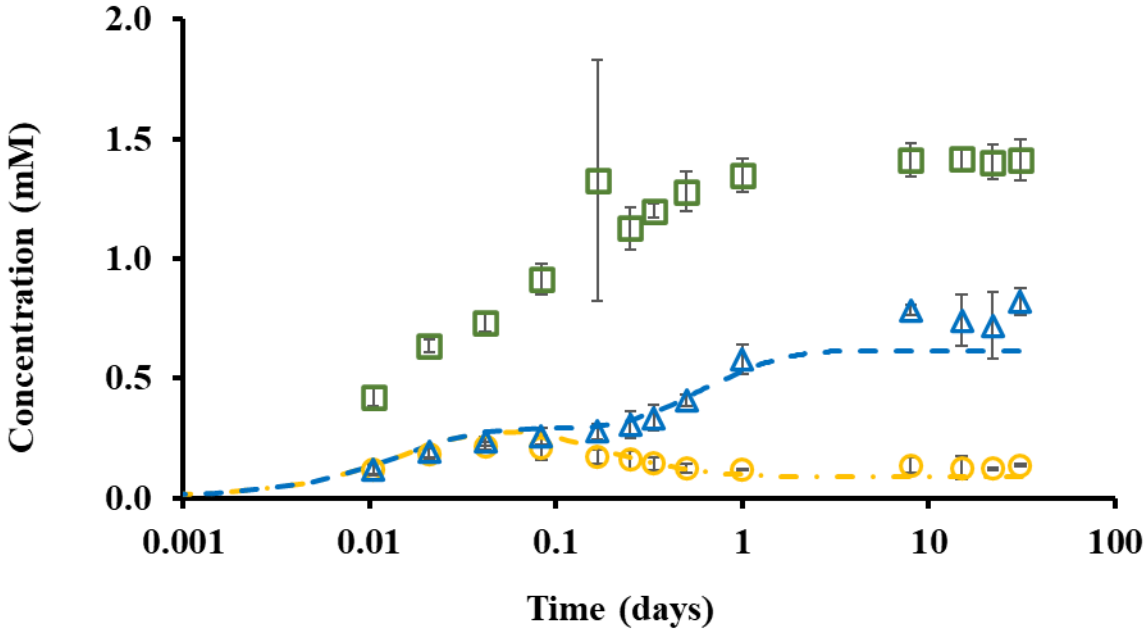

Figure S2. NaUAs dissolution experiments at pH 3 vs modeling with Crunchflow (continuous lines) presenting concentrations of U (open circles), As (open triangles), and Na (open squares).

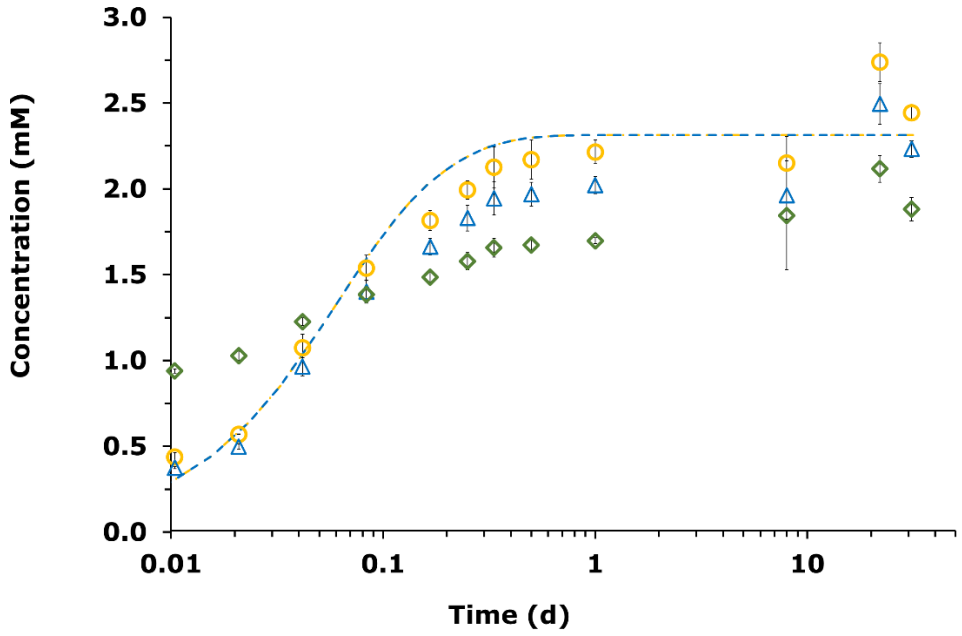

Figure S3. KUAs dissolution experiments at pH 2 vs modeling with Crunchflow (continuous lines) presenting concentrations of U (open circles), As (open triangles), and K (open diamonds).

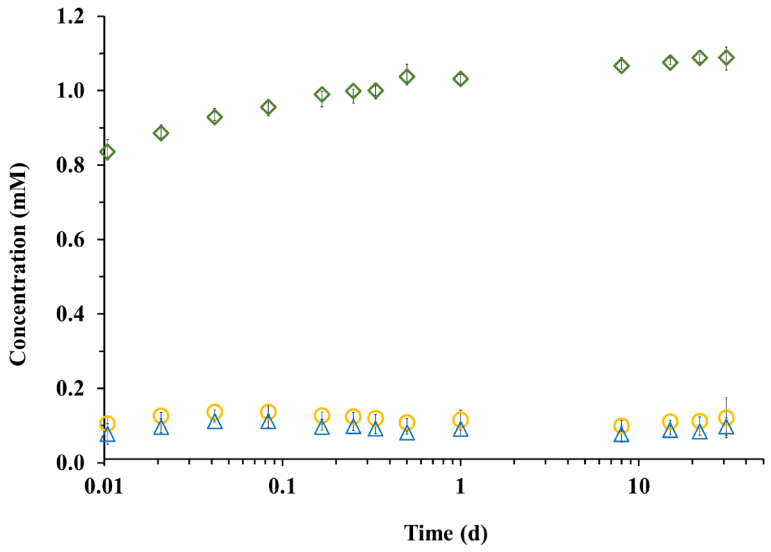

Figure S4. KUAs dissolution experiments at pH 3 presenting concentrations of U (open circles), As (open triangles), and K (open diamonds).

APPENDIX C. SUPPLEMENTARY INFORMATION FROM CHAPTER 5: PRECIPITATION OF AQUEOUS URANYL AND ARSENATE WITH PHOSPHATE AND LIMESTONE

Table S1. XRF concentrations component report from natural limestone used in this study.

Limestone Sample ID	Component (w/o normal) mass %													
	Ca	**Si**	**Fe**	**Na**	**Mg**	**Al**	**P**	**S**	**Cl**	**K**	**Ti**	**Mn**	**Cu**	**Zn**
Top Dustin	44.82	7.33	1.36	0.05	0.59	0.74	0.03	0.02	0.01	0.24	0.09	0.07	0.01	0.01

Table S2. Backscatter electron image by microprobe with % component report from natural limestone used in this study.

Limestone ID	Backscatter electron image make up about 21.5 % of the map area (77352000 sq μm). %				
	Ca	**Si**	**Na**	**Mg**	**K**
Madera	3723600/ 7735200 **48.10**	3723600/ 7735201 **30.30**	not mapped **8.00**	414400/ 7735200 **5.40**	569200/ 7735204 **7.4**

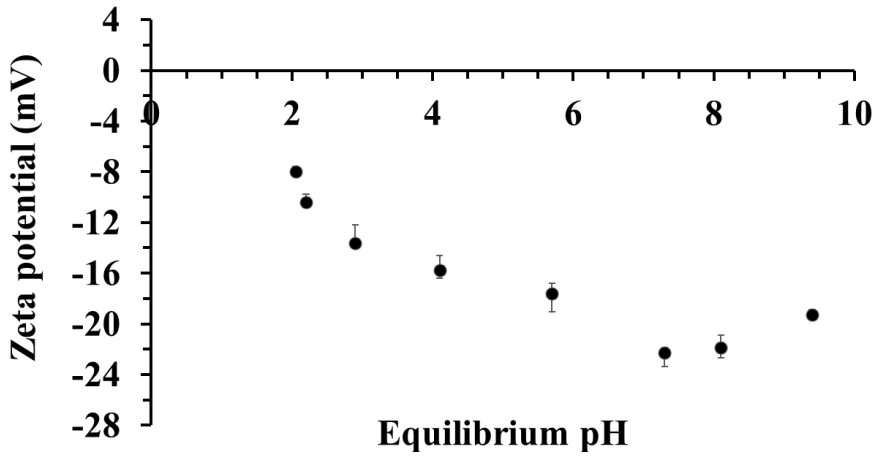

Figure S1. Zeta potential (mV) measurements of limestone used in this research. The reported values are average of three measurements.

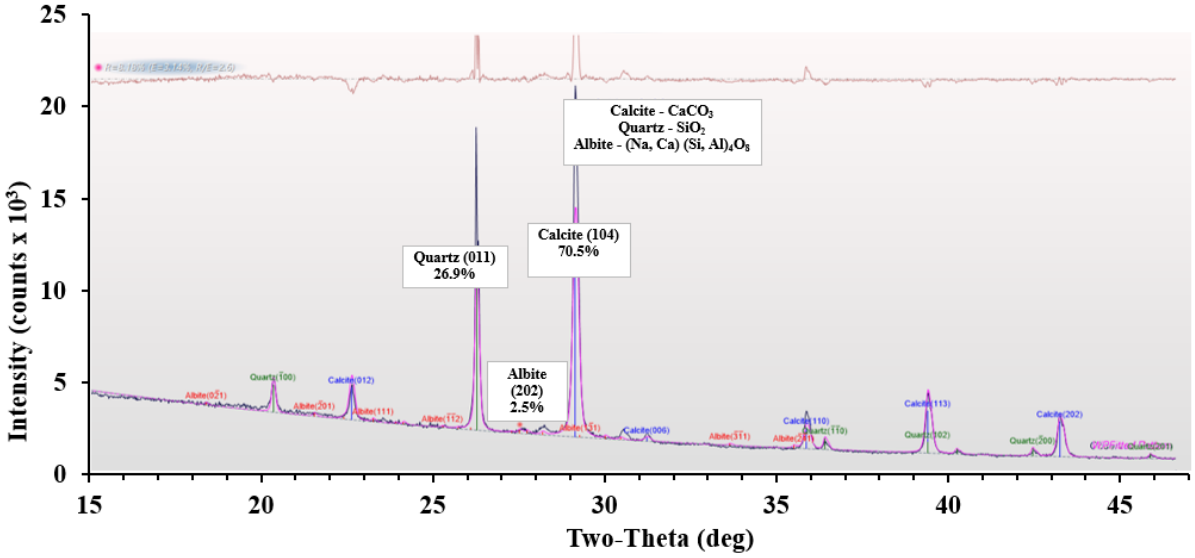

Figure S2. X-ray diffraction from limestone used in this research.

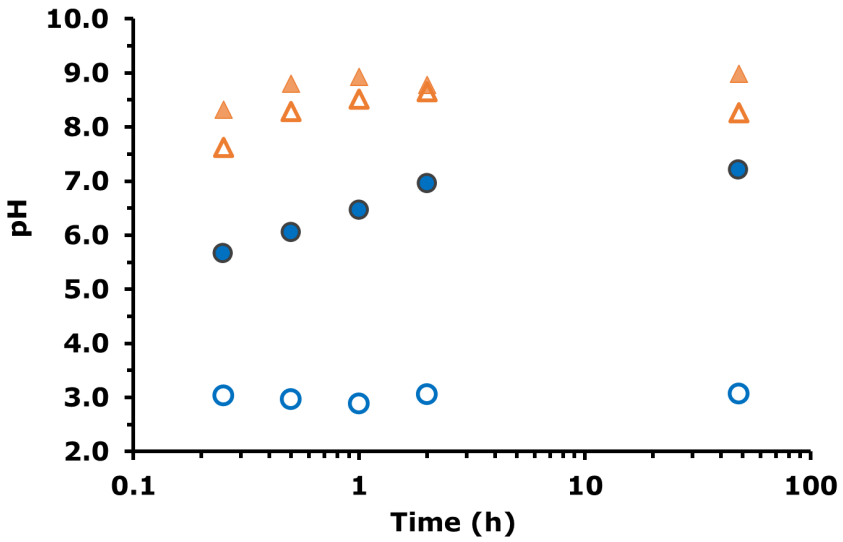

Figure S3. pH for batch experiments with U and As with limestone (close circles and triangles) or without limestone (1000 mg L^{-1}) (open circles and triangles) starting at pH 3 (circles) or pH 7 (triangles).

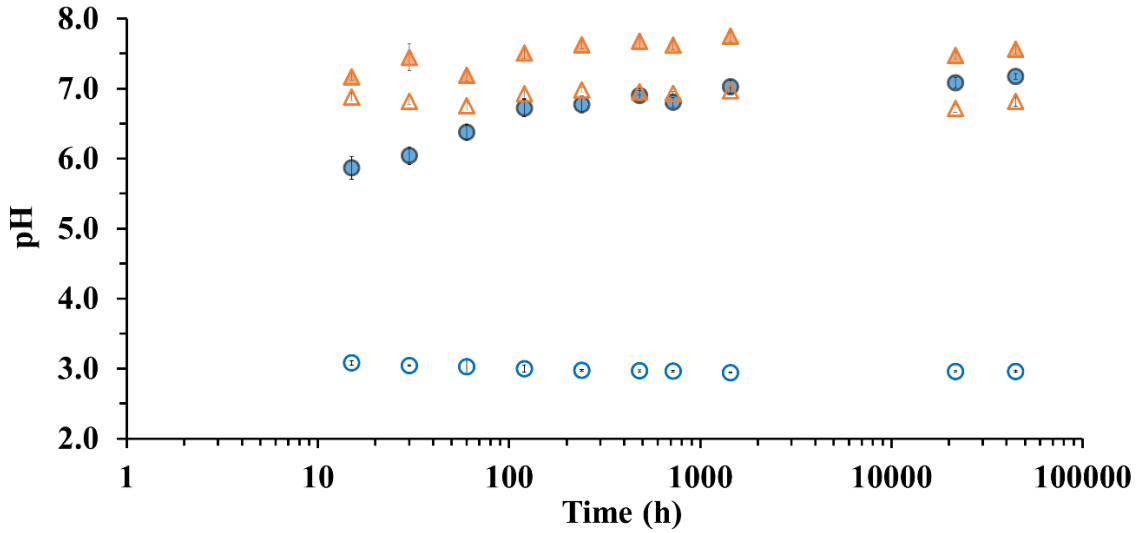

Figure S4. pH for batch experiments with U, As, and PO_4 with (close circles and triangles) or without limestone (400 mg L^{-1}) (open circles and triangles) starting at pH 3 (circles) or pH 7 (triangles) and initial 0.05 mM concentrations of U and As and 1 mM of PO_4.

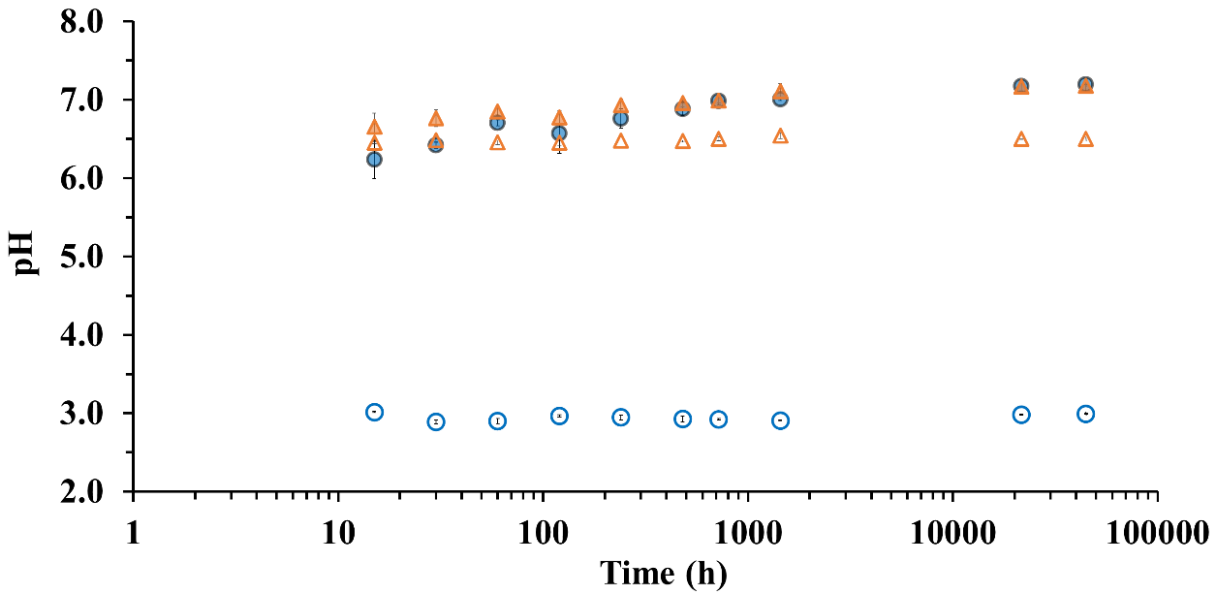

Figure S5. pH of U, As, PO_4, and Ca batch experiments with (close circles and triangles) or without limestone (1000 mg L^{-1}) (open circles and triangles) (starting pH 3 (circles) and pH 7 (triangles) and initial 0.05 mM concentrations of U and As 1 mM of PO_4, and 2 mM of Ca.